SUPERVISORY CONTROL AND INTENT RECOGNITION OF A POWERED KNEE AND ANKLE PROSTHESIS

By

HUSEYIN ATAKAN VAROL

Dissertation

Submitted to the Faculty of the

Graduate School of Vanderbilt University

in partial fulfillment of the requirements

for the degree of

DOCTOR OF PHILOSOPHY

in

Electrical Engineering

August, 2009

Nashville, Tennessee

Approved:

Dr. Michael Goldfarb

Dr. Mitch Wilkes

Dr. George Cook

Dr. Nilanjan Sarkar

Dr. Robert Webster

To my family

ACKNOWLEDGEMENTS

I would like to thank to my advisor, Dr. Michael Goldfarb, for guiding me in this challenging and stimulating research project. I was really lucky to have him as an advisor because he was never hesitant to share his knowledge. I learned so much from him. Also, I would like to express my sincere thanks to my secondary advisor Dr. Mitch Wilkes. He has been always very understanding and helpful. He will be my role model for student-professor interaction. I acknowledge the other members of my thesis committee, Dr.George Cook, Dr. Nilanjan Sarkar, Dr. Robert Webster, for their time and support. I thank to the National Institute of Health for the grant, R01EB005684-01.

The members of Center for Intelligent Mechatronics deserve a special recognition. Together, they create a fantastic research environment, where one would never get bored, if interested in robotics and mechatronics. I especially would like to thank to Frank Sup. I don't know how many hours we spent together with 'The Leg' during our theses. I admire him deeply since he is not only a very tough engineer but also a great father and friend, all in one package. I thank Jason Mitchell and Dr. Thomas Withrow for their great advice and assistance throughout the project. Furthermore, I appreciate greatly what Craig has done for us in testing the prosthesis. Without his dedication, we could not have done this much.

I thank to my friends in Nashville, especially to the Cetin and Erdemir families, for being there whenever I needed them. I would like to express my deepest appreciation to my parents, Dr. Huseyin Selcuk Varol and Gungor Varol, and my brother, Erkan Varol, for their unending love, support and encouragement. I also would like to thank to 'my lonely and beautiful country', Turkey, for giving me a good education and helping me to come this far.

TABLE OF CONTENTS

Page

LIST OF FIGURES

LIST OF TABLES

Page

CHAPTER I

Introduction

1. Background

Though no prior work exists on the development and control of a powered knee and ankle prosthesis, some prior work exists on the development and control of powered knee prostheses, and separately on powered ankle prostheses. Regarding the former, [1] describes the development of an electro-hydraulically powered knee prosthesis, developed as a laboratory test bed for studying the control of powered knee joints during walking. This prosthesis was utilized to develop an echo control approach, in which the authors instrumented the sound-side knee (of a unilateral amputee) with a position sensor, and used a modified version of the measured knee angle profile on the powered prosthesis side one half cycle later, which they term "modified echo control" [2, 3]. Ossur, a prosthetics company, recently introduced a self-contained (battery-powered) powered knee prosthesis, in which they similarly instrument the sound side leg (with accelerometers) and also utilize an echo type approach [4]. Other researchers describe the development of powered prosthesis prototypes, but do not describe a user control and communication interface structure [5, 6]. Recently, an electromyography based pattern recognizer for classifying locomotion modes using artificial neural networks and linear discriminant analysis is proposed in [7]. Regarding the echo control approaches incorporated in [1-3, 8], an obvious drawback is that the sound-side (or unaffected) leg must be instrumented, which requires the user to don and doff additional instrumentation. The echo control approach presumably also restricts the use of the prosthesis to unilateral amputees and also presents a problem for "odd" numbers of steps, in which an echoed step is undesirable. A more subtle, although perhaps more significant shortcoming of the echo-type approach is that suitable motion tracking requires a high output impedance of the prosthesis, which forces the amputee to react to the limb rather than interact with it. Specifically, in order for the prosthesis to dictate the joint trajectory, it must assume a high output impedance (i.e., must be stiff), thus precluding any dynamic interaction with the user and the environment,

which is contrary to the way in which humans interact with their native limbs.

Regarding powered ankle prostheses, a tibia based controller is implemented in [9], in which the ankle angle is adjusted as a function of the tibia angle. In [10], the authors use finite state controllers in combination with torque, impedance and position controllers for the control of a powered ankle prosthesis with a series elastic actuator. They also describe a neural network based high level controller which processes electromyogram (EMG) signals to manage transitions of the finite state controllers for level ground and stair descent. Note that Ossur markets an ankle prosthesis (Proprio Foot [11]) which quasi-statically adjusts the ankle angle for sitting and slope walking, but does not contribute net power to gait.

2. Problem Definition

One of the primary challenges entailed in developing powered lower limb prosthesis is the means by which the user can control the prosthesis. A powered prosthesis is fundamentally different from a passive one in that the latter can only react, while the former can both act and react. In order to effectively implement a powered prosthesis, a control interface must be developed that enables the user to control and communicate intent to the prosthesis in a real-time manner. Clearly, such a communication and control structure must be safe and reliable, and should not require cognition on the part of the user.

This work describes a novel method for the implicit communication with a powered lower limb prosthesis which is an alternative to an echo control approach. The proposed approach infers user intent via pattern recognition based on measured data from sensors on the prosthesis, which provides several advantages relative to an echo approach. First, no additional instrumentation or wiring apart from the prosthesis need be worn by the user. Second, the information flow is much less delayed as compared to the half cycle in the echo control approach. Third, the prosthesis is decoupled from the unaffected side, and thus the user is not constrained to "even" patterns of gait. Lastly, the proposed approach can be utilized on both unilateral and bilateral amputees.

The proposed control architecture for the powered lower limb prosthesis is a three level hierarchy, as diagrammed in Fig. 1-1. At the lowest level, closed-loop joint torque controllers compensate for the

transmission dynamics (i.e., primarily friction and inertia), so that joint torque references (commanded by the middle level controllers) will be tracked with a higher bandwidth and accuracy than would be the case with an open-loop torque control approach. The middle level controllers, which control a given activity mode (such as walking, standing, and sitting), generate torque references for the joints using a finite state machine that modulates the impedance of the joints depending on the phase of the activity, as described in [12]. The high level controller, which is the intent recognizer, consists of three parts: the activity mode intent recognizer, the cadence estimator, and the slope estimator. The latter two estimate the slope and cadence during walking to adjust the parameters of the walking mode controller. The activity mode intent recognizer distinguishes between different activity modes such as standing, sitting, and walking, and switches to the appropriate middle level controller.

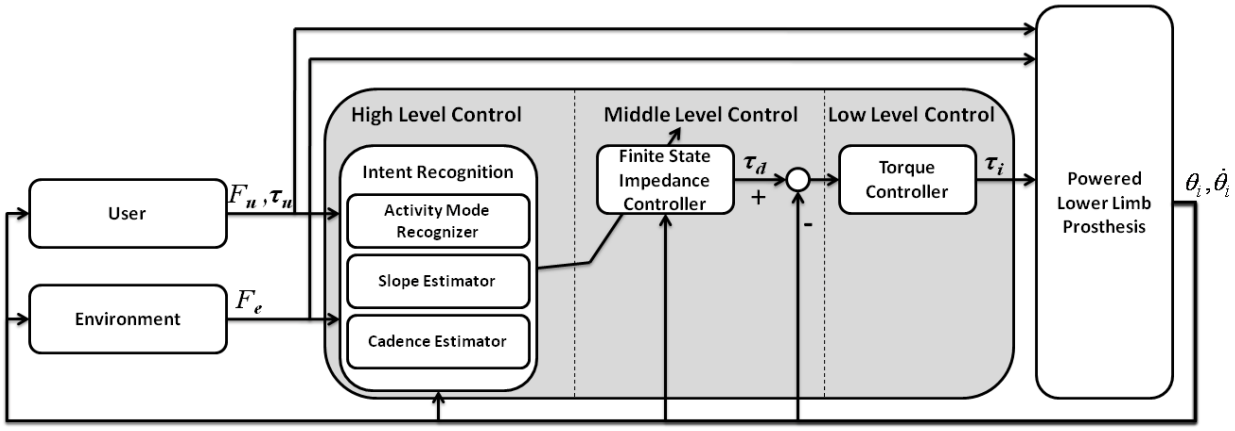

Figure 1-1. Powered prosthesis control architecture.

3. Organization of the Document

This thesis is organized in five chapters. Chapter I presents the motivation for the supervisory control problem of the powered prosthesis, provides an introduction for the remaining parts of the thesis, defines the contributions of the author, and proposes future work. The remaining chapters of this thesis are comprised of three different manuscripts submitted to different journals and conferences to which the author made significant contributions and an additional chapter on supervisory control of a powered prosthesis for ground slope and walking speed adaptation.

Chapter II describes the general design and preliminary testing of an electrical self-contained powered knee and ankle prosthesis. The paper describes the mechanical design, sensors, embedded system, and control architecture. The prosthesis and walking controller is tested on a unilateral amputee subject. Experimental results indicate that the powered knee and ankle prosthesis with the proposed control structure can generate near-normal gait in trials with a unilateral amputee subject. The journal version of this paper has been accepted to the ASME/IEEE Transactions on Mechatronics as a full paper for the focused section on Anthropomorphism in Mechatronic Systems.

The control architecture and intent recognition approach for the real-time supervisory control of a powered lower limb prosthesis is presented in Chapter III. The proposed approach infers user intent to stand, sit, or walk, by recognizing patterns in prosthesis sensor data in real-time, without the need for instrumentation of the sound-side leg. In addition to describing the generalized control approach, this paper describes the implementation of this approach on a single unilateral transfemoral amputee subject, and demonstrates via experiments the effectiveness of the approach. This paper is currently in review with the IEEE Transactions on Biomedical Engineering as a full technical paper.

Chapter IV presents a control framework for the powered knee and ankle prosthesis during sitting and standing and the transitions between the two states. This work describes the extension of the intent recognition algorithm for stand-to-sit and sit-to-stand transitions and the structure of the finite state based impedance controller for the sitting mode. Experiments conducted with a unilateral amputee subject using the self-contained powered prosthesis are also presented to show the effectiveness of the proposed framework. This paper was accepted to the 2009 IEEE International Conference on Rehabilitation Robotics as a technical paper.

Chapter V describes the extension of the high level controller for ground slope and cadence estimation. Experiments conducted with a unilateral transfemoral amputee subject indicate that slope and cadence estimators reliably estimate the ground slope and cadence allowing the modification of walking controller parameters in real-time.

4. References

[1] W. C. Flowers, and R. W. Mann, “Electrohydraulic knee-torque controller for a prosthesis simulator,” ASME J. of Biomechanical Engineering, vol. 99, no. 4, pp. 3-8, 1977.

[2] J. L. Stein, and Massachusetts Institute of Technology. Dept. of Mechanical Engineering., “Design issues in the stance phase control of above-knee prostheses,” Massachusetts Institute of Tech. Dept. of Mechanical Eng. Thesis Ph.D., 1983.

[3] D. L. Grimes, “An active multi-mode above knee prosthesis controller,” Massachusetts Institute of Tech. Dept. of Mechanical Eng. Thesis Ph.D., 1979.

[4] S. Bedard, and P. Roy, Actuated Leg Prosthesis for Above-Knee Amputees, U. S. Patent, 2003.

[5] E. Martinez- Villalpando, J. Weber, G. Elliott, and H. Herr, “Design of an agonist-antagonist active knee prosthesis,” Proc. IEEE/RAS-EMBS Int. Conf. on Biomedical Robotics and Biomechatronics, pp. 529-534, 2008.

[6] D. Popovic, and L. Schwirtlich, “Belgrade active A/K prosthesis,” in de Vries, J. (Ed.), Electrophysiological Kinesiology, Intern. Congress Ser. No. 804, Excerpta Medica, Amsterdam, The Netherlands, pp. 337-343, 1988.

[7] H. Huang, T. A. Kuiken, and R. D. Lipschutz, “A Strategy for Identifying Locomotion Modes Using Surface Electromyography,” IEEE Trans. on Biomedical Engineering, vol. 56, no. 1, pp. 65-73, Jan, 2009.

[8] S. Bedard, and P. Roy, Actuated leg prosthesis for above-knee amputees, 7,314,490, U. S. Patent, June 17, 2003.

[9] M. A. Holgate, A. W. Bohler, and T. G. Sugar, “Control algorithms for ankle robots: A reflection on the state-of-the-art and presentation of two novel algorithms,” Proc. IEEE/RAS-EMBS Int. Conf. on Biomedical Robotics and Biomechatronics, pp. 97-102, 2008.

[10] S. Au, M. Berniker, and H. Herr, “Powered ankle-foot prosthesis to assist level-ground and stair-descent gaits,” Neural Networks, vol. 21, no. 4, pp. 654-666, May, 2008.

[11] W. Koniuk, Self-adusting prosthetic ankle apparatus, 6,443,993, U. S. Patent, March, 23, 2001.

[12] F. Sup, A. Bohara, and M. Goldfarb, “Design and control of a powered transfemoral prosthesis,” Int. J. of Robotics Research, vol. 27, no. 2, pp. 263-273, Feb, 2008.

CHAPTER II

Manuscript I: Preliminary Evaluations of a Self-Contained Anthropomorphic Transfemoral Prosthesis

Frank Sup, Huseyin Atakan Varol, Jason Mitchell, Thomas J. Withrow and Michael Goldfarb

Vanderbilt University

Nashville, TN

Accepted as a Regular Paper to the

IEEE/ASME Transactions on Mechatronics

in the focused section

Anthropomorphism in Mechatronic Systems

1. Abstract

This paper presents a self-contained powered knee and ankle prosthesis, intended to enhance the mobility of transfemoral amputees. A finite-state based impedance control approach, previously developed by the authors, is used for the control of the prosthesis during walking and standing. Experiments on an amputee subject for level treadmill and overground walking are described. Knee and ankle joint angle, torque, and power data taken during walking experiments at various speeds demonstrate the ability of the prosthesis to provide a functional gait that is representative of normal gait biomechanics. Measurements from the battery during level overground walking indicate that the self-contained device can provide over 4,500 strides, or 9 km, of walking at a speed of 5.1 km/h between battery charges.

2. Introduction

There are more than 300,000 transfemoral amputees [1] in the United States (i.e., an incidence of approximately one per thousand people), with 30,000 new transfemoral amputations conducted each year [2]. If similar trends hold across the world population, then one would expect approximately 7 million transfemoral amputees worldwide. One of the most significant limitations of current prosthetic technology is the inability to provide net power at the joints. This loss of net power generation at the lower limb impairs the ability of the prosthesis to restore biomechanically normal locomotive function during many locomotive activities, including level walking, walking up stairs and slopes, running and jumping [3-10]. In the absence of net power generation at the knee and ankle, transfemoral amputees with passive prostheses have been shown to expend 60% more metabolic energy [11] and exert three times the affected-side hip power and torque [9] when compared to healthy subjects during level walking. It is the hypothesis of this work that an actively powered knee and ankle prosthesis with the capability of generating human-scale net positive power over a gait cycle will provide improved functional restoration relative to passive prostheses.

Some of the earliest work in powered transfemoral prostheses was conducted during 1970's and 1980's and is described in [12-18]. Specifically, an electro-hydraulically actuated knee joint, which was tethered to a hydraulic power source and utilized off-board electronics and computation, was developed and tested on

at least one amputee subject. As described in [16], an "echo control" scheme was developed for gait control. In this control approach, the modified knee trajectory from the sound leg was used as a desired knee joint angle trajectory on the contralateral side. Other prior work reported the development of an active knee joint actuated by DC motors and utilized a finite state knee controller with robust position tracking control for gait control [19]. Ossur, a prosthetics company, has recently introduced the "Power Knee" that uses a control approach, which like echo control, utilizes sensors on the sound leg to prescribe a trajectory for the knee joint of the prosthesis [20]. In [21], the authors discuss a biomimetic prosthesis with an agonist-antagonist knee.

Work in powered transtibial prostheses includes [22], which describes the design of an active ankle joint using McKibben pneumatic actuators. Ossur has also introduced a "powered" ankle prosthesis, called the "Proprio Foot," which does not contribute net power to gait, but rather quasistatically adjusts the ankle angle to avoid stumbling and to better accommodate sitting [23]. Bellman et al. describe an active robotic ankle prosthesis with two actuated degrees of freedom [24]. Au and Herr built a powered ankle-foot prosthesis that incorporates both parallel and series elasticity to reduce peak motor torque requirements and to increase bandwidth [25].

Unlike any of the aforementioned prior works, this paper describes a transfemoral prosthesis with both a powered knee and ankle. Note that, as described by Sup et al. [26], the authors have developed previously a pneumatically powered knee and ankle prosthesis prototype, which was designed to leverage recent advances in monopropellant based pneumatic actuation described [27-30]. Despite this, the authors believe that the monopropellant technology in its current state is not ready for commercialization in the near-term. In order to provide a technology that is more appropriate for near-term use, the authors describe in this paper a powered knee and ankle prosthesis powered by a lithium-polymer battery. Such batteries have an energy density approaching 200 W·h/kg [31], which as described herein, enables the development of a transfemoral prosthesis with a reasonable weight and an acceptable, although limited, range of locomotion. The energy density of such batteries is expected to nearly double in the next decade (driven largely by the automotive industry's needs for electrical vehicles) [31], which will provide a significantly improved range of locomotion. Prior to developing the self-contained, battery-powered powered knee and ankle prosthesis

described herein, Sup et al. [32] previously built a tethered electrical powered knee and ankle prototype to explore the electrical power requirements of such a device.

Based on this preliminary work, the authors have developed an electrically powered self-contained active knee and ankle prosthesis, which is described herein. The self-contained prosthesis generates human-scale power at the joints and incorporates a torque-based control framework for stable and coordinated interaction between the prosthesis and the user. This paper describes the mechanical and electrical design of the prosthesis, provides an overview of the finite-state based impedance control framework for walking and standing, presents experimental results on a single transfemoral amputee subject, and discusses the electrical power requirements in different activity modes.

3. Prosthesis Design

The joint torque specifications required of the knee and ankle joints were based on an 85 kg user for a walking cadence of 80 steps per minute, Fig. 2-1, and stair climbing, as derived from body-mass-normalized data [8, 9], while the joint power specifications were based on data from Winter [9], also for an 85 kg user. The design specifications are summarized in Table 2-1. The resulting self-contained powered knee and ankle prosthesis is shown in Fig. 2-2. A detailed discussion of the mechanical, sensor and embedded system design is given in the following sections.

Table 2-1. Design specifications.

Specification	Value
Knee Range of Motion	0° to 120°
Ankle Range of Motion	-45° to 20°
Maximum Knee Torque	75 Nm
Maximum Ankle Torque	130 Nm
Peak Knee Power	150 W
Peak Ankle Power	250 W
Knee Center Height Adjustability	0.45 m to 0.58 m
Maximum Total Weight	4.5 kg
Minimum Factor of Safety	2

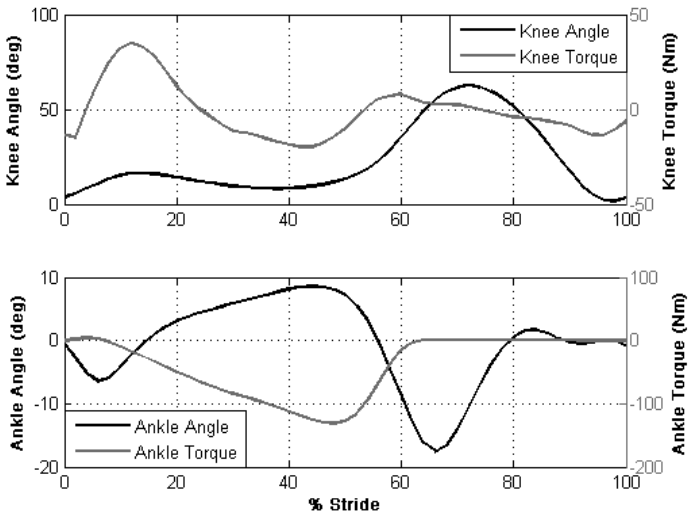

Figure 2-1. Normal biomechanical gait data for an 85 kg subject walking at a cadence of 80 steps per minute [9].

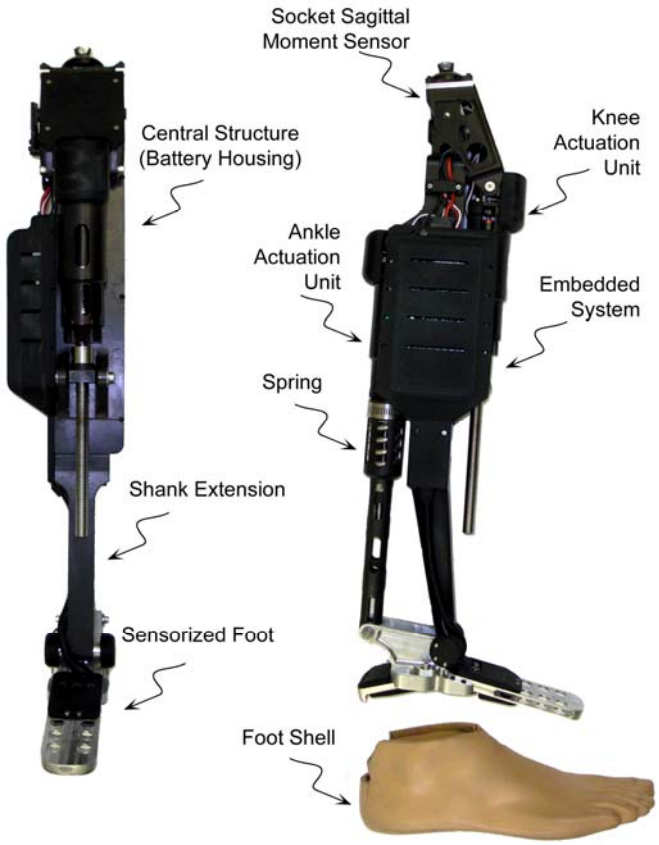

Figure 2-2. The self-contained powered knee and ankle transfemoral prosthesis, front (left) and side (right) views.

Mechanical Design

Actuation for the prosthesis is provided by two motor-driven ball screw assemblies that drive the knee and ankle joints, respectively, through a slider-crank linkage. The prosthesis is capable of 120° of flexion at the knee and 45° of planterflexion and 20° of dorsiflexion at the ankle. Each actuation unit consists of a Maxon EC30 Powermax brushless motor capable of producing 200 W of continuous power connected to a 12 mm diameter ball screw with 2 mm pitch, via helical shaft couplings. The ankle actuation unit additionally incorporates a 302 stainless steel spring (51mm free length and 35mm outer diameter), with 3 active coils and a stiffness of 385 N/cm in parallel with the ball screw. The purpose of the spring is to bias the motor's axial force output toward ankle plantarflexion, and to supplement power output during ankle push off. The stiffness of the spring is maximized to allow for peak force output without limiting the range of motion at the ankle. The resulting axial actuation unit's force versus ankle angle plot, Fig. 2-3, graphically demonstrates for fast walking the reduction in linear force output supplied by the motor at the ankle through the addition of the spring. Note that the compression spring does not engage until approximately five degrees of ankle plantarflexion. Each actuation unit additionally includes a uniaxial load cell (Measurement Specialties ELPF-500L), positioned in series with the actuation unit for closed loop force control of the motor/ballscrew unit. Both the knee and ankle joints incorporate bronze bearings and, for joint angle measurement, integrated precision potentiometers (ALPS RDC503013). A strain based sagittal plane moment sensor, Fig. 2-4, is located between the knee joint and the socket connector, which measures the moment between the socket and prosthesis. The ankle joint connects to a custom foot design, Fig. 2-5, which incorporates strain gages to measure the ground reaction forces on the ball of the foot and on the heel. The central hollow structure houses a lithium-polymer battery and provides an attachment point for the embedded system hardware. To better fit with an anthropomorphic envelope, the ankle joint is placed slightly anterior to the centerline of the central structure. This gives the prosthesis the illusion of flexion when the amputee is standing vertically with the knee fully extended.

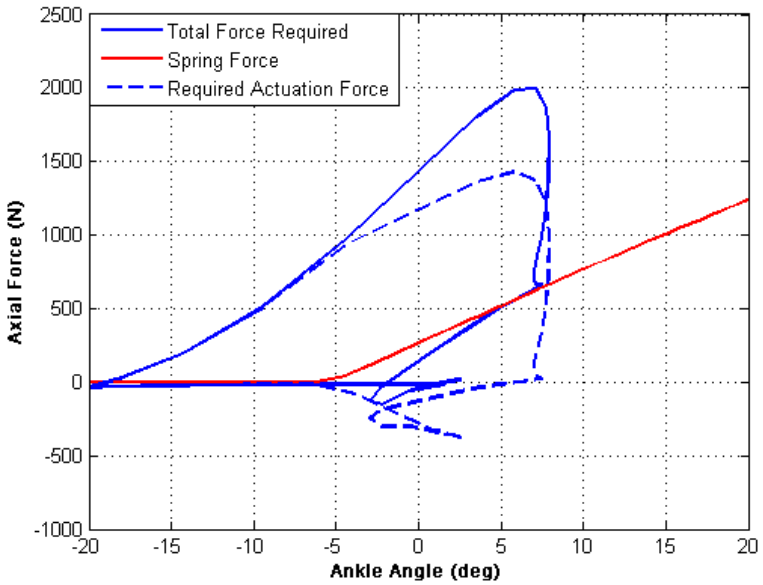

Figure 2-3. The reduction of linear force output required by the ankle motor unit by the addition of a spring in parallel for fast walking, taken from normal biomechanical data [9].

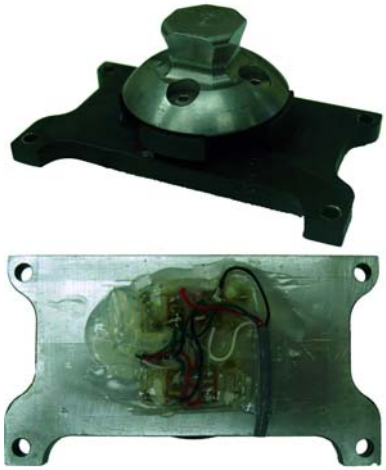

Figure 2-4. Sagittal moment load cell, top and bottom views.

Figure 2-5. Sensorized prosthetic foot with and without strain gage covers.

The length of the shank segment is varied by changing the length of three components; the lower shank extension, the spring pull-down, and the coupler between the ball nut and ankle. Additional adjustability is provided by the pyramid connector that is integrated into the sagittal moment load cell for coupling the prosthesis to the socket (as is standard in commercial transfemoral prostheses). The self-contained transfemoral prosthesis was fabricated from 7075 aluminum and has a total mass of 4.2 kg, which is within an acceptable range for transfemoral prostheses, and comparable to a normal limb segment [33]. A weight breakdown of the device is presented in Table 2-2.

Table 2-2. Mass breakdown of self-contained powered prosthesis.

Component	Mass (kg)
Battery	0.62
Electronics	0.36
Knee Motor Assembly	0.72
Ankle Motor Assembly	0.89
Sensorized Foot	0.35
Foot Shell	0.24
Sagittal Moment Sensor	0.12
Remaining Structure	0.90
Total Weight	4.20

Moment and Force Sensing

The sagittal plane moment between the user and prosthesis, and the force between the prosthesis and ground is sensed in order to infer user intent and coordinate prosthesis control. Based on biomechanical data [8, 9], the required range of measurements was determined to be 100 Nm of sagittal plane moment and a ground reaction force of 1000 N. The sagittal plane moment is measured above the knee joint at the socket interface and the ground reaction force is measured by the custom foot. The location of the sensors was chosen to avoid coupling the desired measured ground reaction force and sagittal moment with the joint torques. In addition, incorporating the ground reaction load cell into the structure of a custom foot

eliminates the added weight of a separate load cell, and also enables separate measurement of the heel and ball of foot load.

The sagittal plane moment sensor, shown in Fig. 2-4, is designed to have a low profile in order to accommodate longer residual limbs. The sensor incorporates a full bridge of semiconductor strain gages which measure the strains generated by the sagittal plane moment. Finite element analysis, using ProEngineer Mechanica, was used to minimize the overall design height and to achieve the desired strains in the load cell. The sensor is fabricated from 7075 aluminum and has an assembled weight of 120 grams including the stainless steel pyramid connector. The overall height of the sensor including the pyramid connector is 32 mm, with a rectangular base of 78 mm by 44 mm. The device was calibrated for a measurement range of 100 Nm, and exhibited linearity within ± 5% error over the full scale output.

The custom foot, shown in Fig. 2-5, was designed to measure the ground reaction force components at the ball of the foot and heel. The foot is comprised of heel and toe beams, rigidly attached to a central fixture and arranged as cantilever beams with an arch that allows for the load to be localized at the heel and ball of the foot, respectively. Each heel and toe beam incorporates a full bridge of semiconductor strain gages that measure the strains resulting from the respective ground contact forces. The foot utilized for the tests described herein measures 220 mm long, 56 mm wide and is 35 mm tall to the top of the central fixture and approximates a US size 12 or EU size 46 foot. The foot is fabricated from 7075 aluminum and weighs 350 grams. The dimensions and weight are similar to commercial low-profile carbon-fiber prosthetic feet, such as the Otto Bock Lo-Rider. The prosthetic foot was designed to be housed in a soft prosthetic foot shell, as shown in Fig. 2-2. The heel and ball of foot load sensors were calibrated for a measurement range of 1000 N, and demonstrated linearity within ± 4% error for the full scale output range.

Embedded System

The powered prosthesis contains an embedded microcontroller that allows for either tethered or untethered operation. The embedded system consists of signal processing, power supply, power electronics, communications and computation modules, Fig. 2-6. The system is powered by a lithium polymer battery with 29.6 V nominal rating and 4000 mA-hr capacity. The signal electronics require ±12 V and +3.3 V, which are provided via linear regulators to maintain low noise levels. For efficiency, the battery voltage is

reduced by PWM switching amplifiers to ±15 V and +5 V prior to using the linear regulators. The power can be disconnected via a microcontroller that controls a solid state relay. The power status is indicated by LED status indicators controlled also by the microcontroller.

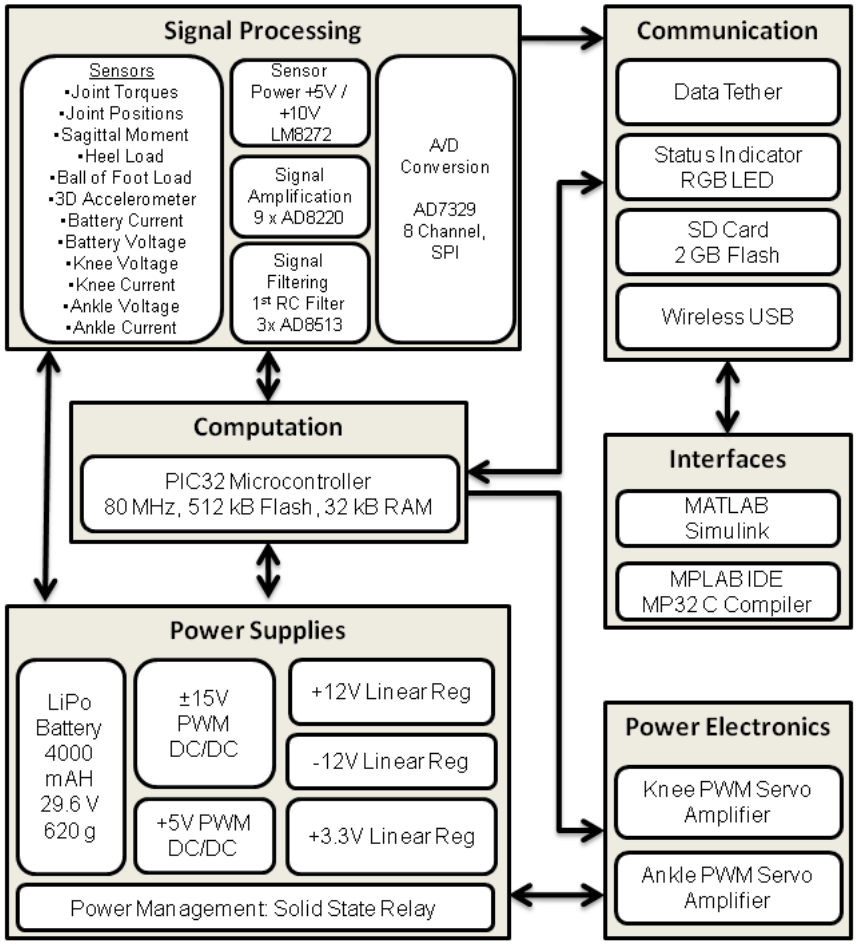

Figure 2-6. Embedded system framework.

The analog sensor signals acquired by the embedded system include the prosthesis sensors signals (five strain gage signals and two potentiometer signals), analog reference signals from the laptop computer used for tethered operation, and signals measured on the board including battery current and voltage, knee and ankle servo amplifier currents and a 3-axis accelerometer. The prosthesis sensor signals are conditioned using input instrumentation amplifiers (AD8220) over a range of +/-10 V. The battery, knee motor and

ankle motor currents are measured by current sensing across 0.02 Ohm resistors and via current sensing amplifiers (LT1787HV). The signals are filtered with a first-order RC filter with 1.6 kHz cut off frequency for the commercial load cells and joint angles and 160 Hz cutoff frequency for the sagittal moment, heel and ball of foot custom load cells and buffered with high slew rate amplifiers before the analog to digital conversion stage. Analog to digital conversion is accomplished by two 8-channel analog to digital convertors (AD7329). The analog to digital conversion data is transferred to the microcontroller via serial peripheral interface (SPI) bus.

The main computational element of the embedded system is an 80 MHz PIC32 microcontroller with 512 kB flash memory and 32 kB RAM, which consumes approximately 0.4 W of power. The microcontroller is programmed in C using MPLAB IDE and MP32 C Compiler. In addition to untethered operation, the prosthesis can also be controlled via a tether by a laptop computer running MATLAB Simulink RealTime Workshop. In the untethered operation state, the microcontroller performs the servo and activity controllers of the prosthesis and data logging at each sample time (1ms). In the tethered operation state, the microcontroller drives the servo amplifiers based on analog reference signals from the laptop computer. A 1 GB SD memory card is used for logging time-stamped data acquired from the sensors and recording internal controller information. The SD card is interfaced to the computer via wireless USB protocol. The microcontroller sends PWM reference signals to two four quadrant brushless DC motor drivers (Advanced Motion Control AZBDC20A8) rated at 12A continuous and 20A peak current output with regenerative capabilities in the second and forth quadrants of the velocity/torque curve.

The embedded system printed circuit board is a 130 mm x 90 mm 4-layer board designed for surface mount technology (SMT) components. To further reduce the footprint of the board, the removable servo amplifiers were raised to allow for the placement of components underneath, as shown in Fig. 3-7. The mass of the embedded system is 0.36 kg, which consists of the board and components (0.10 kg), servo amplifiers (0.19 kg) and protective cover (0.07 kg).

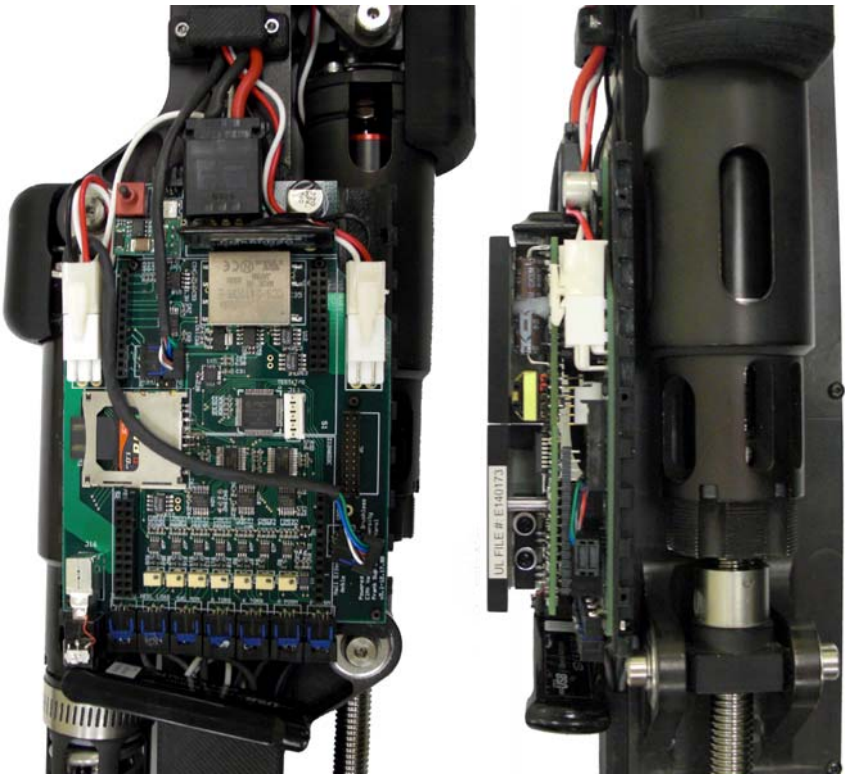

Figure 2-7. Embedded system hardware with (right) and without (left) servo amplifiers.

Control

The general control architecture of the prosthesis consists of three layers, as diagrammed in Fig. 3-8. The high-level supervisory controller, which is the intent recognizer, infers the user's intent based on the interaction between the user and the prosthesis, and switches the middle-layer controllers appropriately. Intent recognition is achieved by first generating a database containing sensor data from different activity modes and training a pattern recognizer that switches between activity modes in real time, as described in [34]. A middle-layer controller is developed for each activity mode, such as walking, standing, sitting, and stair ascent/descent. The middle-layer controllers generate torque references for the joints using a finite state machine that modulates the impedance of the joints depending on the phase of the gait. The low-level controllers are the closed-loop joint torque controllers, which compensate for the transmission dynamics of the ball screw (i.e., primarily friction and inertia), and thus enable tracking of the knee and ankle joint torque references (commanded by the middle-layer controllers) with a higher bandwidth and accuracy than is afforded with an open-loop torque control approach.

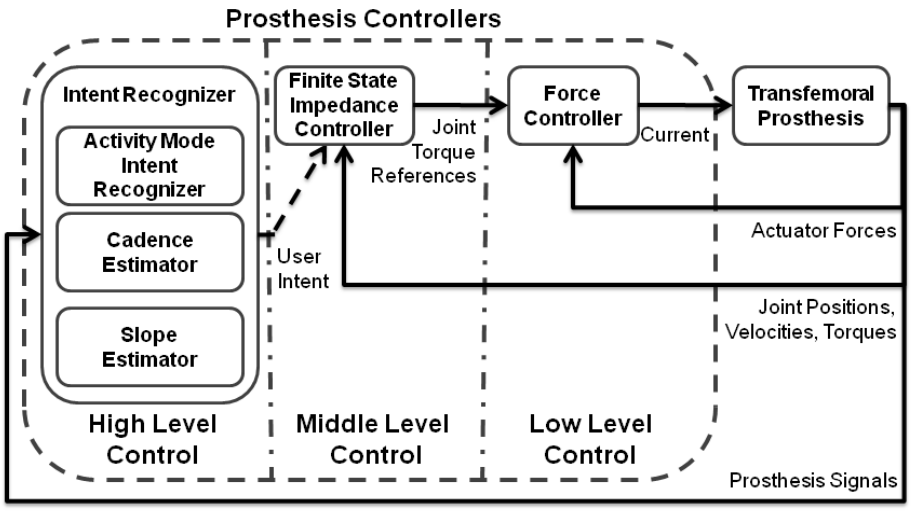

Figure 2-8. Complete control architecture showing high, middle and low levels.

The finite state impedance control developed by the authors utilizes an impedance-based approach to generate joint torques [26]. The joint torques for each activity mode, such as walking, standing, sitting, stair ascent/descent, are governed by separate finite state machines, which modulate the joint impedance according to the phase of gait. The finite state machines for walking and standing are diagrammed in Figs. 2-9 and 2-10, respectively. The state model for walking is described by five phases, three of which are stance phases (early stance, middle stance, and late stance) and two of which are swing phases (swing knee flexion and swing knee extension). The standing state model is described by two phases, which are a weight bearing phase and a non-weight bearing phase. Note that the distinction between torque commands and position commands is largely one of output impedance. That is, accurate tracking of position trajectories requires a high joint output impedance, which is not characteristic of human gait. By generating torques trajectories rather than position trajectories, the output impedance of each joint can be more closely matched to the native limb, thus enabling the user to interact with the prosthesis by leveraging its dynamics in a manner similar to normal gait. In other words, the resulting motion of each prosthesis joint is due to the combination of the user input and the prosthesis input, rather than resulting from the prosthesis input alone (as would be the case with a position-based controller). In each phase, the knee and ankle torques, τ_i, are each described by a passive spring and damper with a fixed equilibrium point, given by:

$$\tau_i = k_i(\theta - \theta_{ki}) + b_i\dot{\theta} \quad (1)$$

where k_i , b_i , and θ_{ki} denote the linear stiffness, damping coefficient, and equilibrium point, respectively, for the i^{th} state. Energy is delivered to the user by switching between appropriate equilibrium points (of the virtual springs) during transitions between phases. In this manner, the prosthesis is guaranteed to be passive within each phase, and thus generates power simply by switching between phases. Since the user initiates phase switching, the result is a predictable controller that, barring phase switching input from the user, will always default to passive behavior.

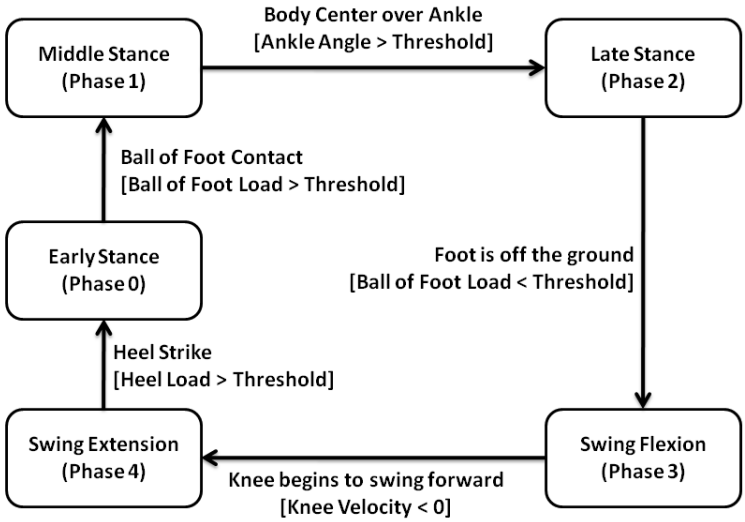

Figure 2-9. The finite state machine for level walking. Blocks represent states and arrows represent the corresponding transitions.

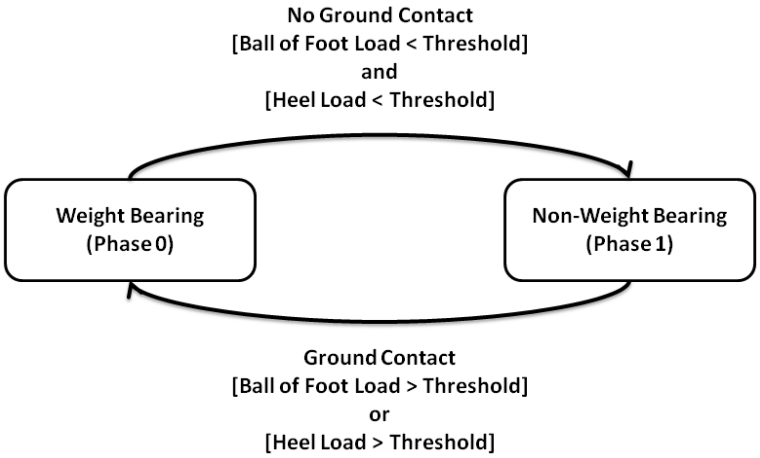

Figure 2-10. The finite state machine for level standing. Blocks represent states and arrows represent the corresponding transitions.

4. Experiments

The powered prosthesis was tested on a 20 year-old male (1.93 m, 75 kg) unilateral amputee three years post amputation. A photograph of the transfemoral amputee wearing the prosthesis is shown in Fig. 2-11. The length of the test subject's residual limb measured from the greater trochanter to the amputated site was 55% of the length of the non-impaired side measured from the greater trochanter to the lateral epicondyle. The subject uses an Ottobock C-leg with a Freedom Renegade prosthetic foot for daily use. For testing of the powered prosthesis prototype, the subject's daily-use socket was used, with the height and varus-valgus alignment of the prosthesis adjusted for the initial trial by a licensed prosthetist.

Figure 2-11. Unilateral transfemoral amputee test subject used for the powered prosthesis evaluation.

Parameter Tuning

Experiments were performed to characterize the knee and ankle joint angles, torques, and power while walking over ground at a self-selected walking speed, and also to characterize the system's electrical power consumption, mechanical power generation, and efficiency. In order to conduct the over-ground characterization, a series of experiments were required to parameterize the middle-layer controller to the subject at various walking cadences. The controller parameterization was conducted on a treadmill at three walking cadences. The nominal cadence used for parameter tuning was the subject's self-selected cadence while wearing his daily-use prosthesis. For over-ground walking, the subject walked comfortably with his daily use (passive) prosthesis at 90 steps per minute at 4.1 km/h. For treadmill walking, the speed indicator on the treadmill was covered and the subject adjusted the treadmill speed until he felt comfortable. The self-selected normal cadence of the subject was determined to be 75 steps per minute at 2.8 km/h. Fast and slow cadences were set at ±15 percent of the normal treadmill cadence resulting in treadmill speeds of 2.2 and 3.4 km/h, respectively. The middle layer control parameters of the powered prosthesis were then tuned (with the prosthesis controlled in the tethered state) while walking on the treadmill at slow, normal and fast walking cadences (as determined by the daily use prosthesis), and also for standing. During the standing mode, the test subject alternately shifted his weight between limbs, turned in place, and stood still. Note that in all cases, the parameters were tuned using a combination of feedback from the user, and from visual inspection of the joint angle, torque, and power data. Note also that the tethered operating mode was utilized during treadmill parameter tuning because it enables quick and easy parameter variation and data visualization, and thus greatly expedites the iterative parameter tuning process. The resulting middle-layer controller parameters of the tuned impedance functions for standing and for the various walking cadences are listed in Tables 2-3 and 2-4.

Table 2-3. Impedance parameters for treadmill walking from experimental tuning.

		Knee Impedance			Ankle Impedance		
Phase	Speed km h^{-1}	k Nm deg^{-1}	b N s m^{-1}	θ_k deg	k Nm deg^{-1}	b N s m^{-1}	θ_k deg
0	2.2	2.5	0.05	8	3.0	0.04	-1
	2.8	2.5	0.05	10	3.0	0.04	-1
	3.4	2.5	0.05	10	3.0	0.04	-1
1	2.2	4.0	0.06	6	5.0	0.04	0
	2.8	5.0	0.06	6	5.0	0.04	0
	3.4	5.0	0.06	6	5.0	0.04	0
2	2.2	3.0	0.02	14	4.0	0.01	-16
	2.8	3.5	0.02	14	5.0	0.01	-16
	3.4	5.0	0.02	14	5.0	0.01	-16
3	2.2	0.15	0.02	65	0.4	0.05	0
	2.8	0.10	0.02	65	0.4	0.05	0
	3.4	0.10	0.01	65	0.4	0.05	0
4	2.2	0.10	0.03	40	0.7	0.03	0
	2.8	0.20	0.03	40	0.7	0.03	0
	3.4	0.25	0.03	40	0.7	0.03	0

Highlighted parameters vary with walking speed.

Table 2-4. Impedance parameters for standing from experimental tuning.

	Knee Impedance			Ankle Impedance		
Phase	k Nm deg-1	b N s m-1	θk deg	k Nm deg-1	b N s m-1	θk deg
0	2.5	0.02	0	4.0	0.05	-6
1	0	0.02	0	2.0	0.05	-6

The measured joint angles from the prosthesis' on-board sensors during level treadmill walking at cadences of 64, 75 and 87 steps per minute are shown in Fig. 2-12. In comparing the knee and ankle angles to prototypical data from normal subject, Fig. 2-1, one can observe that the powered prosthesis and controller provide knee and ankle joint angle profiles quite similar to those observed during normal gait. The ability of the device to provide stance flexion provides cushioning at heel strike and reduces the rise of the body's center of mass to allow for more efficient gait [35].

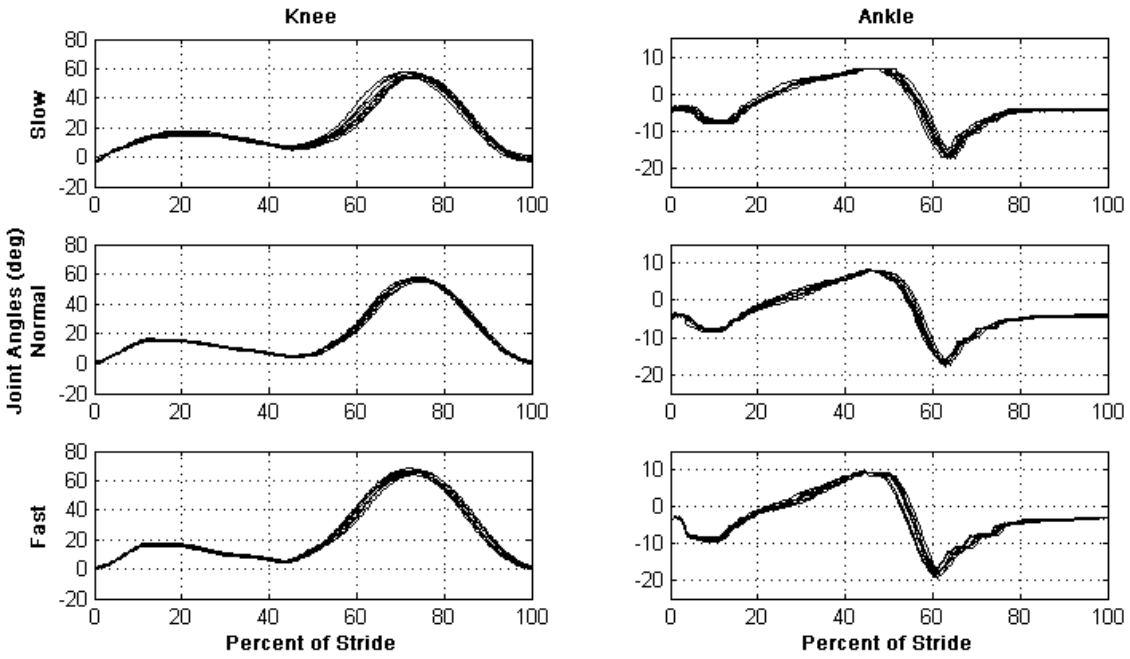

Figure 2-12. Measured joint angles of the powered prosthesis for ten consecutive gait cycles of treadmill walking at slow, normal and fast cadences, 64, 75, and 86 steps per minute, respectively.

Over-ground Walking

Once the middle-layer controllers were fully parameterized for standing and slow, medium (i.e., self-selected), and fast cadences, the prosthesis was switched to the untethered operating mode, so that the subject could walk over-ground with the fully self-contained prosthesis (i.e., without a tether hindering movement). The subject walked on a straight, 50 m track (actually a hallway) at a self-selected cadence. The best walking performance was achieved using the fast (87 steps per minute) impedance controller. As has been documented by others (e.g., see [36]), the mechanics of treadmill walking are not entirely consistent with the dynamics of over-ground walking, and as such the self-selected speeds over-ground are typically significantly faster than self-selected speeds on a treadmill. Consistent with this phenomenon, the subject's self-selected speed during the over-ground walking tests was 87 steps per minute, which corresponded to a walking speed of 5.1 km/h, both of which are significantly greater than the self-selected treadmill walking (which were 75 steps per minute and 2.8 km/h, respectively). Furthermore, the subject's

over-ground self-selected speed increased 24 percent from 4.1 km/h to 5.1 km/h while using the powered prosthesis. The subject walked on the 50 m track at a self-selected speed for a total of 10 trials while prosthesis data (i.e., servo amplifier currents, battery current and voltage, joint positions, velocities and torques, socket sagittal plane moment, heel and ball of foot loads, three dimensional shank accelerations, and controller state information) were collected at a 200 Hz sampling rate.

Measured joint angles, torques and powers from walking on level ground at the self-selected cadence for ten consecutive strides are shown in Fig. 2-13. As indicated by the data, the powered prosthesis provides knee torques over 40 Nm (during stance flexion) and ankle torques approaching 120 Nm during toe-off. As shown in the power data, the prosthesis is contributing significant positive power (during stance) at both the knee joint (peak powers of 50 W) and ankle joint (peak powers approaching 250 W). For each stride, the prosthesis delivers 13.8 J of net energy on average at the ankle. Finally, the torque tracking for the knee and ankle joints, shown in Fig. 2-14, indicates good torque tracking, and further indicates that the torque and power capabilities of the self-powered prosthesis are well-suited to the demands of the controller.

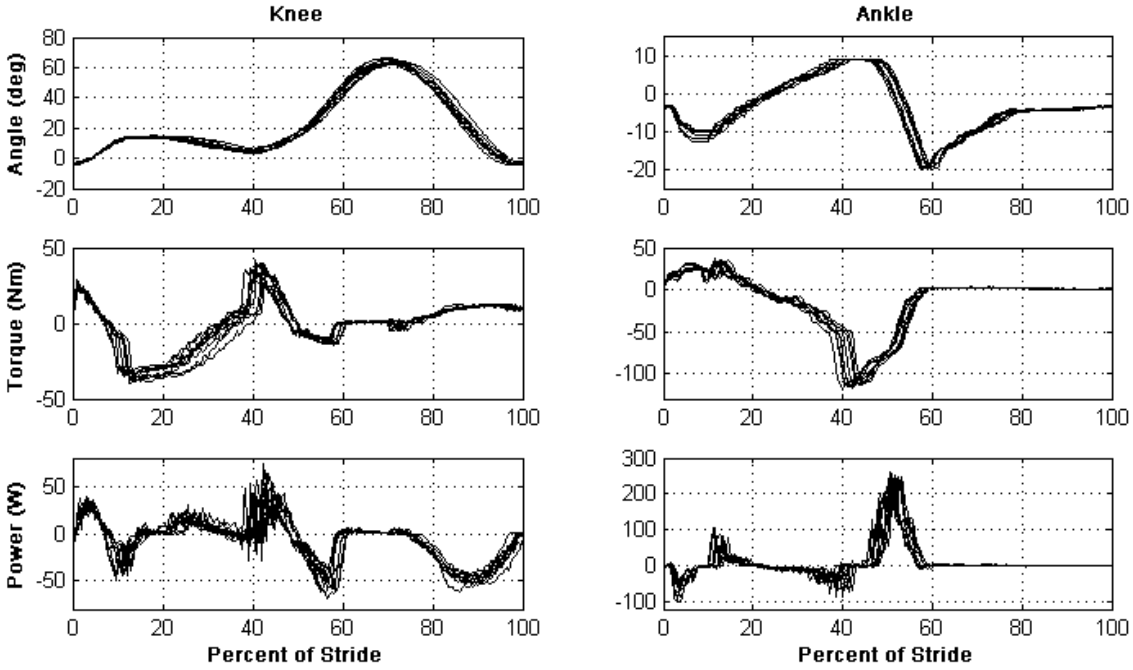

Fig. 2-13. Measured joint angles, torques and powers of the powered prosthesis for ten consecutive gait cycles at self-selected speed (5.1 km/h at 87 steps per minute).

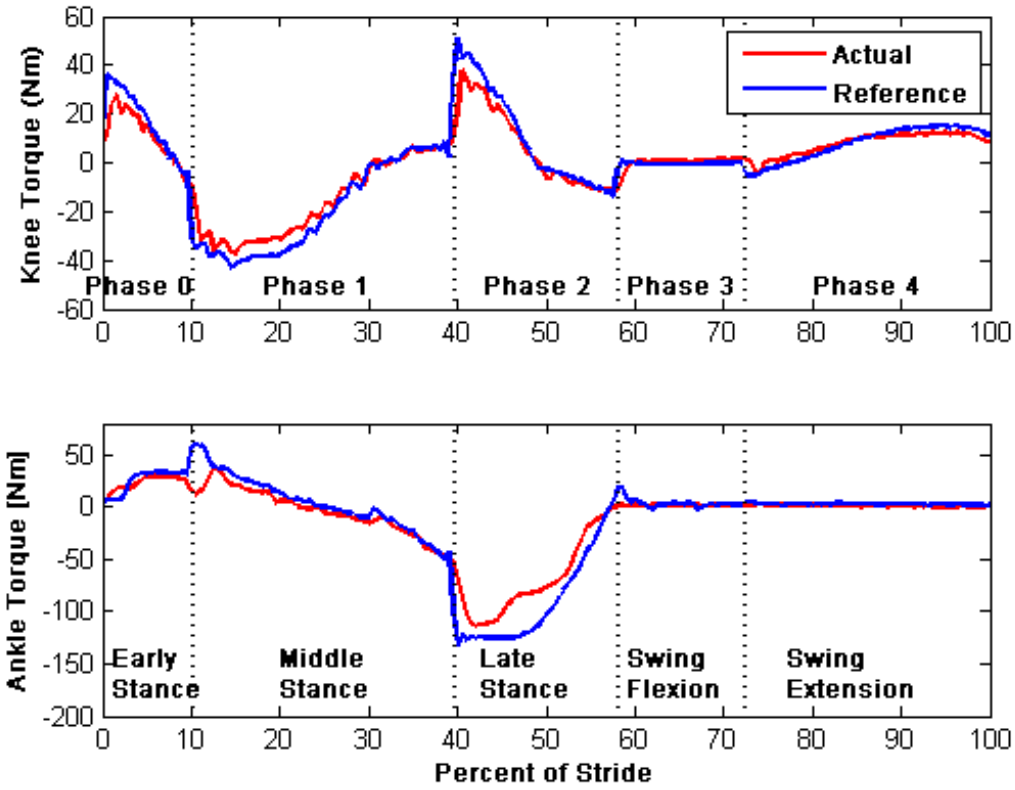

Figure 2-14. References and actual knee and ankle joint torques of the powered prosthesis for one stride at self-selected speed (5.1 km/hr at 87 steps per minute) on normal ground.

Power Consumption and Battery Life

One of the primary constraints of the electrically powered knee and ankle prosthesis design is the power source. As such, the electrical power consumption was measured to characterize the potential battery life and range of the device. The electrical power consumed (at the motor leads) and the mechanical power generated over one gait cycle are shown in Fig. 2-15. Electrical power regeneration (afforded by the regenerative servo amplifiers) is observed in the late swing gait phase in the knee. It is interesting to note that the peak electrical power event for level walking at the knee joint occurs at heel strike. At the ankle joint, a peak mechanical power output of over 200W is experienced at toe-off, which requires approximately 50 percent more electrical power at the motor leads.

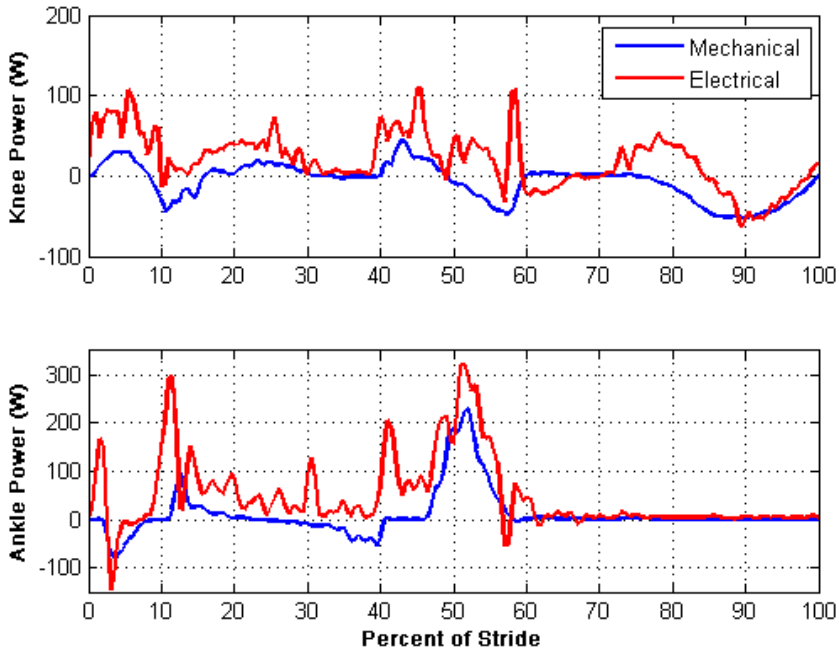

Figure 2-15. Measured electrical and mechanical power at the knee and ankle joints of the powered prosthesis over one gait cycle at self-selected speed (5.1 km/hr at 87 steps per minute) on normal ground.

In order to characterize battery requirements, the average electrical power required by prosthesis (i.e., the embedded system, knee joint, and ankle joint) during standing and walking over level ground (at the self-selected speed of 5.1 km/h) is shown in Fig. 2-16. The total average power consumption for level ground walking and standing is 66 W and 10 W, respectively. Since the prosthesis incorporates a (rechargeable) 118 Watt-hr lithium polymer battery, such electrical power requirements suggest a battery life between charges of approximately 1.8 hours of walking or 12 hours of standing. With these figures, the prosthesis is capable of over 4,500 strides (9,000 steps by the user) with the prosthesis at the self-selected cadence. Given the walking speed of 5.1 km/h, the measured power requirements indicate a walking distance (for the amputee subject) of 9.0 km. Note that if the energy density of lithium ion battery technology doubles over the next five years (as is projected [31]), the walking range between battery charges would similarly double approaching 20 km.

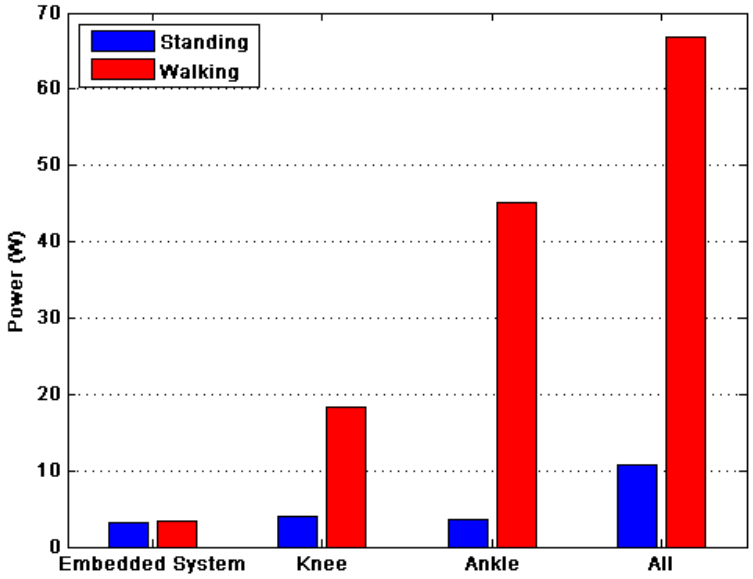

Figure 2-16. Average electrical power consumption of the powered prosthesis for standing and walking at self-selected speed (5.1 km/hr at 87 steps per minute) on normal ground.

5. Conclusion

The paper describes the design and control of a fully self-contained electrically powered knee and ankle prosthesis capable of producing human-scale power. Experimental results with a unilateral amputee indicate that the device can provide transfemoral amputee biomechanics during walking similar to those typically observed during healthy biomechanics. Power consumption measurements on level ground indicate that device consumes 66 W at a walking speed of 5.1 km/h on a 75 kg subject. As such, given the specifications of the on-board battery pack, the prosthesis can provide 9.0 km of level, over-ground walking between recharges. Future works include addressing the audible noise of the device and a comprehensive biomechanical evaluation of the powered prosthesis on multiple amputee subjects.

6. References

[1] P. F. Adams, G. E. Hendershot, and M. A. Marano, "Current estimates from the National Health Interview Survey, 1996," National Center for Health Statistics. Vital Health Stat 10(200), 1999.

[2] J. Feinglass, J. L. Brown, A. LaSasso, M. W. Sohn, L. M. Manheim, S. J. Shah, and W. H. Pearce,

"Rates of lower-extremity amputation and arterial reconstruction in the United States, 1979 to 1996," American J. of Public Health, vol. 89, no. 8, pp. 1222-1227, Aug, 1999.

[3] P. DeVita, M. Torry, K. L. Glover, and D. L. Speroni, "A functional knee brace alters joint torque and power patterns during walking and running," J. of Biomechanics, vol. 29, no. 5, pp. 583-588, May, 1996.

[4] R. Jacobs, M. F. Bobbert, and G. J. van Ingen Schenau, "Mechanical output from individual muscles during explosive leg extensions: The role of biarticular muscles," J. of Biomechanics, vol. 29, no. 4, pp. 513-523, Apr, 1996.

[5] S. Nadeau, B. J. McFadyen, and F. Malouin, "Frontal and sagittal plane analyses of the stair climbing task in healthy adults aged over 40 years: what are the challenges compared to level walking?," Clinical Biomechanics, vol. 18, no. 10, pp. 950-959, Dec, 2003.

[6] A. Nagano, Y. Ishige, and S. Fukashiro, "Comparison of new approaches to estimate mechanical output of individual joints in vertical jumps," J. of Biomechanics, vol. 31, no. 10, pp. 951-955, Oct, 1998.

[7] B. I. Prilutsky, L. N. Petrova, and L. M. Raitsin, "Comparison of mechanical energy expenditure of joint moments and muscle forces during human locomotion," J. of Biomechanics, vol. 29, no. 4, pp. 405-415, Apr, 1996.

[8] R. Riener, M. Rabuffetti, and C. Frigo, "Joint powers in stair climbing at different slopes," Proc. of the First Joint BMES/EMBS Conf., vol. 1, pp. 530 vol.1, 1999.

[9] D. Winter, The Biomechanics and Motor Control of Human Gait: Normal, Elderly and Pathological, 2nd ed.: University of Waterloo Press, 1991.

[10] D. A. Winter, and S. E. Sienko, "Biomechanics of below-knee amputee gait," J. of Biomechanics, vol. 21, no. 5, pp. 361-367, 1988.

[11] R. L. Waters, J. Perry, D. Antonelli, and H. Hislop, "Energy cost of walking of amputees - Influence of level of amputation," J. of Bone and Joint Surgery-American Vol., vol. 58, no. 1, pp. 42-46, 1976.

[12] M. Donath, "Proportional EMG control for above knee prostheses," Massachusetts Institute of Tech.

Dept. of Mechanical Eng. Thesis. M.S., 1974.

[13] W. C. Flowers, "A man-interactive simulator system for above-knee prosthetics studies," Massachusetts Institute of Tech. Dept. of Mechanical Eng. Thesis. Ph.D., 1973.

[14] W. C. Flowers, and R. W. Mann, "Electrohydraulic knee-torque controller for a prosthesis simulator," ASME J. of Biomechanical Engineering, vol. 99, no. 4, pp. 3-8, 1977.

[15] D. L. Grimes, "An active multi-mode above knee prosthesis controller," Massachusetts Institute of Tech. Dept. of Mechanical Eng. Thesis Ph.D., 1979.

[16] D. L. Grimes, W. C. Flowers, and M. Donath, "Feasibility of an active control scheme for above knee prostheses," ASME J. of Biomechanical Engineering, vol. 99, no. 4, pp. 215-221, 1977.

[17] J. L. Stein, and W. C. Flowers, "Stance phase-control of above-knee prostheses - Knee control versus SACH foot design," J. of Biomechanics, vol. 20, no. 1, pp. 19-28, 1987.

[18] J. L. Stein, and Massachusetts Institute of Technology. Dept. of Mechanical Engineering., "Design issues in the stance phase control of above-knee prostheses," Massachusetts Institute of Tech. Dept. of Mechanical Eng. Thesis Ph.D., 1983.

[19] D. Popovic, and L. Schwirtlich, "Belgrade active A/K prosthesis," in de Vries, J. (Ed.), Electrophysiological Kinesiology, Intern. Congress Ser. No. 804, Excerpta Medica, Amsterdam, The Netherlands, pp. 337-343, 1988.

[20] S. Bedard, and P. Roy, Actuated leg prosthesis for above-knee amputees, 7,314,490, U. S. Patent, June 17, 2003.

[21] E. Martinez- Villalpando, J. Weber, G. Elliott, and H. Herr, "Design of an agonist-antagonist active knee prosthesis," Proc. IEEE/RAS-EMBS Int. Conf. on Biomedical Robotics and Biomechatronics, pp. 529-534, 2008.

[22] G. K. Klute, J. Czerniecki, and B. Hannaford, "Muscle-like pneumatic actuators for below-knee prostheses," Proc. 7th Int. Conf. on New Actuators, pp. 289-292, 2000.

[23] W. Koniuk, Self-adusting prosthetic ankle apparatus, 6,443,993, U. S. Patent, March, 23, 2001.

[24] R. Bellman, A. Holgate, and T. Sugar, "SPARKy 3: Design of an active robotic ankle prosthesis with two actuated degrees of freedom using regenerative kinetics," Proc. IEEE/RAS-EMBS Int.

Conf. on Biomedical Robotics and Biomechatronics, pp. 511-516, 2008.

[25] S. Au, and H. Herr, "Powered ankle-foot prosthesis," IEEE Robotics & Automation Magazine, vol. 15, pp. 52-59, 2008.

[26] F. Sup, A. Bohara, and M. Goldfarb, "Design and control of a powered transfemoral prosthesis," Int. J. of Robotics Research, vol. 27, no. 2, pp. 263-273, Feb, 2008.

[27] K. B. Fite, and M. Goldfarb, "Design and energetic characterization of a proportional-injector monopropellant-powered actuator," IEEE/ASME Trans. on Mechatronics, vol. 11, no. 2, pp. 196-204, Apr, 2006.

[28] K. B. Fite, J. E. Mitchell, E. J. Barth, and M. Goldfarb, "A unified force controller for a proportional-injector direct-injection monopropellant-powered actuator," J. of Dynamic Systems Measurement and Control Trans. of ASME, vol. 128, no. 1, pp. 159-164, Mar, 2006.

[29] M. Goldfarb, E. J. Barth, M. A. Gogola, and J. A. Wehrmeyer, "Design and energetic characterization of a liquid-propellant-powered actuator for self-powered robots," IEEE/ASME Trans. on Mechatronics, vol. 8, no. 2, pp. 254-262, 2003.

[30] B. L. Shields, K. B. Fite, and M. Goldfarb, "Design, control, and energetic characterization of a solenoid-injected monopropellant-powered actuator," IEEE/ASME Trans. on Mechatronics, vol. 11, no. 4, pp. 477-487, Aug, 2006.

[31] "In search of the perfect battery," Economist, vol. 386, no. 8570, pp. 22-24, 2008.

[32] F. Sup, H. A. Varol, J. Mitchell, T. Withrow, and M. Goldfarb, "Design and control of an active electrical knee and ankle prosthesis," Proc. IEEE/RAS-EMBS Int. Conf. on Biomedical Robotics and Biomechatronics, pp. 523-528, 2008.

[33] C. E. Clauser, J. T. McConville, and J. M. Young, "Weight, volume and center of mass of segments of the human body," AMRL-TR-69-70, Wright Patterson Airforce Base, Dayton, Ohio, 1969.

[34] H. A. Varol, F. Sup, and M. Goldfarb, "Real-time gait mode intent recognition of a powered knee and ankle prosthesis for standing and walking," Proc. IEEE/RAS-EMBS Int. Conf. on Biomedical Robotics and Biomechatronics, pp. 66-72, 2008.

[35] S. Blumentritt, H. Scherer, U. Wellershaus, and J. Michael, "Design principles, biomechanical data

and clinical experience with a polycentric knee offering controlled stance phase knee flexion: A preliminary report," J. of Prosthetics and Orthotics, vol. 9, no. 1, pp. 18-24, 1997.

[36] M. Traballesi, P. Porcacchia, T. Averna, and S. Brunelli, "Energy cost of walking measurements in subjects with lower limb amputations: A comparison study between floor and treadmill test," Gait & Posture, vol. 27, no. 1, pp. 70-75, Jan, 2008.

CHAPTER III

Manuscript II: Multiclass Real-Time Intent Recognition for a Powered Transfemoral Prosthesis

Huseyin Atakan Varol, Frank Sup and Michael Goldfarb

Vanderbilt University

Nashville, TN

Submitted as a Regular Paper to the

IEEE Transactions on Biomedical Engineering

1. Abstract

This paper describes a control architecture and intent recognition approach for the real-time supervisory control of a powered lower limb prosthesis. The proposed approach infers user intent to stand, sit, or walk, by recognizing patterns in prosthesis sensor data in real-time, without the need for instrumentation of the sound-side leg. Specifically, the intent recognizer utilizes time-based features extracted from frames of prosthesis signals, which are subsequently reduced to a lower dimensionality (for computational efficiency). These data are initially used to train intent models, which classify the patterns as standing, sitting, or walking. The trained models are subsequently used to infer the user's intent in real-time. In addition to describing the generalized control approach, this paper describes the implementation of this approach on a single unilateral transfemoral amputee subject, and demonstrates via experiments the effectiveness of the approach.

2. Introduction

The knee and ankle joints of healthy individuals generate significant net power over a gait cycle during normal walking and during many other locomotive functions, including walking up stairs and slopes [1-8]. Widely available commercial transfemoral prostheses can store and/or dissipate energy, but cannot generate net power over a gait cycle. In the absence of net power, transfemoral amputees during level walking can expend up to 60% more metabolic energy relative to healthy subjects [9] and exert as much as three times the affected-side hip power and torque [7]. Presumably, a prosthesis with power generation capabilities comparable to the native limb could alleviate the need for increased exertion by the amputee during gait.

One of the primary challenges entailed in developing a powered lower limb prosthesis is the means by which the user can control the prosthesis. A powered prosthesis is fundamentally different from a passive one in that the latter can only react, while the former can both act and react. In order to effectively implement a powered prosthesis, a control interface must be developed that enables the user to control and communicate intent to the prosthesis in a real-time manner. Cleary, such a communication and control structure must be safe and reliable, and should not require cognition on the part of the user. This paper

describes a control and communication structure developed by the authors for the control of powered lower limb prostheses, with the emphasis of the paper on the method developed for intent recognition.

Though no prior work exists on the development and control of a powered knee and ankle prosthesis, some prior work exists on the development and control of powered knee prostheses, and separately on powered ankle prostheses. Regarding the former, [10] describes the development of an electro-hydraulically powered knee prosthesis, developed as a laboratory test bed for studying the control of powered knee joints during walking. This prosthesis was utilized to develop an echo control approach, in which the authors instrumented the sound-side knee (of a unilateral amputee) with a position sensor, and used a modified version of the measured knee angle profile on the powered prosthesis side one half cycle later, which they term "modified echo control" [11, 12]. Ossur, a prosthetics company, recently introduced a self-contained (battery-powered) powered knee prosthesis, in which they similarly instrument the sound side leg (with accelerometers) and also utilize an echo type approach [13]. Other researchers describe the development of powered prosthesis prototypes, but do not describe a user control and communication interface structure [14, 15]. Recently, an electromyography based pattern recognizer for classifying locomotion modes using artificial neural networks and linear discriminant analysis is proposed in [16]. Regarding the echo control approaches incorporated in [10-12, 17], an obvious drawback is that the sound-side (or unaffected) leg must be instrumented, which requires the user to don and doff additional instrumentation. The echo control approach presumably also restricts the use of the prosthesis to unilateral amputees and also presents a problem for "odd" numbers of steps, in which an echoed step is undesirable. A more subtle, although perhaps more significant shortcoming of the echo-type approach is that suitable motion tracking requires a high output impedance of the prosthesis, which forces the amputee to react to the limb rather than interact with it. Specifically, in order for the prosthesis to dictate the joint trajectory, it must assume a high output impedance (i.e., must be stiff), thus precluding any dynamic interaction with the user and the environment, which is contrary to the way in which humans interact with their native limbs.

Regarding powered ankle prostheses, a tibia based controller is implemented in [18], in which the ankle angle is adjusted as a function of the tibia angle. In [19], the authors use finite state controllers in combination with torque, impedance and position controllers for the control of a powered ankle prosthesis

with a series elastic actuator. They also describe a neural network based high level controller which processes electromyogram (EMG) signals to manage transitions of the finite state controllers for level ground and stair descent. Note that Ossur markets an ankle prosthesis (Proprio Foot [20]) which quasistatically adjusts the ankle angle for sitting and slope walking, but does not contribute net power to gait.

This paper describes a method for the implicit communication with a powered lower limb prosthesis which is an alternative to an echo control approach. The proposed approach infers user intent via pattern recognition based on measured data from sensors on the prosthesis, which provides several advantages relative to an echo approach. First, no additional instrumentation or wiring apart from the prosthesis need be worn by the user. Second, the information flow is much less delayed as compared to the half cycle in the echo control approach. Third, the prosthesis is decoupled from the unaffected side, and thus the user is not constrained to "even" patterns of gait. Lastly, the proposed approach can be utilized on both unilateral and bilateral amputees.

The authors have recently reported on the development of a powered knee and ankle prosthesis which employs a finite-state based impedance control approach for control of walking [21]. This walking control structure is incorporated as a "middle level" controller in this paper, although in this paper, the middle level walking controller is supplemented with standing and sitting controllers. The coordination between the walking, standing and sitting middle level controllers is supervised by a "high level" controller which infers the user's intent in real-time based on patterns in the prosthesis sensor data. The combined high and middle level controllers, together with a low level controller that enforces joint torques, constitute the full user control and communication interface structure through which a user can implicitly communicate with a powered lower limb prosthesis. The paper describes the structure of the supervisory controller and presents experimental results on a single amputee subject which demonstrate the effectiveness of this interface and control approach.

3. Control Structure

Architecture

The proposed control architecture for the powered lower limb prosthesis is a three level hierarchy, as diagrammed in Fig. 3-1. At the lowest level, closed-loop joint torque controllers compensate for the transmission dynamics (i.e., primarily friction and inertia), so that joint torque references (commanded by the middle level controllers) will be tracked with a higher bandwidth and accuracy than would be the case with an open-loop torque control approach. The middle level controllers, which control a given activity mode (such as walking, standing, and sitting), generate torque references for the joints using a finite state machine that modulates the impedance of the joints depending on the phase of the activity, as described in [21]. The high level controller, which is the intent recognizer, consists of three parts: the activity mode intent recognizer, the cadence estimator, and the slope estimator. The latter two estimate the slope and cadence during walking to adjust the parameters of the walking mode controller. The activity mode intent recognizer distinguishes between different activity modes such as standing, sitting, stair climbing and walking, and switches to the appropriate middle level controller. This work focuses on the activity mode controller (since the middle level control was presented in [21]), and specifically describes an activity mode intent recognition framework that uses Gaussian Mixture Models for the supervisory control of the prosthesis for activity modes of standing, sitting and walking.

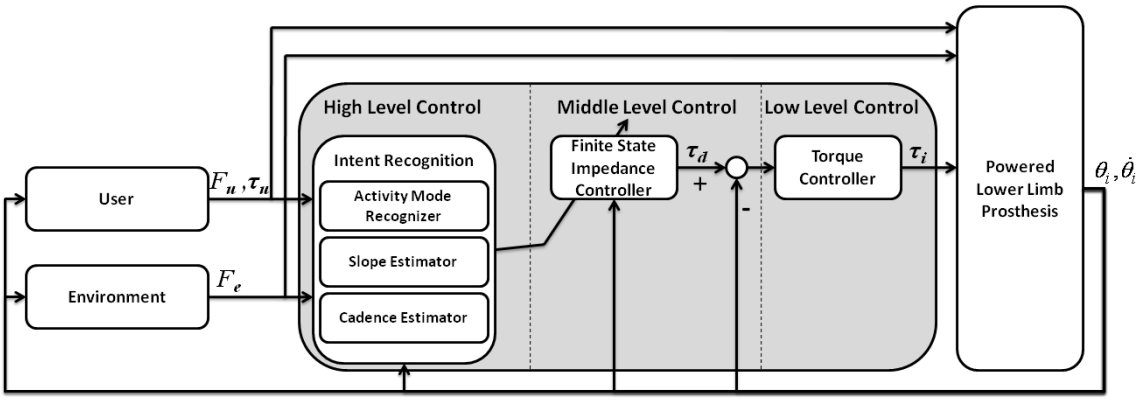

Figure 3-1. Powered prosthesis control architecture.

Finite State Based Impedance Control

In the (middle level) finite state impedance based control, the impedance behavior of healthy biomechanical gait is emulated by modulating joint impedances of the prosthesis according to the phase of gait. In each phase, the knee and ankle torques, τ_i, are each described by a passive spring and damper with a fixed equilibrium point, given by:

$$\tau_i = k_i(\theta - \theta_{ki}) + b_i\dot{\theta} \quad (1)$$

where k_i, b_i, and θ_{ki} denote the linear stiffness, damping coefficient, and equilibrium point, respectively, for the i^{th} state (or phase). Switching joint impedances between the gait phases is initiated by biomechanical cues. For instance, switching from swing extension to the early stance state during walking occurs with the detection of heel strike. With this structure, the prosthesis is guaranteed to be passive within each gait phase, and will deliver power to the user only by switching between the phases. Such switching is a direct result of natural biomechanical cues initiated by the user. As such, the user directly and naturally controls the delivery of power from the prosthesis. The development and implementation of this control framework for level walking is presented in [21]. For the work presented herein, standing and sitting controllers were added to the walking controller (as shown in Fig. 3-2), and all were supervised by the intent recognizer subsequently described.

The walking controller executes in a cyclical fashion over five phases. Early stance, Phase 0, is the shock absorption phase and initiated by heel strike. The leg switches to middle stance mode, Phase 1, when the ball of the foot load exceeds a predefined threshold. Middle stance is followed by late stance, when the body center of mass passes the ankle joint indicated by the angle of ankle joint. Ankle push-off defines late stance and is concluded when the foot leaves the ground. Swing phases (Phases 3 and 4) are defined by the knee flexion and extension phases of swing, respectively.

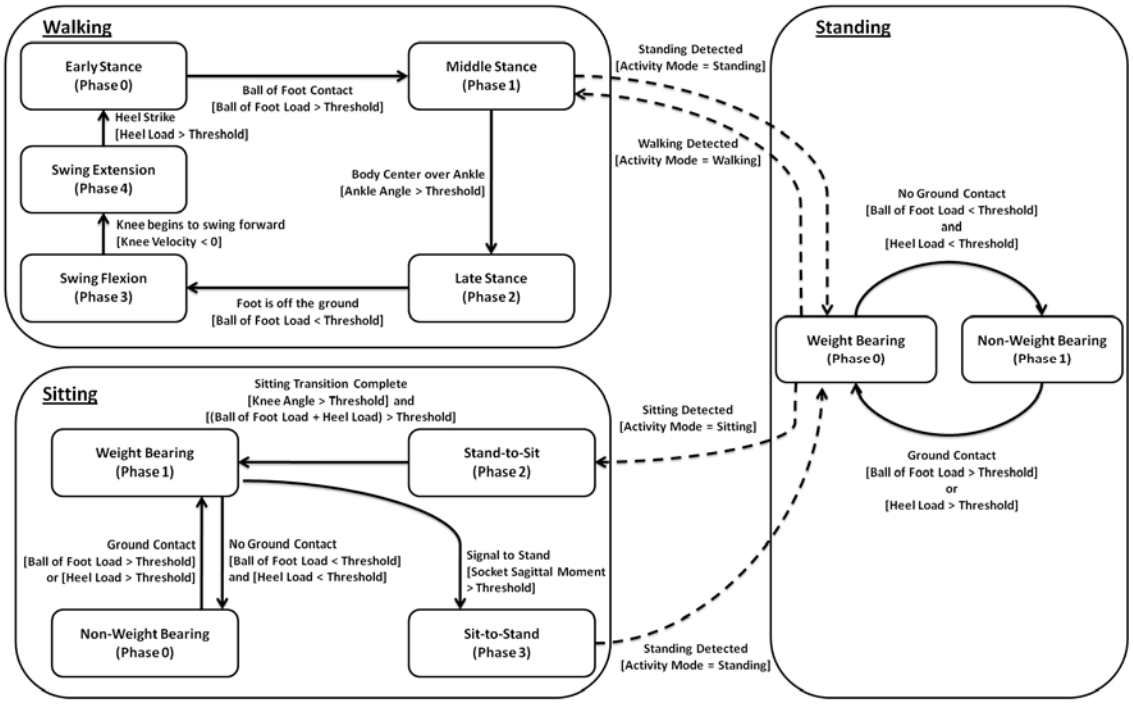

Figure 3-2. The state chart depicting the phase transitions for standing, walking and sitting modes.

The standing impedance controller consists of two phases: weight bearing and non-weight bearing. In the weight bearing phase, the weight of the user is supported with a high impedance at the joints. In the non-weight bearing mode, the knee acts as a soft dashpot to enable freedom of movement and a smooth transition to walking. While using the standing controller, the user can shift his or her weight between the sound side and the prosthesis, balance and shuffle.

The sitting mode controller consists of four phases. Two are true sitting phases, weight bearing and non-weight bearing. The other two encompass the transition phases, sit-to-stand and stand-to-sit, for standing up and sitting down, respectively. The weight bearing and non-weight bearing phases switch the knee and ankle joints between high and low impedances, respectively. The transition phases modulate the stiffness of the knee as a function of knee angle to assist the user in standing up or sitting down. The modulation allows for smoother transitions near the seated position. The ankle joint is slightly dorsiflexed with moderate stiffness during the standing up and sitting down phases. The parameters of the impedance based controllers are tuned using a combination of feedback from the user and joint angle, torque and power

data from the prosthesis.

Intent Recognition

Intent recognition is accomplished by a pattern recognizer that compares the state of the prosthesis to probabilistic models of activity. These models are "trained" with an appropriate database, after which they are utilized for real-time intent recognition. In order to train and use such models, one must first determine the appropriate input. Specifically, an appropriate set of sensors must be selected, an appropriate frame length for that data, and an appropriate set of features to extract from each window. Further, for purposes of real-time implementation, an appropriate reduction in data dimension is typically desirable. Once an appropriate input is selected, models are formulated based on a set of training data. After a probabilistic model for each activity mode (e.g., walking, standing, sitting) is established, the models are used in real-time to determine which activity is most probable at a given instant in time. In order to increase the likelihood of correct mode determination in the real-time implementation, the result is essentially low-pass filtered with a majority voting scheme. The specific procedure is described below, after which it is illustrated on a transfemoral amputee subject.

Sensor Data

The sensor data streams utilized for the intent recognizer should reflect the state of the prosthesis and the user-prosthesis interaction. Appropriate sensor information includes joint angles and angular velocities of the prosthesis joints (i.e., knee and/or ankle joints), in addition to measured interaction forces and/or torques between the user and prosthesis, and between the prosthesis and environment. Additional potentially useful sensor data includes accelerations and electromyography measurements from the residual limb.

Feature Extraction

In this work, features are extracted from frames of data, since a relatively long frame can be condensed into few information rich features. The real-time nature of the intent recognition problem requires that the features extracted from the prosthesis signals be computationally inexpensive, and as such the mean and standard deviation of each frame are used. Thus, for each sensor, two features are extracted, both of which

are normalized to eliminate the scaling and dimensional disparities between the various types of sensor information.

Dimension Reduction

In order to decrease the time required to train the models, to prevent over-fitting, and to facilitate real-time implementation, the feature space should be reduced (at the cost of information content). Though multiple possibilities exist for such dimensional reduction, two effective approaches include Principal Component Analysis (PCA) [22] and Linear Discriminant Analysis (LDA) [23]. Both approaches employ linear transformations, which facilitate computational efficiency due to matrix multiplication operations. In this work, both approaches are considered.

Gaussian Mixture Model Activity Mode Classification

In this work, Gaussian Mixture Models (GMM) are used to characterize the probability that the user and prosthesis is engaged in a given activity mode. Specifically, a separate GMM is used to described each activity mode, w_i. For some set of inputs $\vec{x}$, the probability of being in an activity mode, w_i, is given by:

$$p(\vec{x} \mid w_i) = \sum_{k=1}^{K} \lambda_k^i \, p_k^i(\vec{x}) \tag{1}$$

where

$$p_k^i(\vec{x}) = \frac{1}{\sqrt{(2\pi)^D \left|\sum_k^i\right|}} \exp\left\{-\frac{1}{2}(\vec{x} - \vec{\mu}_k^i)'(\sum_k^i)^{-1}(\vec{x} - \vec{\mu}_k^i)\right\} \tag{2}$$

where K is the number of components of the mixture model, λ_k^i is the mixture parameter of the i^{th} GMM for the k^{th} component, which satisfy the constraints $\sum_{k=1}^{K} \lambda_k^i = 1$ and $\lambda_k^i \geq 0$. The mixture component, $p_k^i(\vec{x})$, is a multivariate Gaussian probability density function with a $D \times 1$ mean vector, $\vec{\mu}_k^i$, and $D \times D$ full covariance matrix, $\sum_k^i$, with $D(D+1)/2$ free parameters. Each GMM can be parameterized by $K(1 + D + D(D+1)/2) - 1$ parameters, which are the mixture parameters, mean vectors and covariance matrices, notated as $w_i = \{\lambda_k^i, \vec{\mu}_k^i, \sum_k^i\}$. Once the GMM's are parameterized, for a given sample feature vector, $\vec{x}_S$, the activity mode, w_m, is selected as the mode with the highest probability:

$$w_m = \arg\max_{w_i}(p(\vec{x}_S \mid w_i)) \quad (3)$$

Parameterization of the GMM's for all desired activity modes is achieved based on training data in an iterative fashion with the Expectation Maximization (EM) algorithm [24]. Several initialization schemes for EM are suggested in [25]. In this work, the reduced dataset for an activity mode, w_i, is roughly clustered using the k-means algorithm [26]. These clusters are used to initialize the EM algorithm for finding the mixtures. A key factor affecting the classification performance of GMM's is the number of mixture components, K. As such, the performance of the models for a range of mixture components should be considered and compared for a given application.

Voting Scheme for Controller Mode Switching

The confidence with which the real-time intent recognizer switches can be increased with various types of low pass filtering. Specifically, in the proposed work, a voting scheme is used, as subsequently described, that requires a majority agreement over a frame of samples in order to switch activity modes. Such an approach enhances confidence, but at the cost of increased switching delay, which at some point will adversely affect the communication between the user and prosthesis. As such, the trade-off between sufficient confidence and switching latency should be assessed for a given application.

4. Implementation

Prosthesis

The proposed control and communication interface structure was implemented on a powered knee and ankle prosthesis, and tested on a unilateral transfemoral amputee subject. Specifically, the control approach was implemented on a self-contained, battery-powered and electric motor actuated prosthesis, which has not previously been reported in the literature. The powered prosthesis, which is shown in Fig. 3-3, is a two degree of freedom robotic device capable of generating human-scale torque and power at the knee and ankle joints. Actuation of each joint is accomplished via slider-crank linkages driven by motor ball screw assemblies. The ankle actuation unit incorporates a spring to bias the motor's axial force output toward ankle plantarflexion, and to supplement power output during ankle push off. The device's sensor package

includes a custom load cell to measure the sagittal socket interface moment above the knee joint, a custom foot to measure the ground reaction force at the heel and ball of the foot, and commercial potentiometers and load cells to measure joint positions and torques, respectively. The self-contained version includes an embedded system which allows both tethered and untethered operation from either a laptop (via MATLAB Simulink) or the PIC32 onboard microcontroller, respectively. The prosthesis is powered by a 118 Watt-hr lithium polymer battery that provides approximately 1.8 hours of level ground walking at 5.1 km/hr (over 4,500 strides with the prosthesis) or 12 hours of standing, based on initial experiments conducted with a single unilateral transfemoral amputee subject.

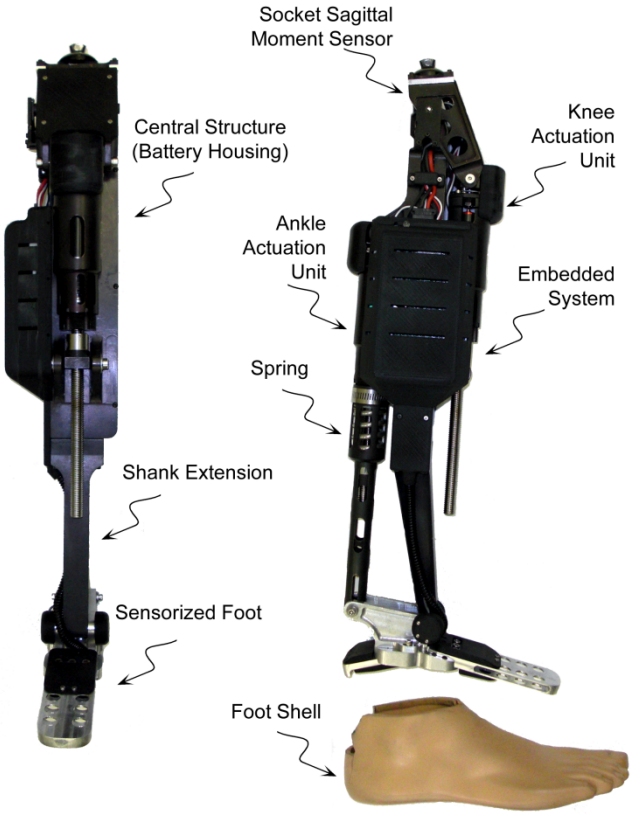

Figure 3-3. Self-contained powered knee and ankle transfemoral prosthesis.

Subject

The prosthesis was tested on a 20-year-old male (1.93 m, 70 kg) unilateral amputee, three years post amputation. The length of the test subject's residual limb, measured from the greater trochanter to the amputated site, was 55% of the length of the non-impaired side measured from the greater trochanter to the lateral epicondyle. The subject uses an Ottobock C-leg with a Freedom Renegade prosthetic foot for daily

use. The subject's daily use socket was used for the experiments, where the powered prosthesis prototype was attached in place of the daily use prosthesis. The overall prosthesis height adjustment and varus-valgus alignment were performed by a licensed prosthetist.

Intent Recognizer Training and Model Selection

The general structure of the intent recognizer, which is illustrated in Fig. 3-4, consists of generating data frames of appropriate sensors, taking the mean and standard deviation of each frame, reducing the dimensionality of these features, using trained models to determine the highest probability class, and using an averaging approach to increase confidence. As previously mentioned, several specific features of this structure are application-dependent, including the set of sensors to use, the length of the data windows, the number of components in the mixture models, and the length of the voting vector. The sensor signals used as input to the intent recognizer consists of seven signals, which include the joint angles and angular velocities of the knee and ankle, socket sagittal plane moment, and heel and ball of foot forces. Note that the joint angles and angular velocities characterize the internal state of the prosthesis, while the forces and torques contain information regarding interaction with the user and environment. At each time step of activity mode intent recognition (10 ms), frames are generated from each sensor signal and the (normalized) average and standard deviation are computed, such that the full feature set includes 14 variables. The frame length, dimensionality of the reduced feature set, method for dimension reduction, number of model components, and voting vector length are all application-dependent trade-offs. In the implementation discussed below, the dimensionality of the reduced feature set, the method of reduction, and the number of components in the mixture model were all determined by selecting the combination that provided the best accuracy of classification for the database that characterized the various activity modes. The frame length and voting vector lengths were then determined as the combination that provided the smallest total delay with a 100% success rate on a given set of test data. This process, and the resulting implementation, is described in the following sections.

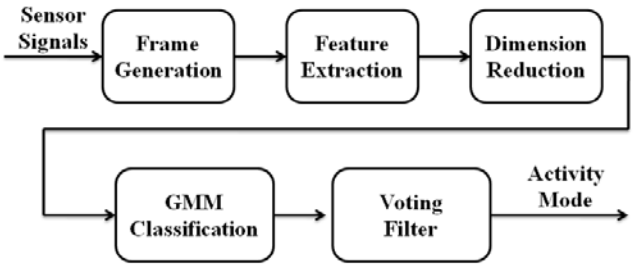

Figure 3-4. Block diagram of the activity mode intent recognizer.

Database Generation

In order to train the GMM's and to select the appropriate options in the intent recognition structure, a database of sensor data was collected to characterize the various activity modes of interest. Specifically, the powered prosthesis was tethered to a laptop computer running MATLAB Real Time Workshop for controller implementation and the middle-level prosthesis controllers were tuned for the subject for walking, standing and sitting. A database was generated that contained the possible walking, standing and sitting scenarios as outlined in Table 3-1. Generation of the database took approximately 2 hours. All data was sampled at 1000 Hz. For the standing mode, two activities were considered: static and dynamic standing. The former consists of activities in which the feet do not leave the ground, such as standing stationary and shifting weight between the limbs. The latter contains more active movements, such as taking small steps, turning in place, and repositioning the limb. Walking includes slow, normal and fast walking with the respective middle level walking controllers. For each walking and standing scenario outlined in Table 3-1, four 100-second trials were measured. Of these, the first two trials were used for model training, while the second two were used for performance evaluation of the intent recognizer.

In order to recognize standing and walking modes, the database generated must contain the possible matched and unmatched activity modes. Specifically, a matched activity mode is when the activity corresponds to the current control mode (e.g., standing while the prosthesis is in standing mode), while an unmatched mode is when the activity corresponds to a different control mode (e.g., walking while the prosthesis is in standing mode). Fig. 3-5 illustrates the timing of mode transitions and makes clear why such unmatched datasets are required for proper intent recognition.

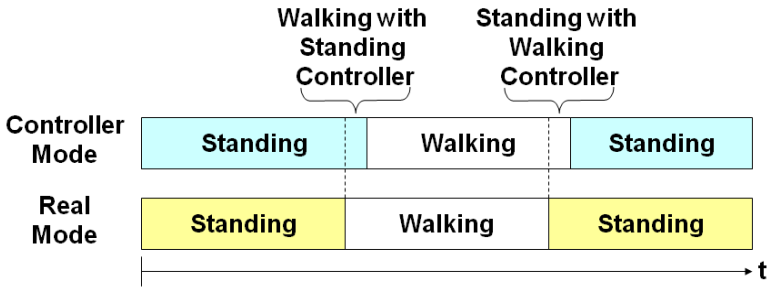

Figure 3-5. Demonstration of the controller and real mode discrepancy during mode transitions.

Generation of the database for the sitting mode is more complicated, since the finite state based impedance controller for sitting includes the standing up and sitting down transitions. These transitions are initiated by the intent recognizer. Without a database containing these transitions, the intent recognizer cannot be designed. In order to overcome this problem, the standing up and sitting down transitions were triggered using knee angle thresholds for generating the database. For generating the sitting database during standing up, an activity mode change occurs from sitting mode to standing mode when the knee angle becomes less than 5 degrees. For sitting down, the activity mode is switched to sitting mode when the knee angle exceeds 5 degrees. Fifteen trials for both cases were conducted. The four seconds after the sitting down transition and four seconds before the standing up transition were recorded for generating the sitting feature frames for the GMM classifier design. From each trial 20 frames of length 50, 100, 200 and 400 samples were generated. Moreover, two 100-second sitting trials were recorded for finding the optimal voting vector length for sitting to standing transitions. During these trials, the subject sat on a stool, performed sitting activities such as repositioning limbs, changing orientation, and reaching an object excluding standing up transition. For each frame length, the database for the GMM classifier design included 1600, 1200, and 600 frames of walking, standing and sitting modes, respectively.

Table 3-1. Different Activity Scenarios For Database Generation

Scenario	Num. of trials	Activity Mode	Activity	Purpose
1	4	Walking	Slow walking with walking controller	GMM, OVVL
2	4	Walking	Normal walking with walking controller	GMM, OVVL
3	4	Walking	Fast walking with walking controller	GMM, OVVL
4	4	Walking	Walking with standing controller	GMM, OVVL
5	4	Standing	Standing with walking controller	GMM, OVVL
6	4	Standing	Static standing with standing controller	GMM, OVVL
7	4	Standing	Dynamic standing with standing controller	GMM, OVVL
8	15	Sitting	Standing up	GMM
9	15	Sitting	Sitting down	GMM
10	2	Sitting	Sitting	OVVL

GMM stands for the task of designing the GMM classifier. OVVL stands for the task of finding the optimal voting vector length for real-time controller switching.

Model Selection

The model search space consisted of 30 models, which in turn consisted of 6 dimension methods (i.e., PCA and LDA for 1 to 3 dimensions) applied to 5 GMM models with number of components K ranging from 2 to 6, for each frame length. In order to find the best classifier for each frame length, the Area under the Receiver Operator Characteristics (AUC) curve [27] was used as the performance metric. This metric was used because it provides a comprehensive metric that computes true and false positives for all possible classification thresholds observed in the data, and because it is insensitive to class distribution. For adapting the AUC score to the multidimensional case, the scores between different classes were computed and the average was used as the final score for a specific model. Ten-fold cross-validation (CV) [28] was employed to avoid over-fitting. In ten-fold CV, the data is split into ten sets of size $N/10$ each. For purposes of model selection, the classifier was trained on 9 datasets and tested for the AUC on the remaining one. This was repeated ten times until all the data splits were tested and the mean AUC score was recorded as the performance metric for a specific classifier.

Voting Scheme for Controller Mode Switching

The real-time implementation of the voting scheme consists of overlapping frames that are classified at each 10 ms interval (Δt). In the voting scheme, the last l classifier decisions are stored in a voting vector and mode switching occurs if more than 80 percent of the classification results are in agreement. The activity mode switching logic based on the voting scheme for the walking, standing and sitting modes is demonstrated in Fig. 3-6. To avoid chattering during transition and increase the robustness of the powered prosthesis control, a rule was introduced to prevent mode switching for 500 ms after the most recent mode switching occurs (i.e., it is assumed a user will not enter and leave a given activity mode in 500 ms).

The combination of the voting length l and the frame length f determines the total delay of activity mode intent recognition. To minimize the total delay in the intent recognizer, the last two trials for each scenario in the experimental database were used to select the minimum voting vector length, corresponding to each frame length, that resulted in no incorrect classifications in the two test trials. In this process, the real-time activity intent recognizer was implemented (offline) with possible voting vector length from 10 to 100 in increments of 5. For each activity mode and for each of the four frame lengths f, the voting vector length was increased until the intent recognizer provided 100% accuracy in the two test trials. Once the optimal voting lengths for each frame size were found, the best frame length/voting vector length combination was determined as that which yielded the smallest overall delay d, where $d = f/2 + 10 l_{\max}$, where $l_{\max}$ is the greatest voting vector length determined among the four transitions shown in Fig. 3-6.

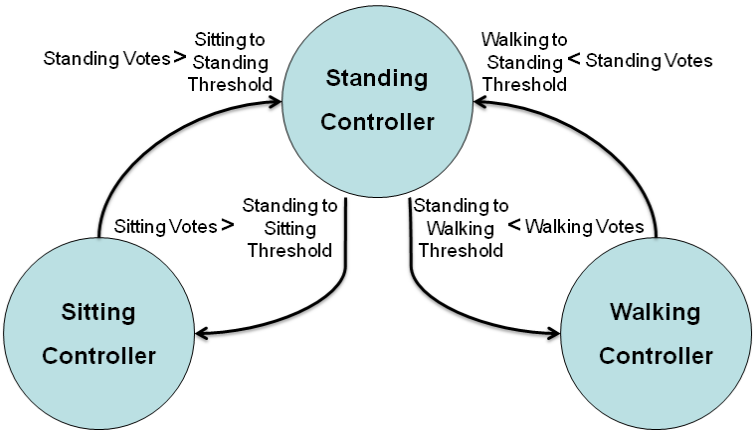

Figure 3-6. Controller mode switching logic for gait mode intent recognition.

5. Results and Discussions

PCA versus LDA for Dimension Reduction

PCA and LDA reduced datasets for the frame length 200 are shown in Figs. 3-7 and 3-8. The inherent characteristics of the transforms are apparent in the figures. Specifically, PCA essentially maximizes the variance of the data, while LDA generates ellipsoid clusters for different classes by maximizing the distance between different class clusters and minimizing the in-class variances. One might think that LDA dimension reduction would result in better classification results compared to PCA, since LDA takes into account the labels of the classes. As stated by [29], however PCA may outperform LDA when the inherent distribution of the data is non-normal. In [30], the authors report that PCA outperformed LDA for the intent recognition between standing and walking classes for a three-dimensional reduction, which was a binary classification problem. In the present three-class problem, LDA outperforms PCA in all cases. As an example, Fig. 3-9 shows the mean AUC scores for both PCA and LDA reduced GMM classification for the frame length 200.

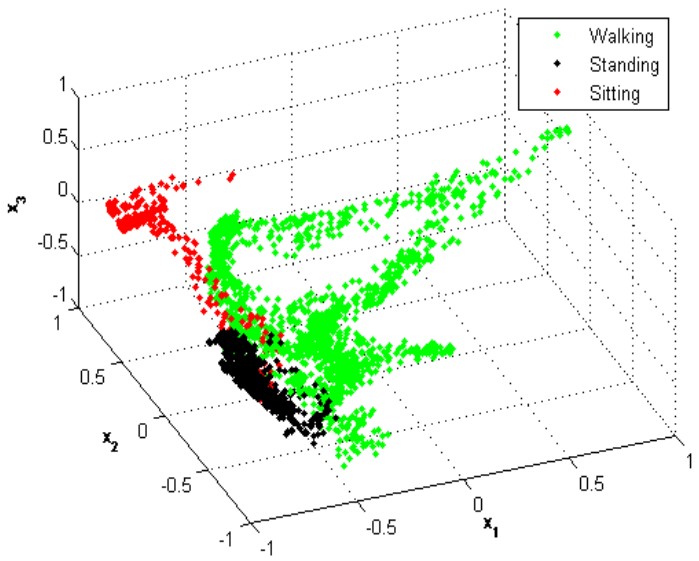

Figure 3-7. PCA dimension reduced features extracted from 200 sample-long frames.

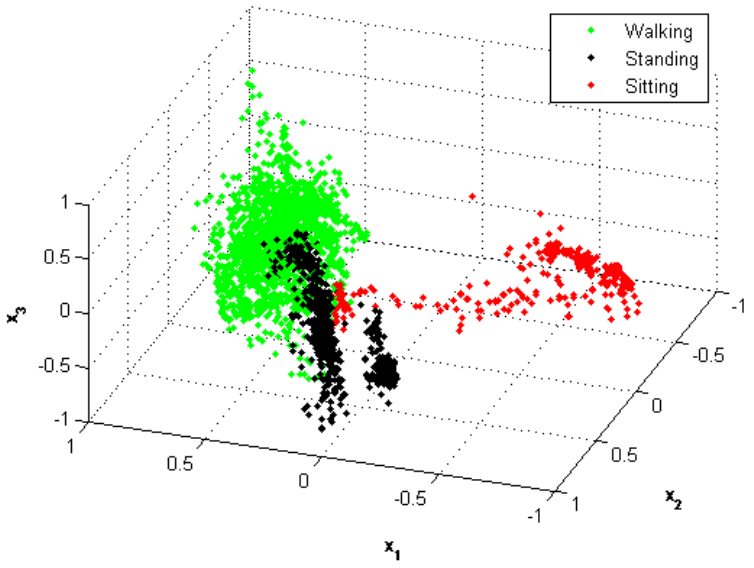

Figure 3-8. LDA dimension reduced features extracted from 200 sample-long frames.

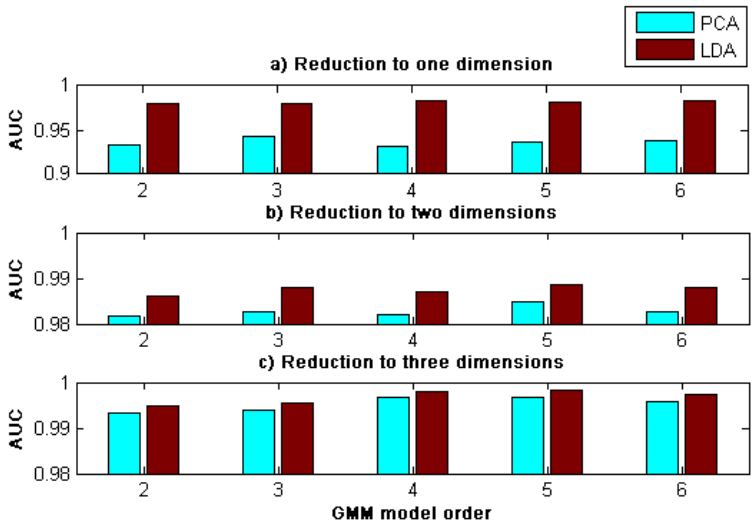

Figure 3-9. Classification performance of different model order GMM's with PCA and LDA dimension reduction to one (a), two (b) and three (c) dimensions for frame length. Note the y-axis scaling for each dimension.

Gaussian Mixture Model Selection

The best AUC scores are obtained from the LDA dimension-reduced three-dimensional GMM's with 5, 6, 5, and 4 mixtures for the frame lengths 50, 100, 200 and 400, respectively. It is observed that the best AUC score increases with increasing frame length. Surface plots of the standing and walking mixture models for frame length 100, showing the portions of the feature space with greater than 0.05 probability densities are presented in Fig. 3-10. The distinct locations of the three different activities in the reduced feature space can be seen in this figure. The dynamic nature of walking is observed in the walking mixture model, which creates a three dimensional loop consisting of several ellipsoids of areas with high probability density. The standing up and sitting down transitions are bridge-like volumes connecting the standing and sitting modes. Lastly, the standing mixture model resides in a small region of the reduced feature space, which connects the walking and sitting regions.

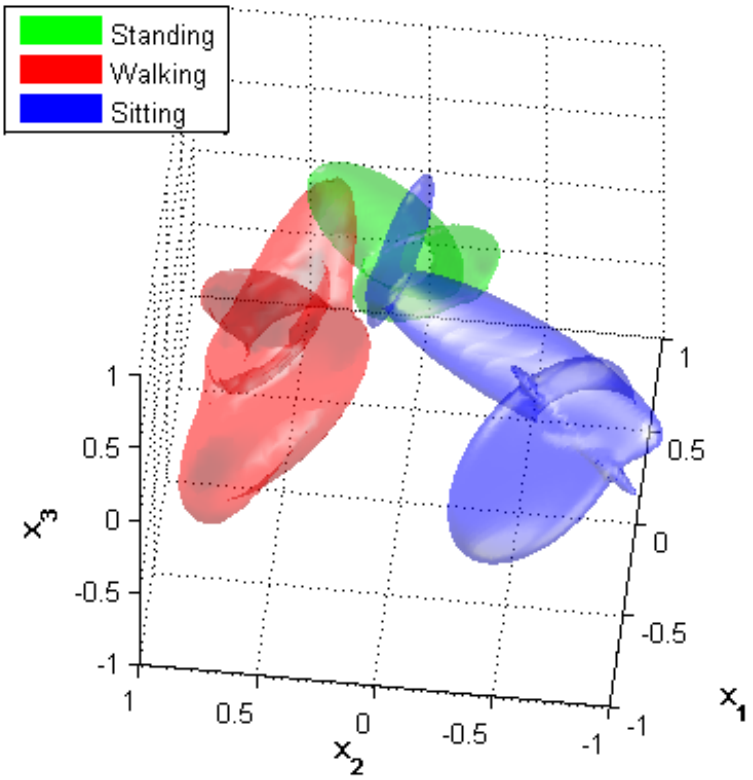

Figure 3-10. Gaussian Mixture Models surface plots for standing, walking and sitting showing the portions of the feature space, where probability density function is greater than 0.05, for three dimensional LDA reduced data.

Voting Vector Length Selection

As previously described, the first two trials of each dataset were used to train the mixture models, while the last two trials were used to select the voting vector lengths that correspond to a minimum total delay and 100% accuracy (in the last two trials). The minimum voting vector lengths that correspond to 100% accuracy are 55, 45, 65, and 60, respectively, which correspond to frame lengths of 50, 100, 200 and 400, respectively, and GMM models of 5, 6, 5, and 4 components, respectively. These and the respective approximate intent recognition delay for each frame length is listed in Table 3-2. As can be observed from the table, the shortest approximate delay for the intent recognition is obtained for the frame length 100 (which corresponds to a voting vector length of 45 and 6-component GMM. With this combination, the intent recognizer will switch to a new mode in approximately one half a second.

Table 3-2. Different Activity Scenarios For Database Generation

Frame Length	Frame Delay (ms)	Voting Delay (ms)	Total Delay (ms)
50	25	550	525
100	50	450	500
200	100	650	750
400	200	600	800

Real-Time Supervisory Control

The intent recognition structure with the selected components (three dimensional LDA dimension reduction with GMM with 6 mixtures using 100 sample-long frames and voting vector length of 45) was tested in real-time gait mode intent recognition. Three trials lasting 190 seconds each on a treadmill were conducted to verify that the method works in a closed feedback loop as a supervisory controller. Each trial began with the test subject standing on a treadmill. The treadmill was started and stopped at arbitrary intervals several times during the trials, requiring the test subject to switch between walking and standing. Note that standing included shifting weight from one side to the other and turning in place. During some of the periods when the treadmill was stopped, a stool was placed on a treadmill and the subject volitionally transitioned between standing and sitting. During these trials, 56 activity mode transitions were made by the subject, and all 56 were correctly identified by the intent recognizer, with no user-perceived latency in mode switching. Despite this, the intent recognizer identified three activity modes during the 570-second trial period that were not intended by the user. Specifically, during the standing mode, the intent recognizer once identified intent to walk, and twice identified intent to sit (and in both cases switched back within one second). Though such incorrect inferences may sound potentially dangerous, they in fact are benign, and in these cases were not noticed by the user. Specifically, as can be seen in Fig. 3-10, when casually shifting weight between legs during standing, the distinction between standing, walking, and the initial transition state from standing to sitting are all quite similar in state and in desired functionality (i.e., both the state of the leg and its behavior are non-unique). That is, the switching errors occurred in a region of the feature space in which both the movement patterns and the leg impedances are similar, and thus they

have little significant effect. For instance, the impedance behavior of the prosthesis for the stand to sit transition is defined by a stiff spring with an equilibrium point of 5 degrees. The virtual spring in the weight bearing standing mode is set to 0 degrees and has a similar stiffness. When the prosthesis makes an erroneous mode switch from standing to sitting, the impedance behavior of the prosthesis does not change significantly. As such, the distinction between these modes is somewhat artificial, and thus there is little importance in distinguishing between them. Thus, the apparent confusion of the intent recognizer is more a problem with the non-uniqueness of these respective activity modes than with a misunderstanding of the user's intent.

An example of an erroneous mode switch is shown in the trial of Fig. 3-11, which shows the activity mode and knee angle for a 190-second trial, with an erroneous stand-to-sit transition at approximately 130 seconds. Even though, there exists an erroneous mode switch, there is no ostensible visual evidence of the incorrect switching.

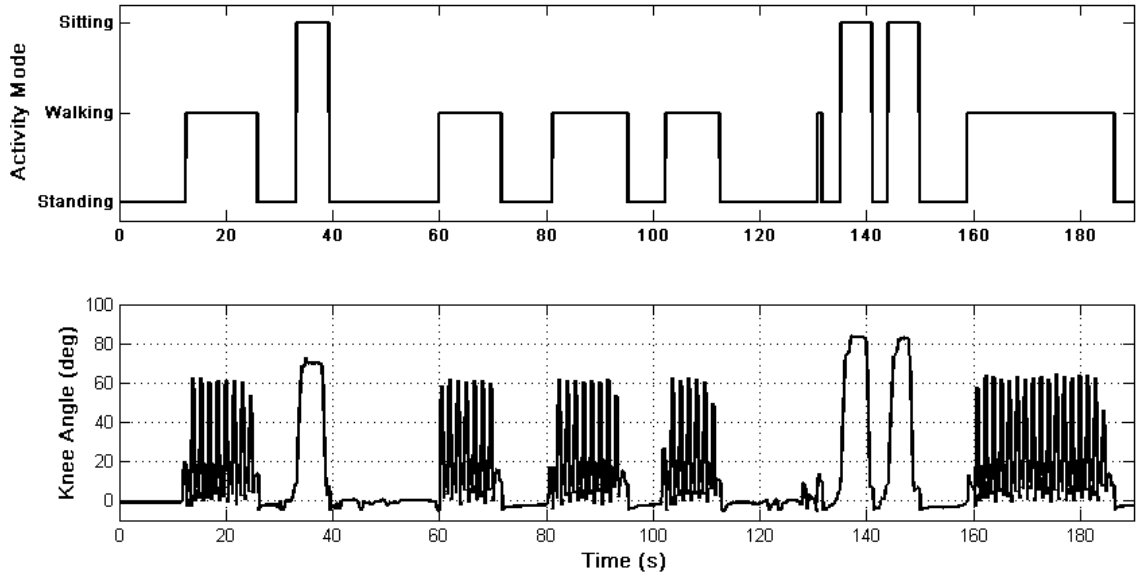

Figure 3-11. Real-time activity mode switching (top) and knee angle (bottom) for a 190 seconds long trial.

One might argue that a simple thresholding scheme such as that implemented for the sitting database generation might suffice for switching between different controllers. The knee angle and the activity mode from a trial during which the subject stood (and shuffled) and made stand-to-sit and sit-to-stand transitions

is shown in Fig. 3-12. As can be observed from the figure, the knee angle threshold used for generating the database (5 degrees) is exceeded several times during dynamic standing. If this threshold were used, many incorrect stand-to-sit transitions would be initiated. In general, the intent recognizer creates an intricate switching function combining many measurements which results in a robust supervisory controller.

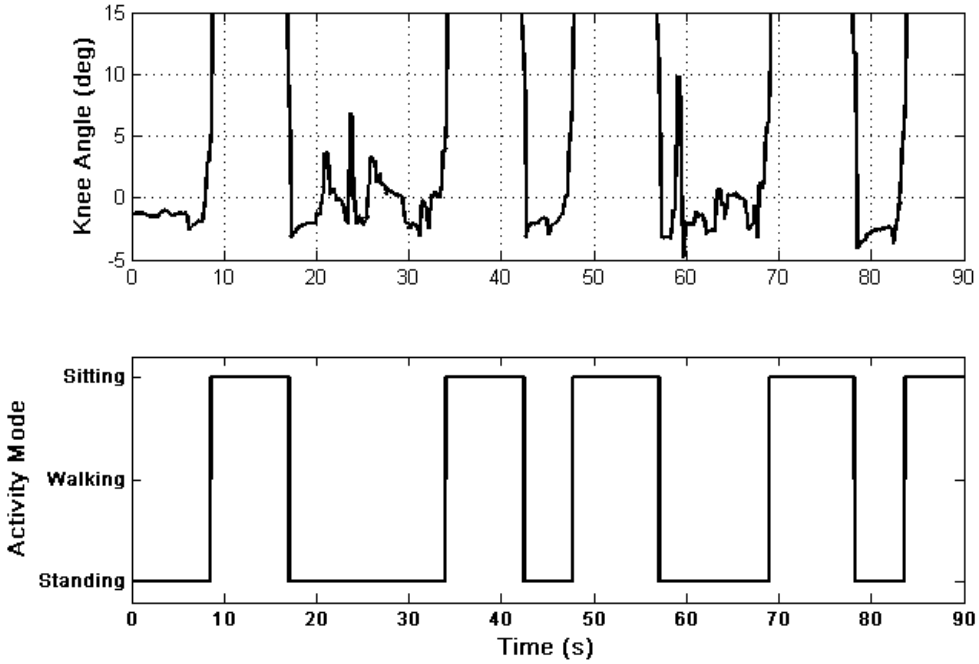

Figure 3-12. Knee angle (top) and real-time activity mode switching (bottom) for a 90 second sit-to-stand and stand-to-transitions trial.

Though the proposed method requires significant computation during the training phase (i.e., generating GMM's for all the combinations, CV and frame length optimization), real-time implementation does not require extensive computation. The entire powered prosthesis control system (lower and middle level controllers, along with the intent recognizer) implemented in real-time using Matlab Real-Time Workshop requires approximately 10% processor utilization for a Pentium 4, 2.0 GHz desktop computer. It should be noted that in real-time implementation, the computation required by the algorithm will scale linearly with the addition of other activity modes, such as stair ascent/descent, and thus should easily allow real-time implementation on an embedded microcomputer.

6. Conclusion

The authors propose an activity mode intent recognition framework for a powered lower limb prosthesis which uses only signals from the prosthesis. The authors describe the approach, and demonstrate it on a powered knee and ankle prosthesis. For this prosthesis, LDA dimension reduction with 100 sample-long frames yielded the best results for standing, sitting and walking mode recognition using GMM as a classifier. Experiments with a unilateral amputee subject showed that the activity mode intent recognition framework extracts the user intent in real-time and switches to the correct underlying activity controller. Some classification errors were observed, although only in highly similar types of activity, and thus the errors in switching were not problematic and were not perceived by the user.

Future work includes testing the proposed framework with multiple amputee subjects and adding new activity modes such as stair ascent and descent.

7. References

[1] P. DeVita, M. Torry, K. L. Glover, and D. L. Speroni, "A functional knee brace alters joint torque and power patterns during walking and running," J. of Biomechanics, vol. 29, no. 5, pp. 583-588, May, 1996.

[2] R. Jacobs, M. F. Bobbert, and G. J. van Ingen Schenau, "Mechanical output from individual muscles during explosive leg extensions: The role of biarticular muscles," J. of Biomechanics, vol. 29, no. 4, pp. 513-523, Apr, 1996.

[3] S. Nadeau, B. J. McFadyen, and F. Malouin, "Frontal and sagittal plane analyses of the stair climbing task in healthy adults aged over 40 years: what are the challenges compared to level walking?," Clinical Biomechanics, vol. 18, no. 10, pp. 950-959, Dec, 2003.

[4] A. Nagano, Y. Ishige, and S. Fukashiro, "Comparison of new approaches to estimate mechanical output of individual joints in vertical jumps," J. of Biomechanics, vol. 31, no. 10, pp. 951-955, Oct, 1998.

[5] B. I. Prilutsky, L. N. Petrova, and L. M. Raitsin, "Comparison of mechanical energy expenditure of joint moments and muscle forces during human locomotion," J. of Biomechanics, vol. 29, no. 4, pp.

405-415, Apr, 1996.

[6] R. Riener, M. Rabuffetti, and C. Frigo, “Joint powers in stair climbing at different slopes,” Proc. of the First Joint BMES/EMBS Conf., vol. 1, pp. 530 vol.1, 1999.

[7] D. Winter, The Biomechanics and Motor Control of Human Gait: Normal, Elderly and Pathological, 2nd ed.: University of Waterloo Press, 1991.

[8] D. A. Winter, and S. E. Sienko, “Biomechanics of below-knee amputee gait,” J. of Biomechanics, vol. 21, no. 5, pp. 361-367, 1988.

[9] R. L. Waters, J. Perry, D. Antonelli, and H. Hislop, “Energy cost of walking of amputees - Influence of level of amputation,” J. of Bone and Joint Surgery-American Vol., vol. 58, no. 1, pp. 42-46, 1976.

[10] W. C. Flowers, and R. W. Mann, “Electrohydraulic knee-torque controller for a prosthesis simulator,” ASME J. of Biomechanical Engineering, vol. 99, no. 4, pp. 3-8, 1977.

[11] J. L. Stein, and Massachusetts Institute of Technology. Dept. of Mechanical Engineering., “Design issues in the stance phase control of above-knee prostheses,” Massachusetts Institute of Tech. Dept. of Mechanical Eng. Thesis Ph.D., 1983.

[12] D. L. Grimes, “An active multi-mode above knee prosthesis controller,” Massachusetts Institute of Tech. Dept. of Mechanical Eng. Thesis Ph.D., 1979.

[13] S. Bedard, and P. Roy, Actuated Leg Prosthesis for Above-Knee Amputees, U. S. Patent, 2003.

[14] E. Martinez- Villalpando, J. Weber, G. Elliott, and H. Herr, “Design of an agonist-antagonist active knee prosthesis,” Proc. IEEE/RAS-EMBS Int. Conf. on Biomedical Robotics and Biomechatronics, pp. 529-534, 2008.

[15] D. Popovic, and L. Schwirtlich, “Belgrade active A/K prosthesis,” in de Vries, J. (Ed.), Electrophysiological Kinesiology, Intern. Congress Ser. No. 804, Excerpta Medica, Amsterdam, The Netherlands, pp. 337-343, 1988.

[16] H. Huang, T. A. Kuiken, and R. D. Lipschutz, “A Strategy for Identifying Locomotion Modes Using Surface Electromyography,” IEEE Trans. on Biomedical Engineering, vol. 56, no. 1, pp. 65-73, Jan, 2009.

[17] S. Bedard, and P. Roy, Actuated leg prosthesis for above-knee amputees, 7,314,490, U. S. Patent, June 17, 2003.

[18] M. A. Holgate, A. W. Bohler, and T. G. Sugar, "Control algorithms for ankle robots: A reflection on the state-of-the-art and presentation of two novel algorithms," Proc. IEEE/RAS-EMBS Int. Conf. on Biomedical Robotics and Biomechatronics, pp. 97-102, 2008.

[19] S. Au, M. Berniker, and H. Herr, "Powered ankle-foot prosthesis to assist level-ground and stair-descent gaits," Neural Networks, vol. 21, no. 4, pp. 654-666, May, 2008.

[20] W. Koniuk, Self-adusting prosthetic ankle apparatus, 6,443,993, U. S. Patent, March, 23, 2001.

[21] F. Sup, A. Bohara, and M. Goldfarb, "Design and control of a powered transfemoral prosthesis," Int. J. of Robotics Research, vol. 27, no. 2, pp. 263-273, Feb, 2008.

[22] I. T. Jolliffe, Principal Component Analysis, 2nd ed., New York: Springer, 2002.

[23] R. A. Fisher, "The statistical utilization of multiple measurements," Annals of Eugenics, vol. 8, pp. 376-386, 1938.

[24] A. P. Dempster, N. M. Laird, and D. B. Rubin, "Maximum likelihood from incomplete data via EM algorithm," J. of the Royal Statistical Society Series B-Methodological, vol. 39, no. 1, pp. 1-38, 1977.

[25] G. J. McLachlan, and D. Peel, Finite mixture models, New York: Wiley, 2000.

[26] J. A. Hartigan, and M. A. Wong, "A K-means clustering algorithm," Applied Statistics, vol. 28, no. 1, pp. 100-108, 1979.

[27] T. Fawcett, "An Introduction to ROC Analysis," Pattern Recognition Letters, vol. 27, no. 8, pp. 861-874, Jun, 2006.

[28] T. M. Mitchell, Machine Learning, New York: McGraw-Hill, 1997.

[29] A. M. Martinez, and A. C. Kak, "PCA versus LDA," IEEE Trans. on Pattern Analysis and Machine Intelligence, vol. 23, no. 2, pp. 228-233, Feb, 2001.

[30] H. A. Varol, F. Sup, and M. Goldfarb, "Real-time gait mode intent recognition of a powered knee and ankle prosthesis for standing and walking," Proc. IEEE/RAS-EMBS Int. Conf. on Biomedical Robotics and Biomechatronics, pp. 66-72, 2008.

CHAPTER IV

Manuscript III: Powered Sit-to-Stand and Assistive Stand-to-Sit Framework for a Powered Transfemoral Prosthesis

Huseyin Atakan Varol, Frank Sup and Michael Goldfarb

Vanderbilt University

Nashville, TN 37235

Accepted as a Technical Paper to the

2009 IEEE International Conference on Rehabilitation Robotics

1. Abstract

This work extends the three level powered knee and ankle prosthesis control framework previously developed by the authors by adding sitting mode. A middle level finite state based impedance controller is designed to accommodate sitting, sit-to-stand and stand-to-sit transitions. Moreover, a high level Gaussian Mixture Model based intent recognizer is developed to distinguish between standing and sitting modes and switch the middle level controllers accordingly. Experimental results with unilateral transfemoral amputee subject show that sitting down and standing up intent can be inferred from the prosthesis sensor signals by the intent recognizer. Furthermore, it is demonstrated that the prosthesis generates net active power of 50 W during standing up and dissipates up to 50 W of power during stand-to-sit transition at the knee joint.

2. Introduction

Standing up is a frequently exercised daily activity which involves the coordinated movement of the entire body to substantially raise the body center of mass in a generally economical manner. It requires significant torque and range of motion at the knee joint and to a lesser extent the ankle joint [1-5]. Fundamentally, the ability to stand up from a seated position is a prerequisite to begin walking and extend one's mobility. In general, transfemoral amputees with prostheses that lack active power can have difficulty standing up or are unable to without aid, thus, predisposing them to a sedentary lifestyle. For a transfemoral amputee to accomplish the sit-to-stand transition unaided, requires twice the torque output from the sound side knee joint as compared to healthy subjects [6] and additionally requires significantly increased compensatory torques in the frontal plane. Furthermore, the amputee does not bear weight on the prosthesis until they are almost in the standing position [6]. To compensate for the lack of power in the lower limb, amputees often rely on the aid of their upper limbs and handrails. Conversely, passive prostheses are more assistive while sitting down. They enable the user to bear weight on both sides reducing excessive torques on the sound side joint. State-of-the-art microcontroller modulated braking knees adjust the damping on the knee joint to control the resistance during stand to sit transition [7]. However, an active prosthesis would

benefit the user during stand-to-sit transition by providing active power to recover to the standing position in case the user changes his or her intent to sit down. The quality of life and mobility of transfemoral amputees could benefit from active assistance provided by a prosthesis with powered joints during the standing up (SU) and sitting down (SD) transitions.

The design of powered transfemoral prostheses is a challenging task due to the large range of motion on the knee joint and the magnitude of the power and torques that need to be applied at both the knee and ankle. Development of powered transfemoral prostheses dates back to the early 1970's with a tethered electro-hydraulically actuated knee joint. This prosthesis was a test bed for studying the feasibility of powered knee joints during walking [8]. Other prior work was conducted on the development of an active knee joint actuated by electrical motors with finite state position controller [9]. Ossur, a prosthetics company, introduced a powered knee prosthesis that is capable of generating net active power [10]. An agonist-antagonist knee design which utilizes the passive dynamics of the knee during walking is presented in [11]. The authors were not able to find any scientific literature on SU and SD transitions for these active transfemoral prostheses.

A self-contained powered knee and ankle prosthesis has been developed by the authors which aims to restore normal locomotive function to transfemoral amputees. The authors have also explored a three level control architecture consisting of a high level intent recognizer, a middle level finite state based impedance controller and low level force-controller for walking and standing. In this work, the control architecture will be expanded to include sitting and the associated SU and SD transitions. The paper is designed as follows. Firstly, the powered prosthesis used in this study is presented. Secondly, the finite state based impedance controller for standing, sitting, and SU and SD transitions is described. Thirdly, the design of the intent recognizer for the sitting mode is described. Finally, experimental results with a unilateral transfemoral amputee are presented and discussed.

3. Methodology

Powered Prosthesis

The authors have previously described a tethered powered knee and ankle prosthesis [12]. A new

(previously unreported) self-contained version of the prosthesis, shown in Fig. 4-1, was used for the powered sit-to-stand and assistive stand-to-sit testing, described herein. The powered prosthesis is a two degree of freedom robotic device capable of generating human-scale torque and power at the knee and ankle joints. Actuation of each joint is accomplished via slider-crank linkages driven by motor ball screw assemblies. The ankle actuation unit incorporates a spring to bias the motor's axial force output toward ankle plantarflexion, and to supplement power output during ankle push off. The device's sensor package includes a custom load cell to measure the sagittal socket interface moment above the knee joint, a custom foot to measure the ground reaction force at the heel and ball of the foot, and commercial potentiometers and load cells to measure joint positions and torques, respectively. The self-contained version hosts an embedded system allowing for both tethered and untethered operation run by either MATLAB Simulink or a PIC32 microcontroller, respectively. The prosthesis is powered by a 118 W·h lithium polymer battery that allows for approximately 1.8 hours of level ground walking at 5.1 km/h (over 4,500 strides with the prosthesis) or 12 hours of standing, estimated in initial trials with one unilateral transfemoral amputee subject.

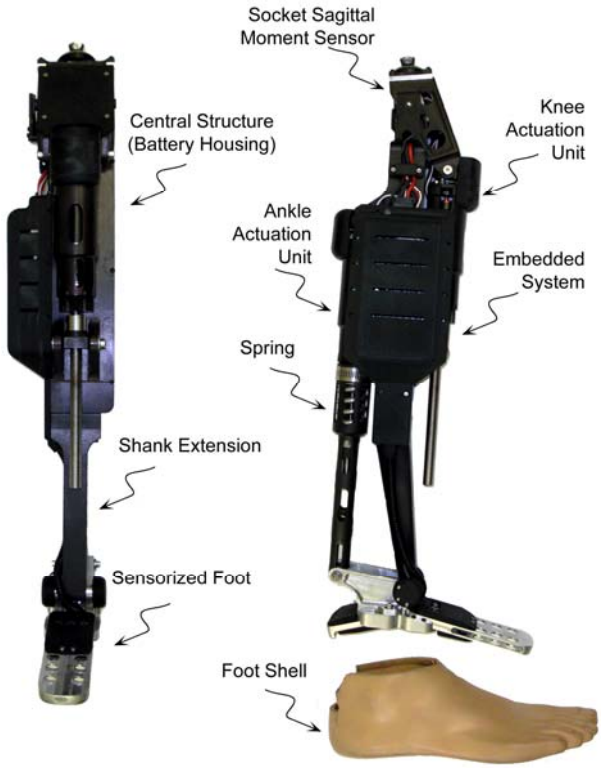

Figure 4-1. The self-contained powered knee and ankle transfemoral prosthesis.

Control Architecture

The control architecture of the prosthesis is a three level hierarchy, as diagrammed in Fig. 4-2. The high level supervisory controller, which is the intent recognizer, infers the user's intent based on the interaction between the user and the prosthesis, and correspondingly switches the middle level controllers. Intent recognition is achieved by first generating a database containing sensor data from different activity modes and then training a pattern recognizer that switches between activity modes in real time, as described in [13]. A middle level controller is developed for each activity mode, such as walking, standing, sitting, and stair ascent/descent. The middle level controllers generate torque references for the joints using a finite state machine that modulates the impedance of the joints depending on the phase of the activity. The low-level controllers are the closed-loop joint torque controllers, which compensate for the transmission dynamics of the ball screw (i.e., primarily friction and inertia), and thus enable tracking of the knee and ankle joint torque references (commanded by the middle level controllers) with a higher bandwidth and accuracy than is afforded with an open-loop torque control approach. In this work, the design of the supervisory intent recognizer and the finite state impedance based controller for the sitting and standing modes will be presented.

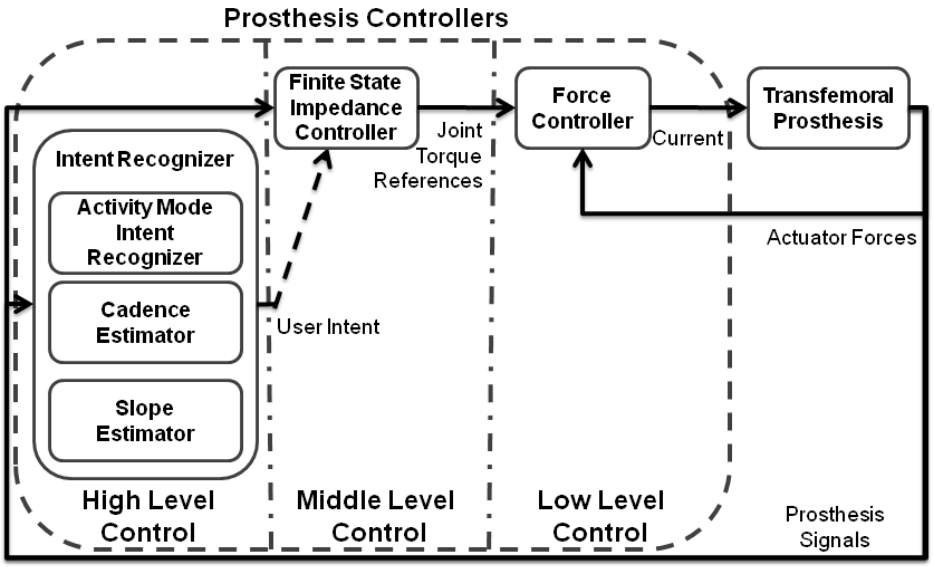

Figure 4-2. Powered prosthesis control architecture.

Finite State Based Impedance Control

In the finite state impedance based control, the impedance behavior of healthy biomechanical gait is mimicked by modulating joint impedances of the prosthesis according to the phase of gait. In each phase, the knee and ankle torques, τ_i, are each described by a passive spring and damper with a fixed equilibrium point, given by:

$$\tau_i = k_i(\theta - \theta_{ki}) + b_i\dot{\theta} \tag{1}$$

where k_i, b_i, and θ_{ki} denote the linear stiffness, damping coefficient, and equilibrium point, respectively, for the i^{th} state. Switching joint impedances between the gait phases is initiated by biomechanical cues. For instance, the switching from swing extension to the early stance state during walking occurs with the detection of heel strike. The approach requires the development of a state machine for each type of user activity such as walking, standing, sitting, and stair ascent and descent. The result is an effective and predictable controller that does not violate passive behavior except when the user requests active power transfer by triggering a transition. The authors previously developed controllers for standing and walking modes using this framework [12]. Within this framework, the finite state based impedance control approach will be extended to include a state machine for sitting and the transitions between sitting and standing, Fig. 4-3.

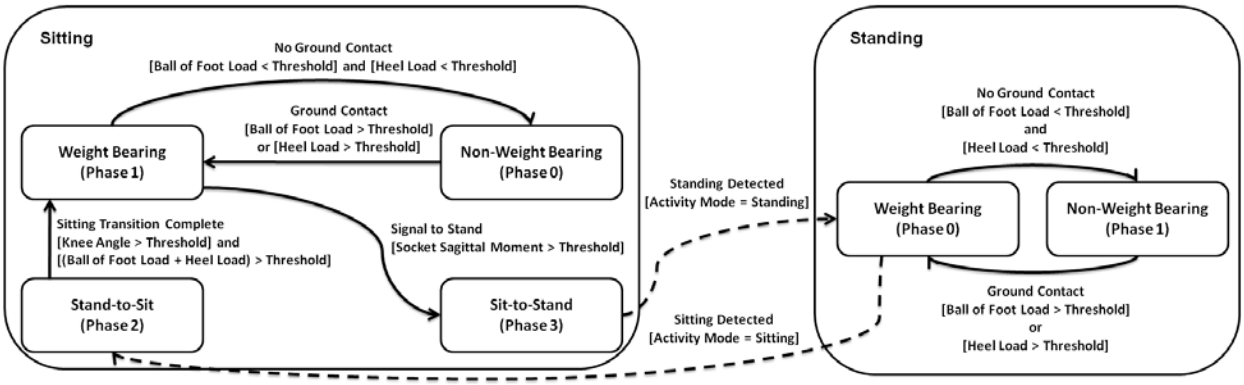

Figure 4-3. The state chart depicting the phase transitions in standing and sitting modes.

The standing impedance controller consists of two phases: weight bearing and non-weight bearing. In the weight bearing phase, the weight of the user is supported with high impedance at the joints. In the non-weight bearing mode, the knee acts as a soft dashpot to enable freedom of movement and a smooth transition to walking. While using the standing controller, the user can shift his or her weight between the sound side and the prosthesis, balance and shuffle. The sitting mode controller consists of four phases. Two are primary sitting phases, weight bearing and non-weight bearing. The other two encompass the transition phases, sit-to-stand and stand-to-sit transitions, for SU and SD, respectively. Weight bearing and non-weight bearing are the active sitting phases that switch the knee and ankle joints between high and low impedances, respectively. The transition phases, sit-to-stand and stand-to-sit, modulate the stiffness of the knee as a function of knee angle, Fig. 4-4, to assist the user in SU and SD. The modulation allows for smoother transitions near the seated position. The ankle joint is slightly dorsiflexed with moderate stiffness during the SU and SD phases. The parameters of the impedance based controllers are tuned using a combination of feedback from the user and joint angle, torque and power data from the prosthesis.

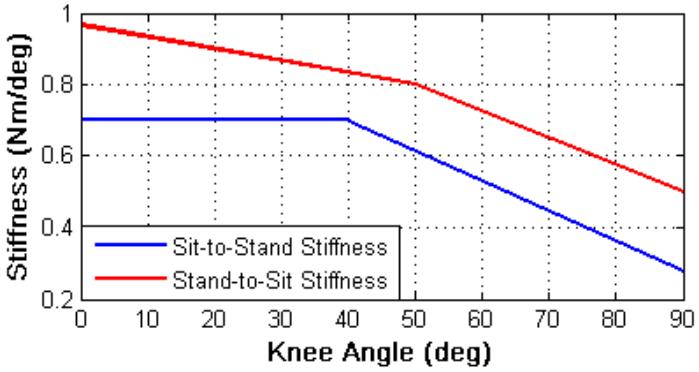

Figure 4-4. Knee angle modulated knee stiffness during sit-to-stand and stand-to-sit phases.

4. Intent Recognition

Database Generation

The prosthesis was tested on a 20-year-old male (1.93 m, 70 kg) unilateral amputee three years post

amputation. The length of the test subject's residual limb, measured from the greater trochanter to the amputated site, was 55% of the length of the non-impaired side measured from the greater trochanter to the lateral epicondyle. The subject uses an Ottobock C-leg with a Freedom Renegade prosthetic foot for daily use. The subject's daily use socket was used on all experiments, where the powered prosthesis prototype was attached on place of the daily use prosthesis. The overall prosthesis height and varus-valgus alignment were performed by a licensed prosthetist. The prosthesis was tuned for the subject. The controller parameters for the standing and sitting mode are given in Table 4-1 and 4-2, respectively, which were obtained by tuning as previously mentioned. The powered prosthesis was tethered to a laptop computer running MATLAB Real Time Workshop for controller implementation and data logging. The prosthesis sensor data for database generation was sampled at 1000 Hz consisted of seven signals: joint positions and velocities for the knee and ankle, socket sagittal plane moment and heel and ball of foot forces.

Table 4-1. Impedance parameters for standing from experimental tuning.

	Knee Impedance			Ankle Impedance		
Phase	k Nm deg^{-1}	b N s m^{-1}	θ_k deg	k Nm deg^{-1}	b N s m^{-1}	θ_k deg
0	2.5	0.02	0	4.0	0.05	-6
1	0	0.02	0	2.0	0.05	-6

Table 4-2. Impedance parameters for sitting from experimental tuning.

	Knee Impedance			Ankle Impedance		
Phase	k Nm deg^{-1}	b N s m^{-1}	θ_k deg	k Nm deg^{-1}	b N s m^{-1}	θ_k deg
0	0	0.05	0	4	0.06	0
1	0	0.02	0	2	0.02	0
2	1.0	0	5	2	0.06	5
3	0.7	0	5	2	0.06	5

In order to recognize standing and sitting modes, a database was generated that contained the possible standing and sitting scenarios as outlined in Table 4-3. The data acquired was used for designing the GMM

classifiers and finding the optimal voting length for real-time controller switching. For the standing mode, two activities were considered: static and dynamic standing. The former consists of activities in which the subject stands still such as standing stationary and shifting weight between the limbs. The latter contains more active movements, such as taking small steps, turning in place, and repositioning the limb. For each of the static and dynamic standing activities, four 100-second trials were measured of which the middle 80 seconds were used for generation of the database. From the first two trials, 200 frames with random initial points for four different frame lengths, *f*, of 50, 100, 200, and 400 samples were extracted to generate the features for the GMM classifier. The remaining standing trials were used for voting vector length determination.

Table 4-3. Different activity scenarios for database generation.

Scenario	#. of trials	Activity Mode	Activity	Purpose
1	4	Standing	Static Standing	GMM, OVVL
2	4	Standing	Dynamic Standing	GMM, OVVL
3	15	Sitting	Standing Up	GMM
4	15	Sitting	Sitting Down	GMM
5	2	Sitting	Sitting	OVVL

Note. GMM stands for the task of designing the GMM classifier. OVVL stands for the task of finding the optimal voting vector length for real-time controller switching.

Generation of the database for the sitting mode was more complicated, since the finite state based impedance controller for sitting includes the SU and SD transitions. These transitions are initiated by the intent recognizer. Without a database containing these transitions, the intent recognizer cannot be designed. In order to overcome this problem, the SU and SD transitions were triggered using knee angle thresholds for generating the database. For generating the database, an activity mode change occurs during standing up in sitting mode to standing mode when the knee angle becomes less than 5 degrees. For sitting down, the finite state based impedance controller is switched to sitting mode when the knee angle exceeds 5 degrees. Fifteen trials for both cases are conducted. The four seconds after the sitting down transition and four seconds before the SU transition are recorded for generating the feature frames for the GMM classifier design. From

each trial 20 frames of length 50, 100, 200 and 400 samples are generated. Moreover, two 100-second sitting trials were recorded for finding the optimal voting vector length for sitting to standing transitions. During these trials, the subject sat on a stool, did sitting activities such as repositioning limbs, changing orientation, and reaching an object excluding SU transition. For each frame length, the database for the GMM classifier design included 800 frames of standing data and 600 frames of sitting data.

Feature Extraction

The real-time nature of the problem requires that the features extracted from the seven prosthesis signals be computationally inexpensive, and as such, the mean and standard deviation were selected as features to extract from each frame, resulting in 14 fundamental simple time domain features. After the features were extracted, they were normalized into the range of [-1, 1] to eliminate the scaling effects between different features. Balancing the information content of a frame against frame length is important since additional delay for intent recognition is introduced as the frame size grows. In order to find the optimal frame length, different frame sizes (50, 100, 200 and 400 samples) were considered.

Dimension Reduction

In order to decrease the time required for real-time intent recognition and training and prevent over-fitting, the feature space was reduced (at the cost of information content) using Principal Component Analysis (PCA) [14] and Linear Discriminant Analysis (LDA) [15], from 14 dimensions to a feature space of 1, 2 and 3 dimensions. Both approaches employ linear transformations, which only necessitate a matrix multiplication operation. Since orthonormal transformations tend to decrease the magnitude of the elements in the transformed matrix as compared to the initial matrix, the reduced features are normalized into the range of [-1, 1] to avoid any possible numerical instability in the GMM classification phase.

Gaussian Mixture Model Activity Mode Classification

Gaussian Mixture Models (GMM) are used to characterize the probability that the user and prosthesis is engaged in a given activity mode. Specifically, a separate GMM is used to describe each activity mode, w_i. For some set of inputs $\vec{x}$, the probability of being in an activity mode, w_i, is given by:

$$p(\vec{x} \mid w_i) = \sum_{k=1}^{K} \lambda_k^i p_k^i(\vec{x}) \tag{1}$$

where

$$p_k^i(\vec{x}) = \frac{1}{\sqrt{(2\pi)^D \left|\sum_k^i\right|}} \exp\left\{-\frac{1}{2}(\vec{x} - \vec{\mu}_k^i)'(\sum_k^i)^{-1}(\vec{x} - \vec{\mu}_k^i)\right\} \tag{2}$$

where K is the number of components of the mixture model, λ_k^i is the mixture parameter of the i^{th} GMM for the k^{th} component, which satisfy the constraints $\sum_{k=1}^{K} \lambda_k^i = 1$ and $\lambda_k^i \geq 0$. The mixture component, $p_k^i(\vec{x})$, is a multivariate Gaussian probability density function with a $D \times 1$ mean vector, $\vec{\mu}_k^i$, and $D \times D$ full covariance matrix, $\sum_k^i$, with $D(D+1)/2$ free parameters. Each GMM can be parameterized by $K(1 + D + D(D+1)/2) - 1$ parameters, which are the mixture parameters, mean vectors and covariance matrices, notated as $w_i = \{\lambda_k^i, \vec{\mu}_k^i, \sum_k^i\}$. Once the GMM's are parameterized, for a given sample feature vector, $\vec{x}_S$, the activity mode, w_m, is selected as the mode with the highest probability:

$$w_m = \arg\max_{w_i}(p(\vec{x}_S \mid w_i)) . \tag{3}$$

Parameterization of the GMM's for all desired activity modes is achieved based on training data in an iterative fashion with the Expectation Maximization (EM) algorithm [16]. Several initialization schemes for EM are suggested in [17]. In this work, the reduced dataset for an activity mode, w_i, is roughly clustered using the k-means algorithm [18]. These clusters are used to initialize the EM algorithm for finding the mixtures. A key factor affecting the classification performance of GMM's is the number of mixture components, K. As such, the performance of the models for a range of mixture components should be considered and compared for a given application.

Model Selection

The model search space consists of 42 models, which in turn consist of 6 dimension methods (i.e., PCA and LDA for 1 to 3 dimensions) applied to 7 GMM models ranging from order 2 to 8, for each frame length. In order to find the best classifier for each frame length, the Area under the Receiver Operator Characteristics curve (AUC) [19] is used as the performance metric. The reason for choosing AUC is twofold. Firstly, it provides a comprehensive metric that computes true and false positives for all possible

classification thresholds observed in the data. Secondly, the AUC metric is insensitive to class distribution. 10-fold cross-validation (CV) [20] is employed to avoid over-fitting. In 10-fold CV, the data is split into 10 sets of size $N/10$. For purposes of model selection, the classifier is trained on 9 datasets and tested for the AUC on the remaining one. This is repeated ten times until all the data splits are tested and the mean AUC score is recorded as the performance metric of a specific classifier.

Voting Scheme for Controller Mode Switching

The activity mode intent recognizer is a component of the supervisory controller for the powered prosthesis and has two performance objectives. The first objective is to switch to another mode in the shortest time possible when a mode transition occurs, and the second objective is to avoid switching to another mode when there is no real transition. With respect to the first objective, a longer switching time will decrease the quality of movements since the user will have a perceived latency of the assistance from the prosthesis. However, failure to meet the second objective could have more severe consequences (i.e. causing loss of balance and even a fall). Therefore, to increase assurance of correct mode switching, a voting scheme is used.

In the real-time implementation, overlapping frames are classified at each 10 ms interval (Δt). In the voting scheme, the last l classifier decisions are stored in a voting vector and mode switching occurs if more than 90 percent of the classification results are in agreement. To avoid chattering during transition and increase the robustness of the powered prosthesis control, a rule was introduced to not allow the controller mode to switch for 500 ms after a mode switching occurs.

The combination of the voting length, l, and the frame length, f, determines the delay of activity mode intent recognition. To optimize the voting vector length, l, the last two trials for each scenario in the experimental database were used. In this process, the real-time activity intent recognizer is implemented offline with possible voting vector length from 10 to 100 in increments of 10. For a specific frame length, f, the smallest voting length, l_s, which does not switch to standing for the sitting trials and to standing for sitting trials, is selected as the optimal voting vector length.

Once the optimal voting length for each frame is found, the best frame length for the real-time activity intent mode recognition needs to be determined. It is assumed that the two trials for each scenario

encompass all the possible cases and the best models for each frame length are reliable, meaning they do not result in incorrect controller switching. Hence, the problem becomes to select the frame length which yields the least amount of delay, *d,* in the intent recognition. This is accomplished by computing an approximate delay score, $d = f/2+10l$, for each frame length.

5. Results and Discussions

Real-time Intent Recognition

The intent recognition analysis returns the GMM with 6 mixtures using three dimensional PCA reduction using 100 sample frames as the best model. The voting vector length for this model is 40 resulting in an approximate delay of 450 ms. Surface plots of the standing and sitting GMMs showing the regions of the feature space with greater than 0.05 probability densities are presented in Fig. 4-5. The distinct locations of the two different activities in the reduced feature space can be seen in this figure. It should be noted that the SU and SD transitions look like a bridge connecting the standing and sitting modes in this plot. The best model (the model with the least delay) is used for real-time intent recognition between the standing and sitting activity modes. Five trials lasting 90 seconds were conducted to verify that the supervisory controller works in a closed feedback loop. During each trial, the experimenter gave audio cues to the subject to stand up and sit down. During the five trials, no erroneous mode changes were observed. The prosthetic knee angle and the activity mode for one of the trials are shown in Fig. 4-6. The subject stated that there was no perceived latency during transitions. This also agrees with the fact that the knee trajectories for SU and SD transitions are smooth. One might argue that instead of designing a complex intent recognizer a simple thresholding scheme such as implemented for the database generation might suffice for initiating SU and SD transitions. As can be observed from Fig. 4-6, however, the knee angle threshold used for generating the database (5 degrees) is exceeded many times during standing. If this threshold were used, many incorrect stand-to-sit transitions would be initiated. The intent recognizer creates an intricate switching function combining many measurements which results in a robust supervisory controller.

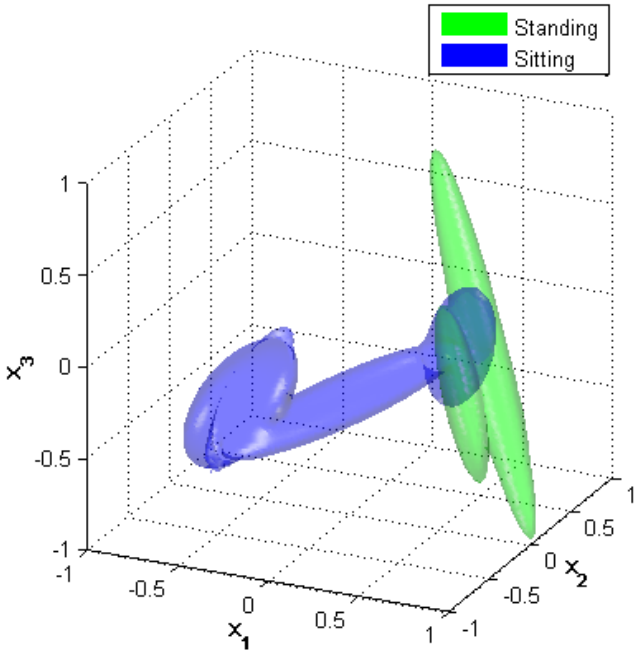

Figure 4-5. Gaussian Mixture Model surface plots of the standing and sitting modes showing the regions of the feature space, where the probability density function is greater than 0.05, for the three dimensional PCA reduced data.

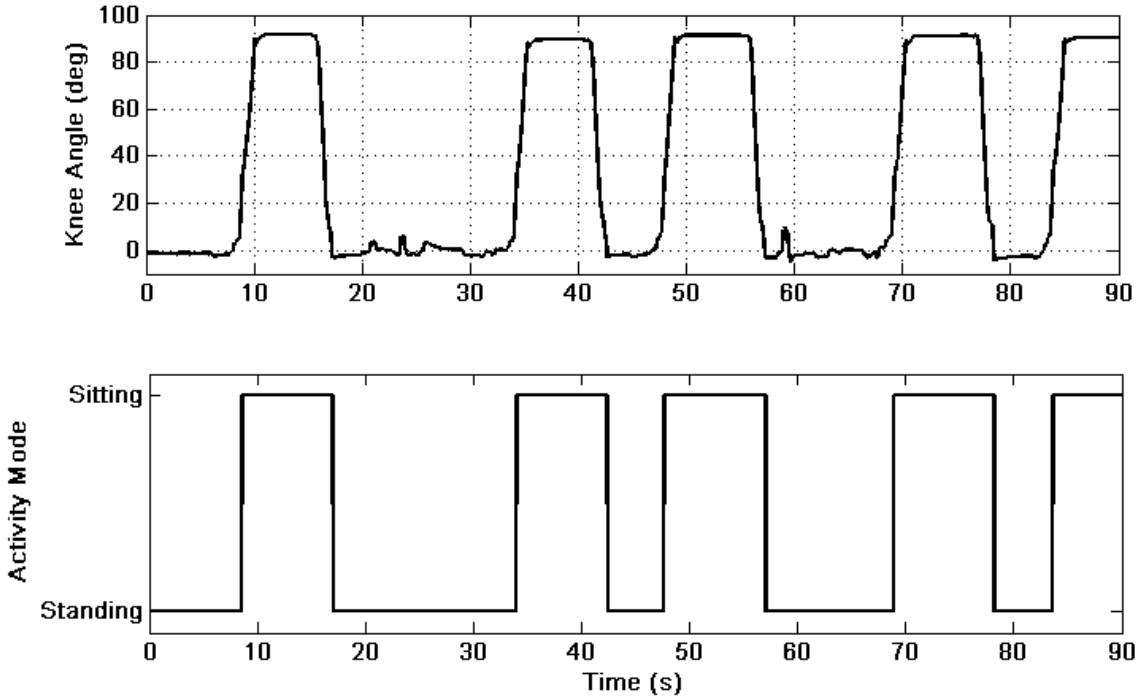

Figure 4-6. Prosthetic knee angle (top) and the real-time activity mode switching (bottom) for a 90 seconds standing and sitting trial.

Biomechanical Evaluation

The knee and ankle angles, torques and powers are shown in Figs. 4-7 and 4-8 for SU and SD, respectively. The corresponding video frame plot showing the middle two second period of these transitions are in Fig.4-9. In standing up, the prosthesis generates peak torque of around 25 Nm and positive peak power of 50 W at the knee during SU. During SD, a smooth descent with up to 50 W of power dissipated at the knee is observed. Even though no significant power and torque was registered at the ankle, the active ankle joint increases stability by adjusting the ankle angle to keep the foot flat during the SU and SD transitions. It should be noted that the powered prosthesis is capable of generating higher torques than those in Figs. 4-7 and 4-8 but the parameters were tuned such that the subject feels most comfortable. The relatively short residual limb length of the subject could limit the maximum comfortable knee torque during SU. The subject stated while using the powered prosthesis it was easier for him to stand up and he feels more support from the prosthesis relative to using his passive one. Presumably, the increased support from the powered prosthesis reduced the joint torques and powers required during standing up from the sound side, although these were not measured in the experimental trials.

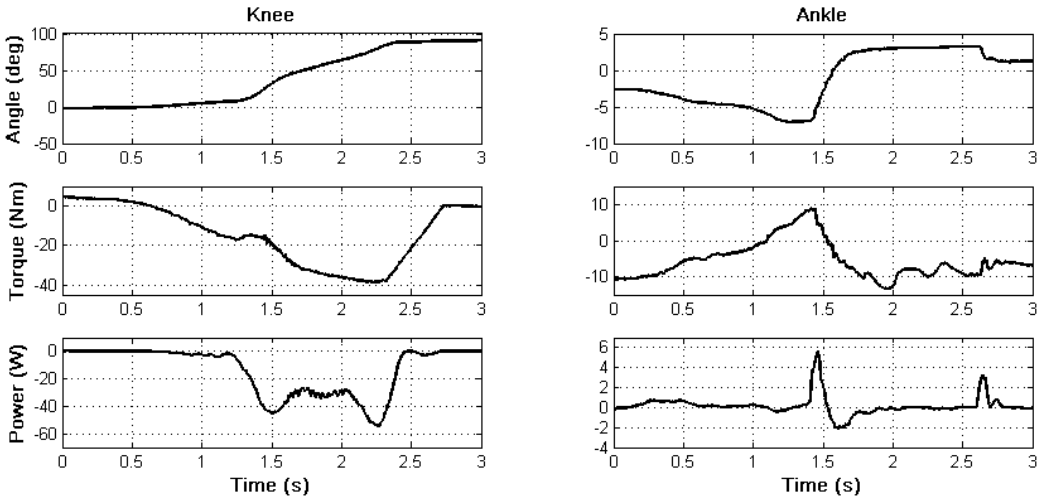

Figure 4-7. Knee and ankle angles (top), torques (middle) and powers (bottom) during sitting down.

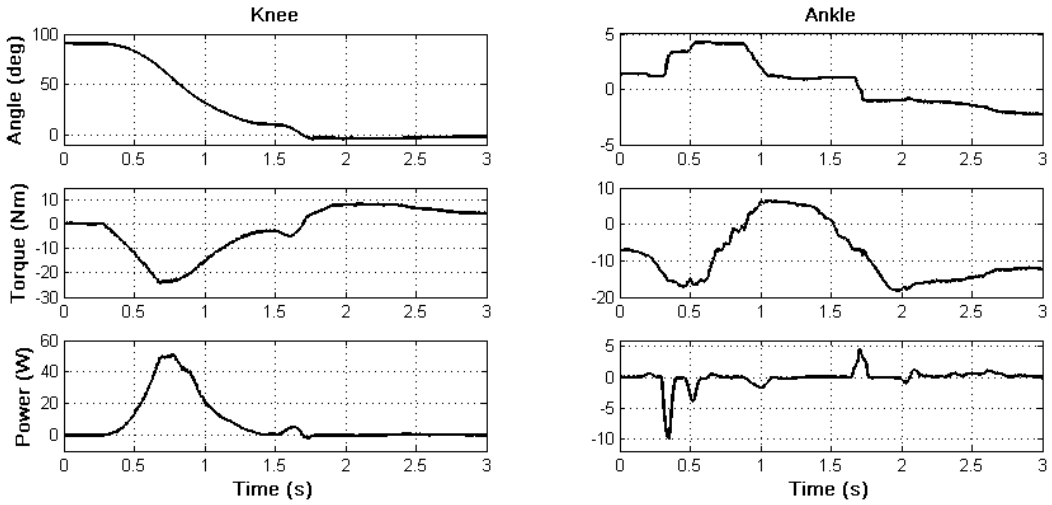

Figure 4-8. Knee and ankle angles (top), torques (middle) and powers (bottom) during standing up.

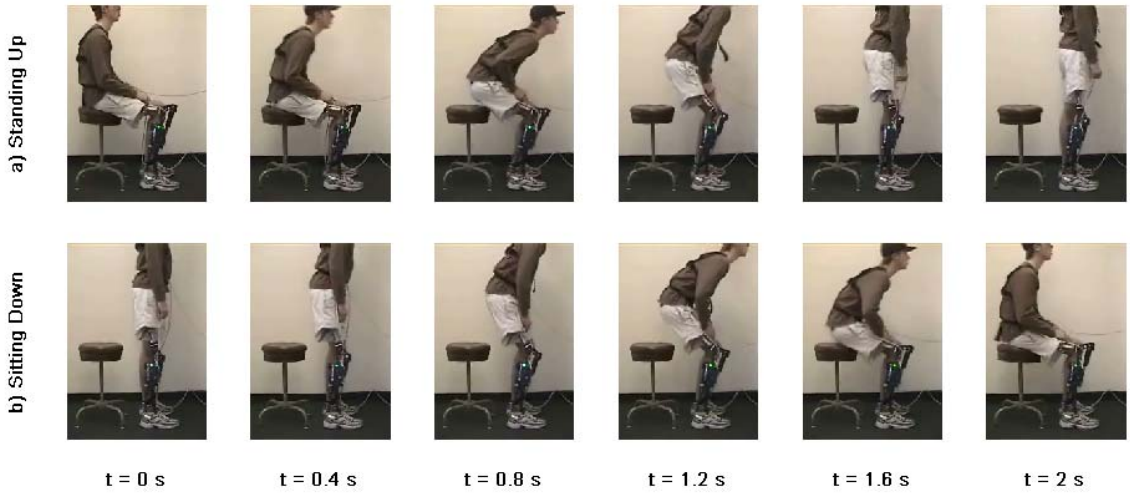

Figure 4-9. Video frames of standing up (a) and sitting down (b) transitions.

6. Conclusion

This paper describes a novel control framework for standing and sitting down with a powered knee and ankle prosthesis. The results indicate that the high level controller (intent recognizer) infers user's intent without perceived latency by the user and switches the underlying controllers correctly. Operating in the proposed control framework, the powered prosthesis was able contribute significant net power to the user at the knee joint during standing up that could not have been achieved with passive prostheses. Further work

includes comprehensive biomechanical evaluation of the assistive sit-to-stand and stand-to-sit control framework on multiple amputee subjects.

7. References

[1] U. Lindemann, H. Claus, M. Stuber, P. Augat, R. Muche, T. Nikolaus, and C. Becker, "Measuring power during the sit-to-stand transfer," European J. of Applied Physiology, vol. 89, no. 5, pp. 466-470, Jun, 2003.

[2] M. Galli, V. Cimolin, M. Crivellini, and I. Campanini, "Quantitative analysis of sit to stand movement: Experimental set-up definition and application to healthy and hemiplegic adults," Gait & Posture, vol. 28, no. 1, pp. 80-85, Jul, 2008.

[3] A. Kralj, R. J. Jaeger, and M. Munih, "Analysis of Standing up and Sitting down in Humans - Definitions and Normative Data Presentation," J. of Biomechanics, vol. 23, no. 11, pp. 1123-1138, 1990.

[4] W. G. M. Janssen, H. B. J. Bussmann, and H. J. Stam, "Determinants of the sit-to-stand movement: A review," Physical Therapy, vol. 82, no. 9, pp. 866-879, Sep, 2002.

[5] M. Schenkman, R. A. Berger, P. O. Riley, R. W. Mann, and W. A. Hodge, "Whole-body movements during rising to standing from sitting," Physical Therapy, vol. 70, no. 10, pp. 638-648, Oct, 1990.

[6] H. Burger, J. Kuzelicki, and C. Marincek, "Transition from sitting to standing after trans-femoral amputation," Prosthetics and Orthotics International, vol. 29, no. 2, pp. 139-151, Aug, 2005.

[7] D. Berry, "Microprocessor prosthetic knees," Phys Med Rehabil Clin N Am, vol. 17, no. 1, pp. 91-113, vii, Feb, 2006.

[8] W. C. Flowers, and R. W. Mann, "Electrohydraulic knee-torque controller for a prosthesis simulator," ASME J. of Biomechanical Engineering, vol. 99, no. 4, pp. 3-8, 1977.

[9] D. Popovic, and L. Schwirtlich, "Belgrade active A/K prosthesis," in de Vries, J. (Ed.), Electrophysiological Kinesiology, Intern. Congress Ser. No. 804, Excerpta Medica, Amsterdam, The Netherlands, pp. 337-343, 1988.

[10] S. Bedard, and P. Roy, Actuated Leg Prosthesis for Above-Knee Amputees, U. S. Patent, 2003.

[11] E. Martinez- Villalpando, J. Weber, G. Elliott, and H. Herr, “Design of an agonist-antagonist active knee prosthesis,” Proc. IEEE/RAS-EMBS Int. Conf. on Biomedical Robotics and Biomechatronics, pp. 529-534, 2008.

[12] F. Sup, H. A. Varol, J. Mitchell, T. Withrow, and M. Goldfarb, “Design and control of an active electrical knee and ankle prosthesis,” Proc. IEEE/RAS-EMBS Int. Conf. on Biomedical Robotics and Biomechatronics, pp. 523-528, 2008.

[13] H. A. Varol, F. Sup, and M. Goldfarb, “Real-time gait mode intent recognition of a powered knee and ankle prosthesis for standing and walking,” Proc. IEEE/RAS-EMBS Int. Conf. on Biomedical Robotics and Biomechatronics, pp. 66-72, 2008.

[14] I. T. Jolliffe, Principal Component Analysis, 2nd ed., New York: Springer, 2002.

[15] R. A. Fisher, “The statistical utilization of multiple measurements,” Annals of Eugenics, vol. 8, pp. 376-386, 1938.

[16] A. P. Dempster, N. M. Laird, and D. B. Rubin, “Maximum likelihood from incomplete data via EM algorithm,” J. of the Royal Statistical Society Series B-Methodological, vol. 39, no. 1, pp. 1-38, 1977.

[17] G. J. McLachlan, and D. Peel, Finite mixture models, New York: Wiley, 2000.

[18] J. A. Hartigan, and M. A. Wong, “A K-means clustering algorithm,” Applied Statistics, vol. 28, no. 1, pp. 100-108, 1979.

[19] T. Fawcett, “An Introduction to ROC Analysis,” Pattern Recognition Letters, vol. 27, no. 8, pp. 861-874, Jun, 2006.

[20] T. M. Mitchell, Machine Learning, New York: McGraw-Hill, 1997.

CHAPTER V

Supervisory Control of a Powered Transfemoral Prosthesis for Walking Speed and Ground Slope Adaptation

Note: The work presented in this chapter will be combined with the slope ascent finite state based impedance controller and submitted to IEEE Transactions on Neural Systems and Rehabilitation Engineering.

1. Abstract

This work presents the supervisory control of a powered knee and ankle prosthesis for walking speed and ground slope adaptation. A cadence estimator computes the cadence by measuring the time intervals between the peaks of the ball of the foot load. Slope adaptation is based on the orientation of an accelerometer mounted on the prosthetic foot. Experimental results with a unilateral transfemoral amputee subject indicate that slope and cadence estimators reliably estimate the ground slope and cadence allowing the modification of walking controller parameters in real-time.

2. Introduction

Current commercial lower limb prostheses are generally passive devices lacking the ability to generate net power at the joints. The loss of net power generation at the lower limb impairs the ability of the prosthesis to restore biomechanically normal locomotive function during many activities, including level walking, ascending stairs and slopes, and rising from a seated position [1-6]. Among all of these locomotion activities, walking provides the primary means to extend ones mobility and improve one's quality of life. Presumably, a prosthesis with the capability of generating net human scale power at the joints with a suitable controller could better restore functionality to lower limb.

Previously, the authors have shown that near normal gait can be achieved with a powered prosthesis in

level walking [7]. To maximize the benefits of such a powered prosthesis while walking requires an intelligent controller that can adjust to the walking speed of the user and the slope of the walking surface. Two main challenges exist in the control structure of the device for different walking conditions. First the prosthesis must be tuned for each condition (i.e. walking speed and ground slope). The second is the development of a supervisory controller that modifies walking controller parameters in coordination with changes in walking conditions.

Prior work in walking speed and incline estimation primarily focus on the use of accelerometer based data and, in the case of prostheses and orthoses, signals such as angles and reaction forces. In [8] and [9], the authors estimate the walking speed and incline of healthy experimental subjects using neural networks using features based on the accelerometer data. Three similar approaches use accelerometers and gyroscopes to estimate the ground slope and walking speed in healthy subjects. In these works, the sensors are mounted in different locations depending on the application (foot [10], shank [11] and hip [12]). The foot mounted system was able to estimate both slope and speed, while the shank mounted system could only reliably identify walking speed. The hip mounted system is part of an active gait orthosis and combines the accelerometer data with hip, knee and ankle angles and ground reaction force measurements. A control method for a passive knee prosthesis described by [13] uses the timing of six controller state transition events at each gait cycle to calculate cadence. There are two prosthetic foot/ankle devices that adjust the ankle angle during swing to accommodate changes in ground slope. The work in [14] uses an accelerometer and its orientation with respect to gravity to estimate ground slope. The other is a commercial device, "Proprio Foot" [15], developed by the prosthetics company Ossur. To the authors' knowledge, no scientific literature exists for this device.

In this work, the supervisory control structure of a powered knee and ankle prosthesis is extended to perform the supervisory control task of adjusting the walking controller parameters to adapt to different walking speeds and ground slopes. The paper begins with an overview of the control architecture and is followed by the development of the cadence and slope estimators. Next, the powered prosthesis, test subject and experimental procedure are explained. Results are then presented along with discussion of their significance. The paper is concluded with highlights of the research and the direction of future work.

Control Architecture

The control architecture of the prosthesis is a three level hierarchy, as diagrammed in Fig. 5-1. The high level supervisory controller, which is the intent recognizer, infers the user's intent based on the interaction between the user and the prosthesis, and correspondingly switches the middle level controllers, as described in [16, 17]. In addition, the high level control is responsible for estimating the cadence and ground slope. The middle level controllers generate torque references for the joints using a finite state machine that modulates the impedance of the joints depending on the phase of the activity. A middle level controller is developed for each activity mode, such as walking, standing, sitting, and stair ascent/descent. The low level controllers are the closed-loop joint torque controllers. In this work, the high level controller will be extended to include the cadence and slope estimators.

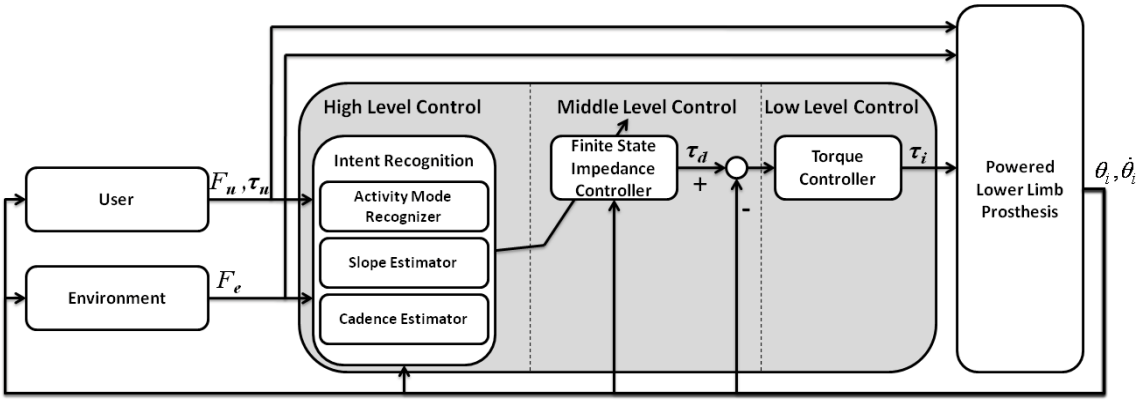

Figure 5-1. Powered prosthesis control architecture.

Finite State Based Impedance Control

In the finite state impedance based control, the impedance behavior of healthy biomechanical gait is mimicked by modulating joint impedances of the prosthesis according to the phase of gait. In each phase, the knee and ankle torques, τ_i, are each described by a passive spring and damper with a fixed equilibrium point, given by:

$$\tau_i = k_i(\theta - \theta_{ki}) + b_i\dot{\theta} \tag{1}$$

where k_i, b_i, and θ_{ki} denote the linear stiffness, damping coefficient, and equilibrium point, respectively, for

the i^{th} state. The approach requires the development of a state machine for each type of user activity such as walking, standing, sitting, and stair ascent and descent. The state chart for walking showing different gait phases is shown in Fig 5-2. Switching joint impedances between the gait phases is initiated by biomechanical cues. For instance, the switching from swing extension to the early stance state during walking occurs with the detection of heel strike. The result is an effective and predictable controller that does not violate passive behavior except when the user requests active power transfer by triggering a transition. The authors previously developed controllers for standing, walking, sitting, and the sit-to-stand and stand-to-sit transition modes using this framework [7, 17].

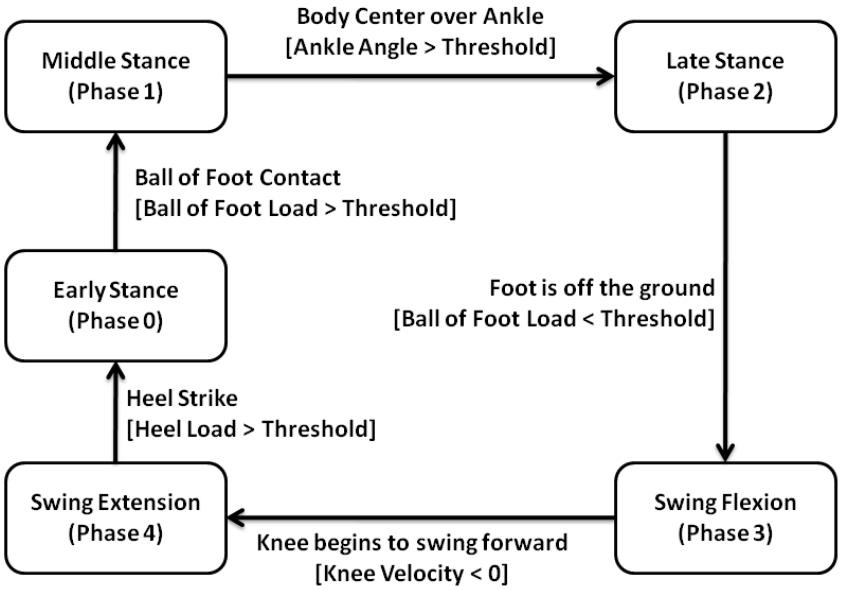

Figure 5-2. The state chart depicting the phase transitions in walking mode.

In walking middle level controller, Phase 0 begins with a heel strike, upon which the knee immediately begins to flex so as to provide impact absorption and begin loading. Once the ankle plantarflexes to reach a flat foot state, Phase 1 is initiated. Both knee and ankle joints have relatively high stiffness during this phase to prevent buckling and allow for appropriate stance knee flexion. Phase 2 is the push-off phase and begins as the ankle dorsiflexes beyond a given angle (i.e. user's center of mass lies forward of stance foot). The knee stiffness decreases in this phase to allow knee flexion while the ankle

provides a plantarflexive torque for push-off. Phase 3 begins as the foot leaves the ground as indicated by the ground reaction force and lasts until the knee reaches maximum flexion. Phase 4 is active during the extension of the knee joint, which begins as the knee velocity becomes negative and ends at heel strike. In both of the swing phases, the ankle torque is small and is represented in the controller as a spring regulated to a neutral position, corresponding to the estimated ground slope. The knee is modeled as a damper and a weak spring regulated to a flexed position in both swing phases to generate a smooth swing motion which lands at the desired angle.

Ground Slope Estimation

The principle of ground slope estimation is estimating the orientation of the prosthetic foot relative to gravity while the foot is flat on the ground. A 3-axis accelerometer capable of measuring ±3 g accelerations (ADXL330, Analog Devices) is embedded into the ankle joint coupler where the prosthetic foot is connected. In order to estimate the ground slope, the accelerometer data in the tangential direction is used, see Fig. 5-3. Assuming the foot is flat on the ground, the ground slope angle, θ_s, can be calculated as in Eqn. 2 where *g* is the gravitational constant.

$$\theta_s = \sin^{-1}\left(\frac{a_t}{g}\right) \tag{2}$$

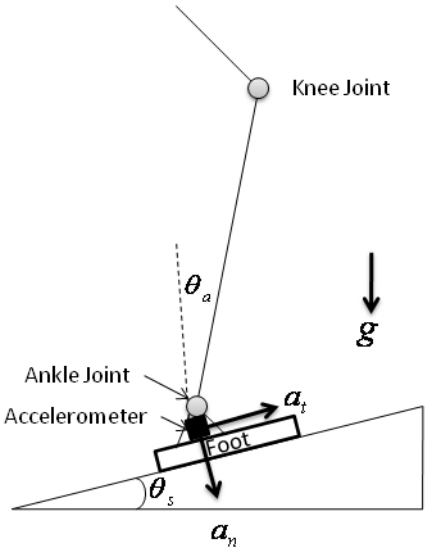

Figure 5-3. Diagram of prosthesis and accelerometer location and angle convention used.

In order to find the ground slope estimate, $\hat{\theta}_S$, the accelerometer data is collected while the foot is flat on the ground, as determined by the heel and ball of the foot load sensors. During this time interval, Eqn. 2 is computed and the mean of the frame is used as the ground slope estimate, $\hat{\theta}_S$. Once the slope is estimated, the intent recognizer selects the corresponding middle layer controller based on some predefined thresholds as in Fig. 5-4.

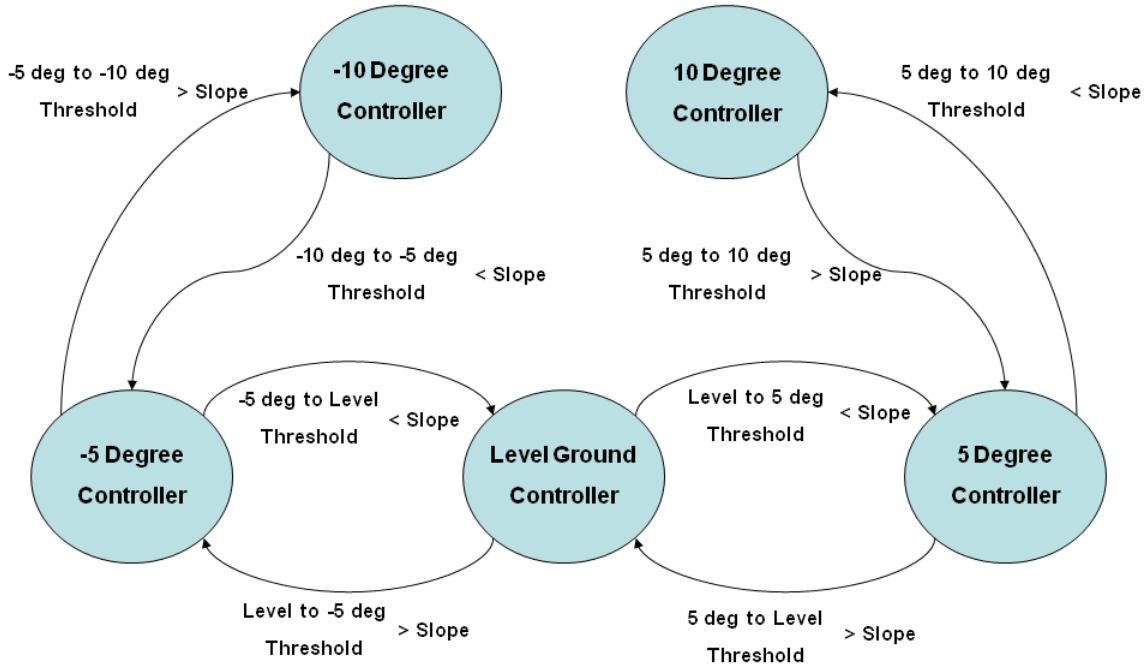

Figure 5-4. Controller switching logic based on slope.

Positive and negative 5 and 10 degree slopes are considered in this study. The 5 degree slope is selected since the building code in the United States dictates that the maximum slope of a ramp cannot exceed a slope of 1:12 (5 deg) [18]. The 10 degree slope is chosen for outdoor conditions in which extreme ground slopes might occur. It should be also noted the controllers are quite tolerant to the ground slope over a large range. For instance, the subject will be able to walk with the 5 degree parameters on a 10 degree slope, although the gait will not be optimal.

Cadence Estimation

As reported in [19], there is a close correlation between walking speed and cadence. Since measuring a period is easier than measuring a velocity with the given sensor set, cadence is used in this work as an indicator of user's intended walking speed. Further, it has been observed in preliminary trials with the prosthesis that parameter variation is most closely correlated with cadence rather than gait speed. Specifically, cadence estimation is accomplished by measuring the time between successive peaks in the ball of the foot loads. In the real-time implementations, cadence estimation is accomplished by recording the foot toe load after heel strike when it exceeds 400 N till the load decreases below 350 N (See Fig. 5-5). Then, the time of occurrence of the peak toe load in this window is found and the previous peak time is subtracted from the new peak time to find the cadence. Once the cadence is estimated, the intent recognizer selects the corresponding middle layer controller based on some predefined thresholds as in Fig. 5-6.

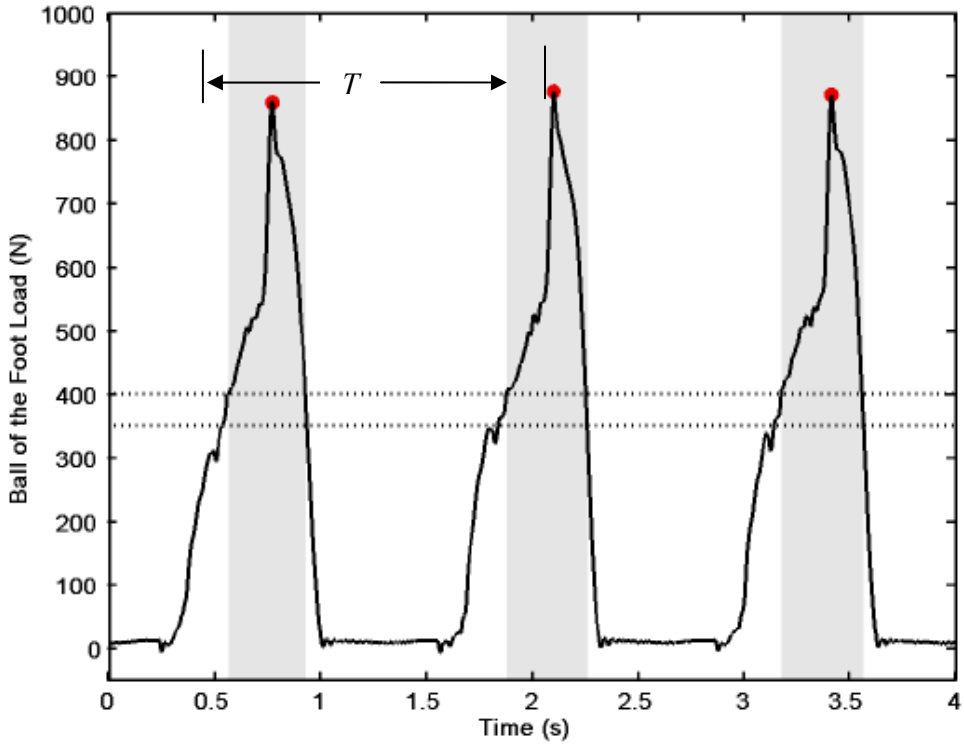

Figure 5-5. Ball of the foot load from a walking trial with self selected cadence. The gray area denotes the region where the ball of the foot sensor data is collected to find the peak. The time interval between two successive peaks, *T*, is used to find the cadence.

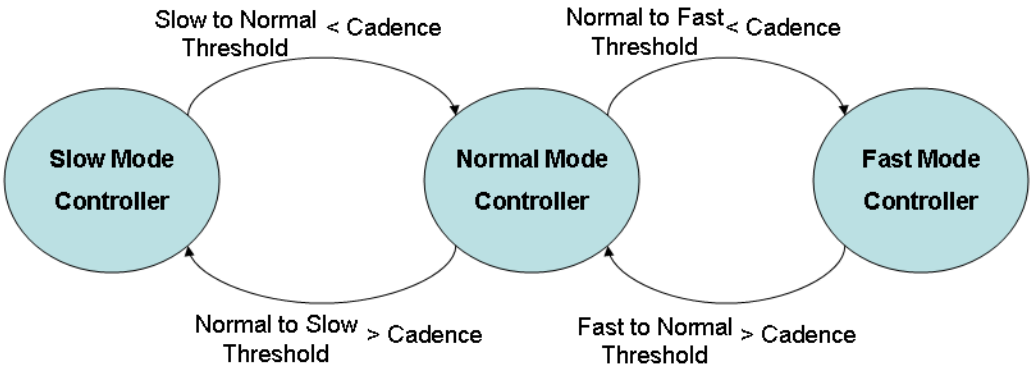

Figure 5-6. Controller switching logic based on cadence.

3. Experimental Procedure

Powered Prosthesis

The authors have described a self-contained powered knee and ankle prosthesis [7], Fig. 5-7, that was used in the supervisory control for a walking speed and ground slope adjustment experiments in this work. The powered prosthesis is capable of generating 70 and 120 Nm at the knee and ankle joints, respectively. The range of motion of the device is comparable to the native human limb. The device's sensor package includes a custom load cell to measure the sagittal socket interface moment above the knee joint, a custom foot to measure the ground reaction force at the heel and ball of the foot, and commercial potentiometers and load cells to measure joint positions and torques, respectively. The self-contained version hosts onboard power and an embedded system allowing for both tethered and untethered operation.

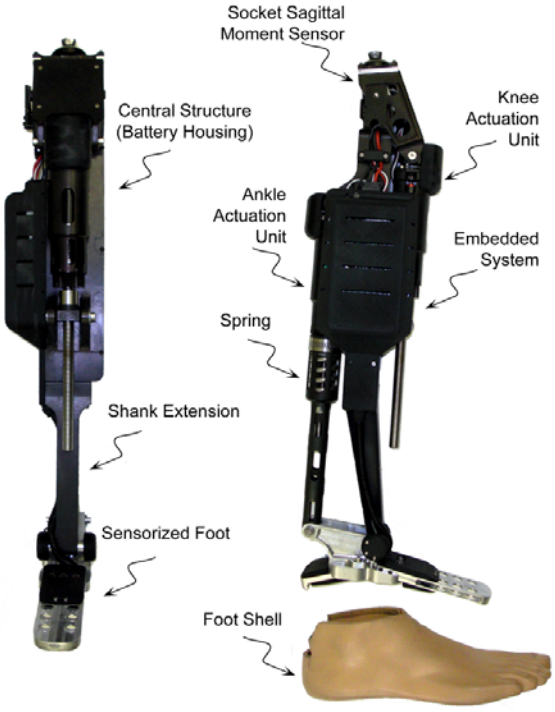

Figure 5-7. The self-contained powered knee and ankle transfemoral prosthesis.

Experimental Subject

The prosthesis was tested on a 20-year-old male (1.93 m, 70 kg) unilateral amputee four years post amputation, Fig. 5-8. The length of the test subject's residual limb, measured from the greater trochanter to the amputated site, was 55% of the length of the non-impaired side measured from the greater trochanter to the lateral epicondyle. The subject uses an Otto Bock C-leg with a Freedom Renegade prosthetic foot for daily use. The subject's daily use socket was used on all experiments, where the powered prosthesis prototype was attached on place of the daily use prosthesis. The overall prosthesis height and varus-valgus alignment were performed by a licensed prosthetist. The subject spent over 200 hours of time using the prosthesis in a laboratory setting and was proficient in using the device.

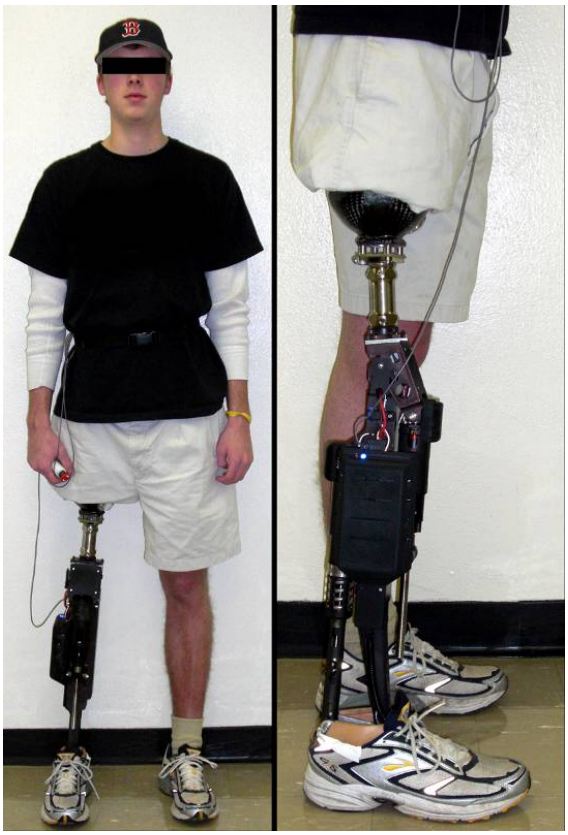

Figure 5-8. Unilateral transfemoral amputee test subject used for the powered prosthesis evaluation.

Experimental Procedure

To test the cadence estimator, the powered prosthesis was tuned for level walking at self-selected speed (90 steps/min) and for ±15 percent of the self-selected speed of the test subject. The resulting cadences of the subject at these three speeds were calculated. The cadence thresholds of the estimator were updated. The estimator was first tested on 50 m track (actually an indoor hallway) and the test subject was asked to self-adjust his speed as he walked the track. In the second experiment, the subject was asked to walk on a 400 m outdoor running track and again asked to self-adjust his speed as he progressed along on the track. In addition, the subject was asked to walk both in a straight line and in a zigzag pattern to test the robustness of the estimation.

For slope estimation, the device was tuned for level, 5 and 10 degrees upslope walking with the slope estimator working, but not modulating the underlying controllers. The output of the slope estimator was recorded and verified that it corresponded to the actual slope. Once the operation of the slope estimator was

verified, a second set of trials was conducted on a 170 m track (actually a residential sidewalk) that progressively increased in inclination from level to 10 deg. The slope of this 170 m track was measured at every 9 m using an inclinometer. In this trial, the slope estimator switched the underlying controllers and the test subject walked the 170 m track. For all of the above experiments, internal controller states, knee and ankle joint angles, torques, and powers for the prosthesis were recorded for the duration of the walk.

4. Results and Discussions

The average cadences on level ground for slow, normal and fast walking are found to be 79, 92 and 106, respectively. The thresholds for controller mode switching which are set based on these average cadences are summarized in Table I. The results of the cadence estimator showing the real-time cadence estimates, mode switchings and the cadence estimates computed from the recorded signals in the post-processing for the 50 m indoor and 400 m outdoor track are shown in Fig. 5-9 and 5-10, respectively. The post-processed cadence estimate is found by computing the cadence from the intervals between consecutive heel strikes. As it can be seen from the figures, the real-time estimated cadence is accurate with respect to the cadence estimate from post-processing and the prosthesis shows correct mode switching behavior based on this estimated cadence.

Table 5-1. Cadence Threshold Values for the Walking Speed Supervisory Control

Threshold	Value (cadence)
Slow to Normal	89
Normal to Slow	83
Fast to Normal	96
Normal to Fast	102

In the experiments where the subject walked on constant level ground, 5 and 10 degree upslopes, it is verified that the slope estimator predicts the ground slope in real-time. Since the prosthesis was not tuned yet for the downhill slopes, no experiments were conducted for -5 and -10 degrees slopes. The thresholds for controller mode switching for supervisory ground slope adaptation control are summarized in Table II. The ground slope estimate, measured ground slope and real-time mode switching plotted versus time in a

supervisory ground slope adaptation experiment on a 170 m hill starting with 0 degree slope and ending with 10 degree slope is shown in Fig. 5-11. The figure indicates that the slope estimates are accurate enough to allow for real-time supervisory control. Fig 5-12 shows the estimated and measured ground slopes versus distance. It should be noted that there is an observed difference up to two degrees between the estimated and measured valued.

Table 5-2. Slope Threshold Values for the Slope Adaptation Supervisory Control

Threshold	Slope (deg)
Level to 5 Degree	3.5
5 Degree to Level	2
5 Degree to 10 Degree	7
10 Degree to 5 Degree	5.5

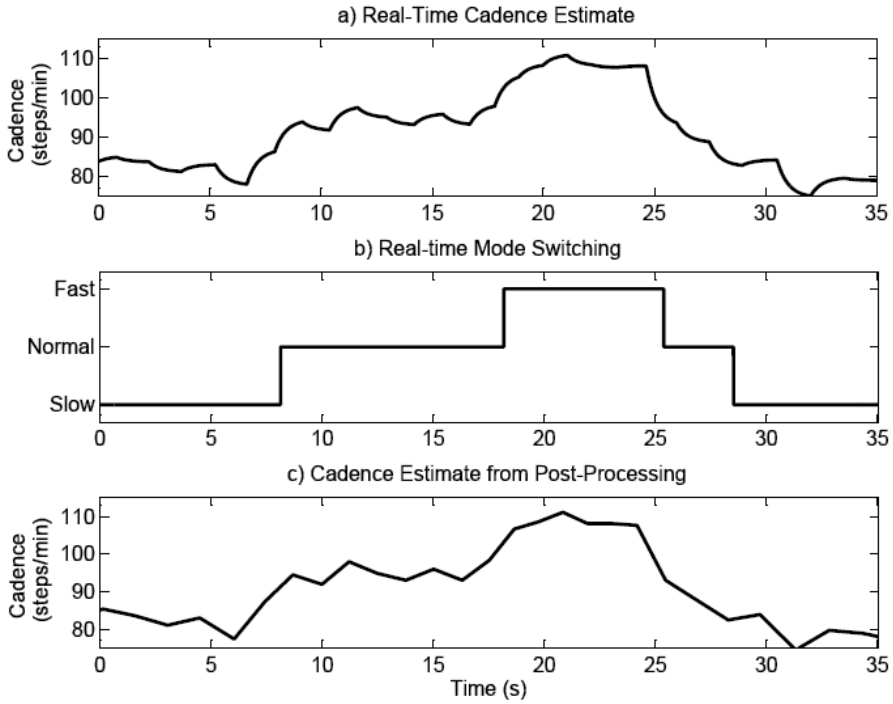

Figure 5-9. Real-time cadence estimate (a), supervisory control mode switching (b), and the cadence estimate from post-processing (c) for a 35 second walking trial on the 50 meter track.

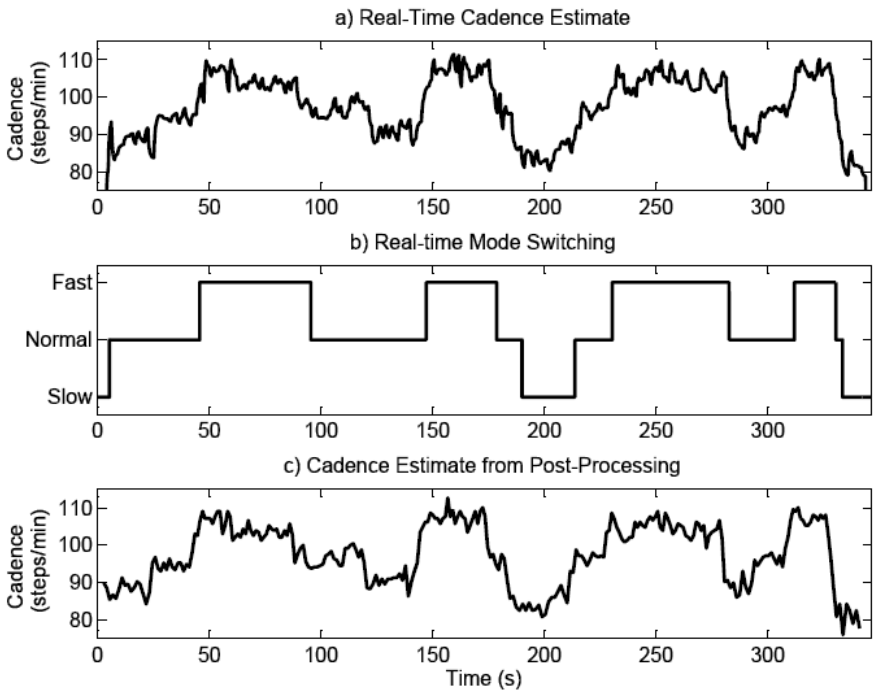

Figure 5-10. Real-time cadence estimate (a), supervisory control mode switching (b), and the cadence estimate from post-processing (c) for a 340 second walking trial on the 400 meter track.

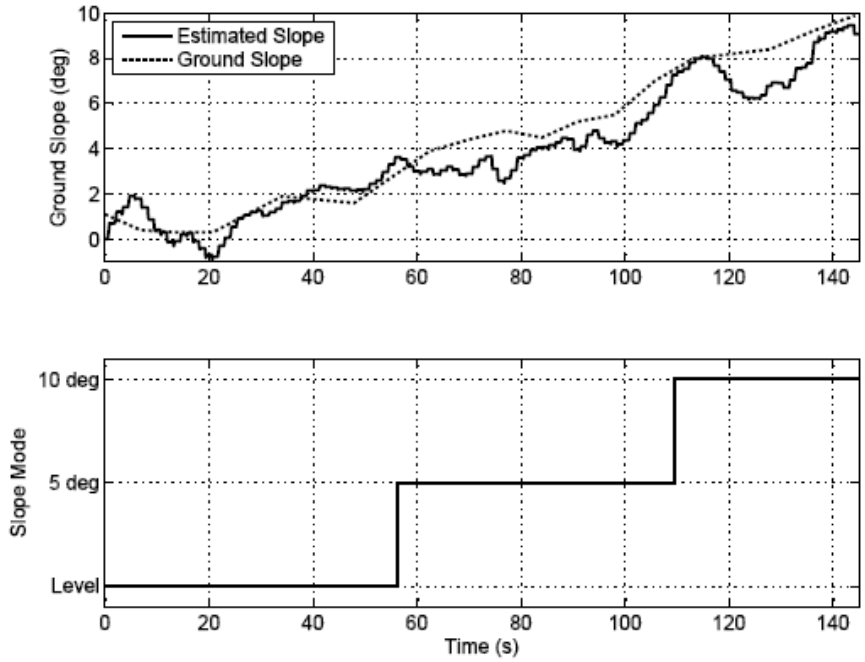

Figure 5-11. Measured and real-time estimated ground slope versus time (a) and supervisory control mode switching (b) for the 170 m supervisory control walking trial on the hill track.

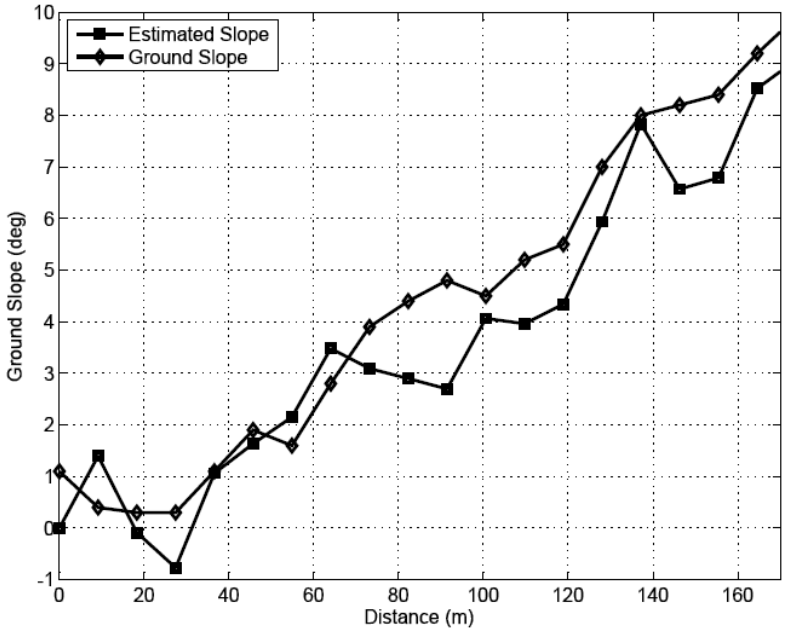

Figure 5-12. Measured and real-time estimated ground slope versus distance traveled for the 170 m supervisory control walking trial on the hill track.

5. Conclusion

The supervisory control of a powered knee and ankle prosthesis for walking speed and ground slope adaptation can be done reliably using the slope and cadence estimators outlined that rely only on the prosthesis' sensors. Future work with the powered prosthesis should focus on the tuning for downhill slopes and supervisory control experiment on tracks containing both positive and negative slopes. Further extensions of the work include the ability to navigate uneven terrain and slope estimation while standing for enhanced stability.

6. References

[1] H. Burger, J. Kuzelicki, and C. Marincek, "Transition from sitting to standing after trans-femoral amputation," Prosthetics and Orthotics International, vol. 29, no. 2, pp. 139-151, Aug, 2005.

[2] T. Schmalz, S. Blumentritt, and B. Marx, "Biomechanical analysis of stair ambulation in lower limb amputees," Gait & Posture, vol. 25, no. 2, pp. 267-278, Feb, 2007.

[3] M. Traballesi, P. Porcacchia, T. Averna, and S. Brunelli, "Energy cost of walking measurements in

subjects with lower limb amputations: A comparison study between floor and treadmill test," Gait & Posture, vol. 27, no. 1, pp. 70-75, Jan, 2008.

[4] R. L. Waters, J. Perry, D. Antonelli, and H. Hislop, "Energy cost of walking of amputees - Influence of level of amputation," J. of Bone and Joint Sur-American Vol., vol. 58, no. 1, pp. 42-46, 1976.

[5] D. Winter, The Biomechanics and Motor Control of Human Gait: Normal, Elderly and Pathological, 2nd ed.: University of Waterloo Press, 1991.

[6] D. A. Winter, and S. E. Sienko, "Biomechanics of below-knee amputee gait," J. of Biomechanics, vol. 21, no. 5, pp. 361-367, 1988.

[7] F. Sup, H. A. Varol, J. Mitchell, T. J. Withrow, and M. Goldfarb, "Self-Contained Powered Knee and Ankle Prosthesis: Initial Evaluation on a Transfemoral Amputee," IEEE 11th Int. Conf. on Rehabilitation Robotics, pp. 638-644, 2009.

[8] K. Aminian, P. Robert, E. Jequier, and Y. Schutz, "Estimation of speed and incline of walking using neural network," IEEE Trans. on Instrumentation and Measurement, vol. 44, no. 3, pp. 743-746, 1995.

[9] S. Yoonseon, S. Seungchul, K. Seunghwan, L. Doheon, and K. H. Lee, "Speed Estimation From a Tri-axial Accelerometer Using Neural Networks," 29th Annual Int. Conf. of the IEEE Engineering in Medicine and Biology Society, pp. 3224-3227, 2007.

[10] A. M. Sabatini, C. Martelloni, S. Scapellato, and F. Cavallo, "Assessment of walking features from foot inertial sensing," IEEE Trans. on Biomedical Engineering, vol. 52, no. 3, pp. 486-494, Mar, 2005.

[11] Q. Li, M. Young, V. Naing, and J. M. Donelan, "Walking Speed and Slope Estimation Using Shank-mounted Inertial Measurement Units," IEEE 11th Int. Conf. on Rehabilitation Robotics, pp. 839-44, 2009.

[12] Y. Hirata, T. Iwano, and K. Kosuge, "Control of Wearable Walking Helper on slope based on integration of acceleration and GRF information," IEEE/RSJ Int. Conf. on Intelligent Robots and Systems, pp. 3731-3736, 2008.

[13] D. Zlatnik, B. Steiner, and G. Schweitzer, "Finite-state control of a trans-femoral (TF) prosthesis,"

IEEE Trans. on Control Systems Technology, vol. 10, no. 3, pp. 408-420, 2002.

[14] W. S. Holmberg, “An autonomous control system for a prosthetic foot ankle,” 4th IFAC Symposium on Mechatronic Systems, pp. 856-61, 2006.

[15] W. Koniuk, Self-adusting prosthetic ankle apparatus, 6,443,993, U. S. Patent, March, 23, 2001.

[16] H. A. Varol, F. Sup, and M. Goldfarb, “Real-time gait mode intent recognition of a powered knee and ankle prosthesis for standing and walking,” Proc. IEEE/RAS-EMBS Int. Conf. on Biomedical Robotics and Biomechatronics, pp. 66-72, 2008.

[17] H. A. Varol, F. Sup, and M. Goldfarb, “Powered Sit-to-Stand and Assistive Stand-to-Sit Framework for a Powered Transfemoral Prosthesis,” IEEE 11th Int. Conf. on Reh. Robotics, pp. 645-651, 2009.

[18] 42 U.S.C. § 12101 et seq., Americans with Disabilities Act of 1990, 1994.

[19] R. L. Waters, B. R. Lunsford, J. Perry, and R. Byrd, “Energy Speed Relationship of Walking - Standard Tables,” J. of Orthopaedic Research, vol. 6, no. 2, pp. 215-222, Mar, 1988.

CHAPTER VI

Conclusions and Future Work

1. Conclusions

In this work, it is shown that the safe and reliable control of a powered transfemoral prosthesis can be accomplished using a three level control structure consisting of a high level supervisory intent recognizer, middle layer finite state based impedance controller and low level torque controller. All the control development has been tested and verified with a unilateral amputee subject. The main contributions of this work can be listed as:

- Development of a three level control structure consisting of high level supervisory control intent recognizer, middle level finite state based impedance activity controllers and low level torque controllers.
- Design of activity mode intent recognizer which infers user intent to stand, sit, or walk, by recognizing patterns in prosthesis sensor data in real-time, without the need for instrumentation of the sound-side leg.
- Design of a cadence estimator which is used to modify the walking controller parameters based on the user's walking cadence.
- Design of a slope estimator which allows real-time ground slope adaptation.
- The expansion of the finite-state impedance control structure to accommodate sitting and the associated sit-to-stand and stand-to-sit transitions.
- Development of embedded system hardware and software for a powered prosthesis for tethered and untethered operation with data logging and wireless transmission capabilities.
- Initial biomechanical and power consumption results when walking at different speeds.

2. Future Work

The future research objectives aim to improve the powered prosthesis which will create an intelligent and highly robust device that could benefit a significant amputee population in the case of device commercialization. In order to achieve this, future research should focus on the following three areas: hardware development, control system design and biomechanical assessment.

Hardware

One of the main drawbacks of the current prosthesis is the audible noise during operation due to the fast movement of the ball screw. This is not only a problem related to the Vanderbilt powered knee and ankle prosthesis. Nearly all of the powered prostheses being developed or in the market (the powered knees and the powered ankles) are using ball screw based transmissions. Therefore, future research on hardware should mainly focus to fix this problem by creating a quiet and efficient transmission that can transmit human scale torque and power for the required knee and ankle joint ranges. Moreover, use of sealed roller bearings instead of bushing might increase the efficiency of the prosthesis slightly. Since many different commercial feet are available in the market, it might be more suitable to use one of these instead of the present custom built foot. Besides efficiency, mechanical robustness and weight; ease of manufacturing should also be considered as one of the mechanical design objectives to decrease the production costs of the prosthesis in case of a possible commercialization.

Some hardware improvement might be accomplished regarding the embedded system and sensors of the prosthesis as well. Rather than using a centralized embedded system, a distributed embedded system with small localized printed circuit boards embedded in the prosthesis can be used. This way, the structure can be used as heat sinks for the servo amplifiers decreasing the weight of the prosthesis by eliminating need for the additional heat sinks used on the present embedded system. In general, no cables should cross over moving joints of the prosthesis to prevent failures on these cables due to continuous flexing and twisting. Sensing side of the prosthesis might be improved by replacing the analog potentiometer with high count digital encoders. This way, a cleaner velocity signal which will allow higher gains for the damping parameters in the finite state based impedance control framework might be

achieved. The present prosthesis contains the battery pack in the central housing. The replacement of the battery requires removal of several screws. A new design should incorporate an easily replaceable battery pack similar to one in a notebook computer. In general, the prosthesis should have external covers to have a splash safe rugged design, which will be more suitable for outdoor working conditions.

The socket interface of the amputees is one of the main limitations of the current prostheses. Current sockets have compliance and act as an additional joint between the hip and the knee, distorting the gait dynamics. Research should be conducted on better socket technologies which don't affect the gait dynamics negatively. Osseointegration is one of the promising new technologies that might be considered in conjunction with a powered prosthesis.

Control Design

Amputees using passive prosthesis have difficulty in stair ascent and descent, both of which require highly coordinated motions requiring significant power and torque in knee and ankle joints. The present control structure does not contain the stair ascent and descent controllers. Firstly, the middle layer controllers for the stair ascent and descent modes should be developed. Then the activity mode intent recognizer should be trained using a database containing these two new classes and supervisory control for these modes should be accomplished. The present slope walking controller is tuned for 5 and 10 degree slope ascent. Tuning of the slope walking controller for -5 and -10 degree slope descent is also necessary.

The powered prosthesis is tested on two subjects and it is seen that the parameters for the middle layer controller do not change very significantly. In general, use of optimal parameters would maximize the biomechanical merits of the prosthesis. Nonetheless, achieving the optimal parameter set for each user might require a long tuning time. In this case, the initial guess for the parameters becomes important. Once the prosthesis is tuned for multiple subjects, look-up tables for initial parameters might be created based on few variables such as height, weight and residual limb length. These look-up can be used to create the initial parameter set for a subject and possibly decrease the tuning time.

The present tuning procedure for the middle layer control tries to achieve joint trajectories for population average of healthy subjects by generating torque references. The symmetry of the gait is

evaluated only qualitatively based on visual inspection of the subject's gait. Use of motion capture for tuning might allow the prosthesis to improve the symmetry of gait. A further area of work might be to design an adaptive auto-tuner which minimizes a cost function based on the symmetry using processed motion capture data.

Supervisory controller requires generation of a database. Once the pattern recognizer is trained using the database, the pattern recognizer is fixed. After creating an initial database, the database might be stored on the memory of the prosthesis and the database might be replenished continuously with new data logged during the daily operation of the prosthesis. When the prosthesis is taken off for a long duration, the pattern recognizer might be trained on this new database. This way, the change in gait (for instance change in gait due to gaining weight) over long periods of time will be taken into account.

After the development of the middle layers controllers are finished, another middle layer controller based on the active passive decomposition might be implemented for control. The active passive decomposition based controller generates the torque reference of the joints by combining two components. The first component is the passive one defined by nonlinear spring-dashpot relations. The second one is the active part which is a function of the sensory inputs which are under direct influence of the user. The sensory information to use for this controller might include the ground reaction forces, socket interface torques and forces, and accelerometer and gyroscope measurement on the residual limb.

Matlab/Simulink is being used for interfacing the prosthesis with a computer for tuning and diagnostics in laboratory setting. Since Matlab is an expensive program developed mainly for scientists and engineers, a simple graphical user interface based tuning and diagnostics tool would be beneficial by decreasing the costs and allowing non-engineer users such as prosthesists to tune the prosthesis for amputees.

Biomechanical Evaluation

Extensive biomechanical evaluation of the prosthesis using motion capture and metabolic energy consumption setups for different walking conditions, sit-to-stand and stand-to-sit transitions should conducted.

A powered prosthesis with a high actuator bandwidth is capable of simulating passive prosthesis.

Different combinations such as passive knee and passive ankle, active ankle and passive knee, and both active joints can be evaluated with respect to symmetry of gait, metabolic energy consumption and hip torque for different activity scenarios with multiple subjects. If the results of this study favor the powered prosthesis, this might be used as an argument to support the powered prosthesis.

Another area for biomechanical studies with the prosthesis can include long term studies. In these studies, subjects can take the prosthesis out of the lab and use as their daily use prosthesis for a long duration. The information acquired can be used to refine the hardware and the control structure of the prosthesis. Additionally, average numbers of daily steps, number of falls and stumbles can be inferred from the logged data to investigate to compare the affects the powered prostheses in the daily life of amputees to the passive prostheses.